IASF/INAF
BOLOGNA
Project System Team

Planck LFI

TITLE: **In flight evaluation of LFI radiometers thermal susceptibilities**

DOC. TYPE: **TECHNICAL NOTE**

PROJECT REF.: **PL-LFI-PST-TN-098** **PAGE:** **1, 82**

ISSUE/REV.: **1.0** **DATE:** **October 2011**

Prepared by	**F. CUTTAIA** **L. TERENZI** **LFI System Team**	**Date:** **October 17th, 2011** **Signature:** _____
Agreed by	**C. BUTLER** **LFI Program Manager**	**Date:** **September 6th, 2011** **Signature:** _____
Approved by	**N. MANDOLESI** **LFI Principal Investigator**	**Date:** **September 6th, 2011** **Signature:** _____

DISTRIBUTION LIST

Recipient	Company / Institute	E-mail address
J. TAUBER	ESA – Noordwijk	Jan.Tauber@esa.int
N. MANDOLESI	IASF/INAF – Bologna	mandolesi@iasfbo.inaf.it
C. BUTLER	IASF/INAF – Bologna	butler@iasfbo.inaf.it
G. MORGANTE	IASF/INAF – Bologna	morgante@iasfbo.inaf.it
M. BERSANELLI	UNIMI – Milano	Marco.bersanelli@mi.infn.it
A. MENNELLA	UNIMI – Milano	Aniello.Mennella@fisica.unimi.it
A. ZACCHEI	INAF - OA Trieste	zacchei@oats.inaf.it
LFI Systematics		lfi_systematics@iasfbo.inaf.it
LFI SPCC	IASF/INAF – Bologna	lfispcc@bo.iasf.cnr.it

CHANGE RECORD

Issue	Date	Sheet	Description of Change	Release
Issue 0.1	Sep '11	All	Draft issue of document	1.0

Abstract

In this technical note we provide a preliminary estimation of the impact of temperature fluctuations at the level of different thermal stages on the output signal of the Planck-LFI radiometers. Thermal susceptibilties at the level of Front End Modules (FEMs), Back End Modules (BEMs) and 4K Reference Loads have been evaluated throughout the ground test phases of the instrument. Due to bias optimization and different environmental conditions an in-flight measurement is needed to get an estimate of the temperature fluctuations impact on science and to setup an attempt of reduction of such a systematic effect by using houskeeping informations.

References

[1] M. Seiffert, A. Mennella, C. Burigana, et al., *1/f noise and other systematic effects in Planck-LFI radiometers*, A&A, 391, 1185-1197 (2002)

[2] A. Mennella, M. Bersanelli, M. Seiffert, et al., *Offset balancing in pseudo correlation radiometers for CMB measurements*, A&A, to be published (2003)

[3] L. Terenzi, et al *Planck LFI CPV: Thermal Susceptibility Test Report* (ref: P_PVP_LFI_0016_01) PL-LFI-PST-RP-075, Issue 1.1, October 2009

[4] G. Morgante, et al. *Cryogenic characterization of the Planck sorption cooler system flight model*, Journal of Instrumentation, Volume 12, Issue 12, pp. T12016 (2009)

[5] L. Terenzi, et al. *Thermal susceptibility of the Planck-LFI receivers.* Journal of Instrumentation, Volume 12, Issue 12, pp. T12012 (2009)

[6] L. Valenziano et al., *Planck-LFI: Design and Performance of the 4 Kelvin Reference Load Unit*, Journal of Instrumentation, Volume 12, Issue 12, pp. T12006 (2009)

[7] L.Terenzi et al., *Preliminary evaluation of the impact of temperature fluctuations in the HFI 4K stage on LFI*, Technical Note PL-LFI-PST-TN-048 – Issue 2.0, June 2006

[8] A. Mennella, M. Bersanelli, C. Burigana, et al., *Planck: systematic effects induced by periodic fluctuations of arbitrary shape*, A&A, 384, 736-742 (2002)

[9] E. Artal et al., *LFI 30 and 44 GHz receivers Back-End Modules*, Journal of Instrumentation, Volume 12, Issue 12, pp. T12003 (2009)

[10] A. Mennella, M. Tomasi, *Susceptivity of the LFI radiometers to the BEM temperature*, wiki page at: http://belzebu.lambrate.inaf.it/lfiWiki/bin/view/LFI/BEMTemperatureSusceptivity#Analysis_by_linear_voltage_tempe

1. Introduction

The Planck-LFI radiometric receivers are pseudo-correlation radiometers [1, 2] that continuously compare the sky signal with the reference load signal in order to minimise spurious effects from gain instabilities..

Fig. 1 shows a sketch of the baseline LFI front-end.

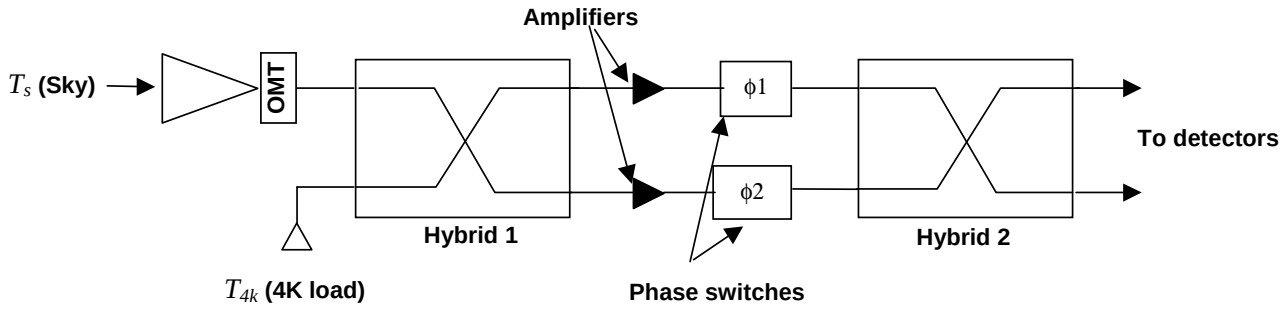

Figure 1. Schematic of the baseline LFI front end.

The output signal on each of the two lines exiting the second hybrid is constituted by a sequence of alternating sky and load signals that are detected and integrated over the phase switch period. Neglecting imperfect isolation and non-ideal behaviours in the phase switches we can write the difference between integrated sky and load power outputs as (see [1] for detailed calculations):

$$p(t) = \frac{ak\beta}{4}(1-r)\left[G_1(\tilde{T}_s + \tilde{T}_{4K} + 2T_{n1}) + G_2(\tilde{T}_s + \tilde{T}_{4K} + 2T_{n2})\right] + \frac{ak\beta}{2}(1+r)\sqrt{G_1 G_2}(\tilde{T}_s - \tilde{T}_{4K}) \quad \textbf{(1)}$$

where:

G_1, G_2 are the amplifiers power gains;

T_s, T_{4K}, T_{n1}, T_{n2} represent signal, reference load and front end amplifier noise temperatures, respectively;

$\tilde{T}_s = \frac{T_s}{L} + \left(1 - \frac{1}{L}\right) T_{FEM}$ represents the sky signal after the OMT (which is input to the first hybrid);

$L = 10^{\frac{1}{10}(L_{dB}(\text{feed}) + L_{dB}(OMT))}$ is the feed horn + OMT attenuation;

$\tilde{T}_{4K} = \frac{T_{4K}}{L_{4K}} + \left(1 - \frac{1}{L_{4K}}\right) T_{FEM}$ represents the reference signal after the 4K horn entering the first hybrid;

$L_{4K} = 10^{\frac{1}{10}(L_{dB}(4K-horn))}$ is the 4K feed horn attenuation;

T_{FEM} is the front-end physical temperature;

r is the gain modulation factor;

k is the Boltzmann constant, β is the bandwidth and *a* is the proportionality constant of the square-law detectors.

If we assume two identical amplifier ($G_1 = G_2 = G_{FE}$ and $T_{n1} = T_{n2} = T_{nFE}$) in the front end and consider the warm stage of amplification in the back end (with gain G_{BE} and noise temperature T_{nBE}), we can write the differential detectors output power as:

$$p(t) = ak\beta G_{\mathrm{FE}} G_{\mathrm{BE}} \left[\tilde{T}_{\mathrm{sky}} + T_{\mathrm{n_{FE}}} + \frac{T_{\mathrm{n_{BE}}}}{G_{\mathrm{FE}}} - r\left(\tilde{T}_{\mathrm{4K}} + T_{\mathrm{n_{FE}}} + \frac{T_{\mathrm{n_{BE}}}}{G_{\mathrm{FE}}} \right) \right] \qquad (1)$$

To calculate the induced signal fluctuation let us write the physical temperature of the relevant LFI stages as $T_{phys}(t) = T^0_{phys} + \delta T_{phys}(t)$ where $T^0_{phys} \cong \begin{cases} 20K \rightarrow T_{FEM} \\ 4.5K \rightarrow T_{4K} \\ 300K \rightarrow T_{BEM} \end{cases}$ and $\delta T_{phys}(t)$ is the oscillation. The induced signal oscillation, $\delta T_s(t)$, can be determined by solving the equation $\frac{\partial p}{\partial T_s}\delta T_s(t) = \frac{\partial p}{\partial T_{phys}}\delta T_{phys}(t)$ (see [2, 3]) for each of the three stages taken into account, obtaining:

$$\delta T_s = \begin{cases} L\left\{ \left(1-\frac{1}{L}\right) - r\left(1-\frac{1}{L_{4K}}\right) + \left[\tilde{T}_s + T_n - r(T_{4K}+T_n)\right]\frac{\log_e(10)}{10}\frac{\partial G(dB)}{\partial T_{FE}} + (1-r)\frac{\partial T_n}{\partial T_{FE}} \right\}\delta T_{FE} \\ \qquad -r\frac{L}{L_{4K}}\delta T_{4K} \\ L\frac{\log_e(10)}{10}\left(\frac{\partial G_{BE}(dB)}{\partial T_{BE}} + \frac{\partial a(dB)}{\partial T_{BE}}\right)\left\{\left[\tilde{T}_s + T_{n_{FE}} + \frac{T_{n_{BE}}}{G_{FE}} - r\left(\tilde{T}_{4K} + T_{n_{FE}} + \frac{T_{n_{BE}}}{G_{FE}}\right)\right]\right\}\delta T_{BE} \end{cases} \qquad \textbf{(2)}$$

Where, in the back end transfer function evaluation, we have neglected the term in $\left(\frac{\partial T_{n_{BE}}}{\partial T_{BE}}\right)$ because it is largely reduced by a factor G_{FE}.

In summary we expect that fluctuations in the focal plane temperature, by modulating the first stage of low noise amplifiers gain and noise temperature, are impacting the sky and reference signal; the 4K reference load temperature fluctuations are impacting in an almost direct way the corresponding signal and also the sky signal at a minor level, depending on the isolation.
The back end temperature fluctuations, at a first order, modulate the sky and reference signal by impacting the back end amplifiers gain and the square law detector constant, while the effect on the differenced signal is almost nulled at the time scale the gain modulation factor is evaluated.
Due to different bias settings and environmental boundary conditions a direct estimate of transfer functions and thermal susceptibilities is needed from flight data.

2. In flight thermal stability

In Figure 1 an overview of the three stages temperature curve since the early phase of the mission (from Operation Day 125 to 830) is given.

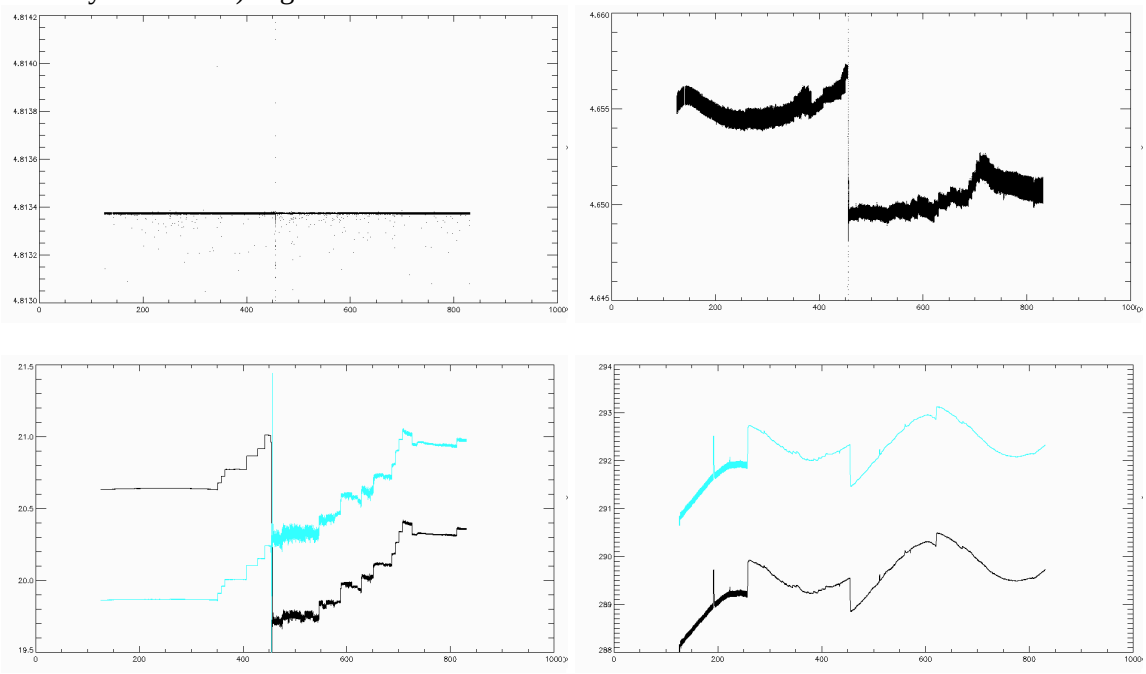

Figure 1 An overall view of the relevant LFI temperature stages curves during the mission (from OD125 to 830). Top plots show the temperature of the HF 4K shield close to the 70 GHz reference loads (left plot, PID controlled very stable temperature) and 30 and 44 GHz reference loads (right plot, about 1 mK p-p fluctuations at the cooler periods together with the seasonal drifts). In the bottom left plot the temperature curves of a left side (TS1R, black curve) and of a right side (TS1L, light blue curve) FPU sensors. In the bottom right plot the temperature curves of a left side (LBEM1, blue curve) and of a right side (RBEM1, light blue curve) back end unit sensors.

It is evident how the overall seasonal/orbital satellte temperature drift is accompanied, for each of the different stages, to lower timescale fluctuations in well defined time ranges of the mission.
As a general approach in the evaluation of the three different thermal susceptibilities (back end, front end and 4K), we selected time intervals where the temperature stage under test was varying while the others were sufficiently stable, in order to be confident in considering negligible other variation sources than the measured one.
So in the very first part of the mission, from OD 125 to 350, FPU and 4K sensors were quite steady apart a slow seasonal variation, while the back end sensors suffered of a daily modulation due to the switching on and off of the transponder for the data link, visible in the plot above, as the thickest curves in the corresponding period. This time range was then considered optimal for the evaluation of the back end induced thermal susceptibility, reported in Section 3. After OD 258, when the transponder was left on for the rest of the mission, the temperature of the warm part mainly suffered of orbital slow fluctuation, except the Switch over between nominal and redundant 20 K cooler that, around OD 450, affected for some hours the thermal setup of the whole satellite. The period between OD 350 and 450 was then considered effective to measure the front end induced thermal susceptibilities taking advantage from some TSA setpoint adjustments

(visible as evident steps in the FPU sensors curves). Results from this analysis also compared with those obtained in the CPV dedicated test (see report [3]) are reported in Section 4 (TBW).
An optimal time range for the evaluation of the impact of 4K load fluctuations is harder to be focussed, so the corresponding analysis will be performed after the BEM and FEM detailed characterization.

3. In flight back end modules thermal susceptibility

3.1 Temperature fluctuations

The back end temperature fluctuations in the first part of the mission were due to the switching on and off of the antenna transponder dedicated to the routine daily telecommunication period (DTCP).

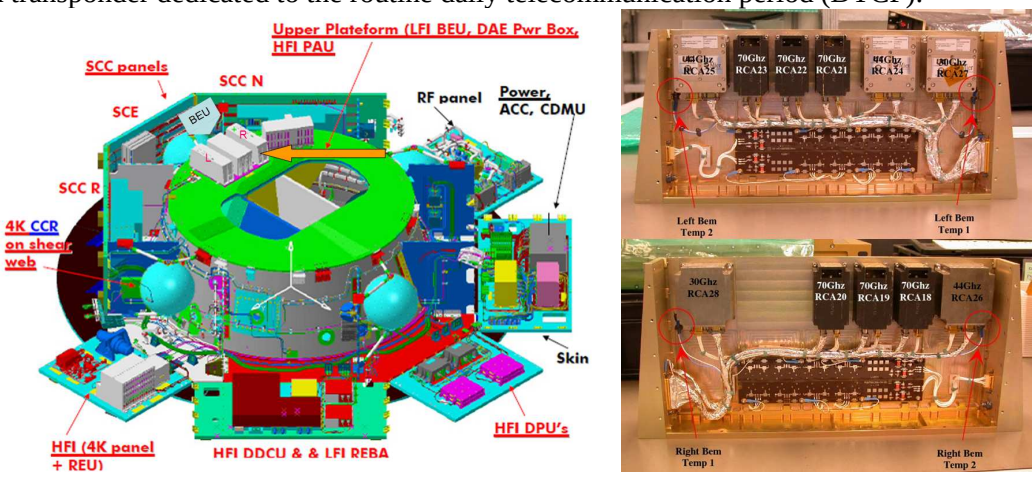

Figure 2 Left: An overall scheme of the Planck SVM. Fluctuations run from the RF Panel to the LFI BEU following the yellow arrow direction. Right: sensor location in the LFI back end boxes.

This operation phase lasting about three hours a day (with a dissipation of about 25 W) caused a typical fluctuation of the whole warm part of the satellite with a period of about 24 hours. This fluctuation of about 200 mK peak to peak impacts the total power of the radiometers. It is measured at the level of the LFI back end unit by means of the Left and Right BEM 1 and 2 sensors, whose locations close to the back end modules (and corresponding amplifiers and diodes) are shown in **Figure 2**. In the same Figure also an overall scheme of the Service Vehicle Module (SVM) and subplatform is shown. It is evident how, in the thermal path starting from the RF and power panels, the Right BEMs are expected to be reached from a perturbation before the Left BEMs sensor. This is actually visible from the corresponding temperature curves (**Figure 3**, top left). Furtherly filtering the data (**Figure 3**, top right) a small delay between sensors of the same box side.
As also discussed in the dedicated sections below, when analyzing the radiometers output, a good correlation is found with the corresponding box side (LEFT or RIGHT) while it is, in general, more difficult to assign one of the two sensors of a single side even though it is physically close to the BEM. This is mainly due to the slow timescale of fluctuations which is not resolved also heavily low passing the signals as shown in the **Figure 3** bottom plots and in the **Figure 4** to **Figure 7**. A deeper and accurate analysis will be useful to optimize a tool dedicated to a fine fluctuation removal. In the figures below an overview of all detecors from the RCAs whose BEMs are close to the described sensors is given.

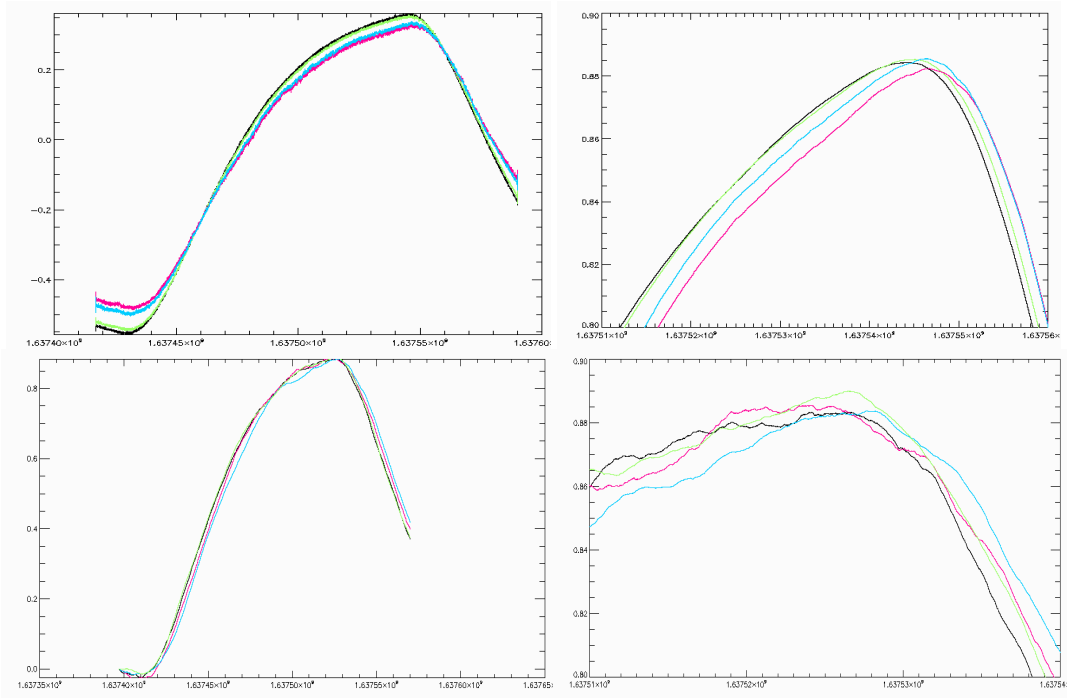

Figure 3 Top Left: An overall plot of the back end temperature rise event between the ODs 191 and 193. Curves are smoothed and mean subtracted: black is R_BEM1, green R_BEM2, light blue is L_BEM1, purple L_BEM2. Top Right: curves are furtherly filtered and normalized in order to have a similar height around the peak. Bottom Left and Right: normalized curves of sky outputs of RCAs color coded the same way of the sensors on top plots by physical proximity: black is RCA28-01, green RCA26-11, purple is RCA27-11 and light blue is RCA25-01

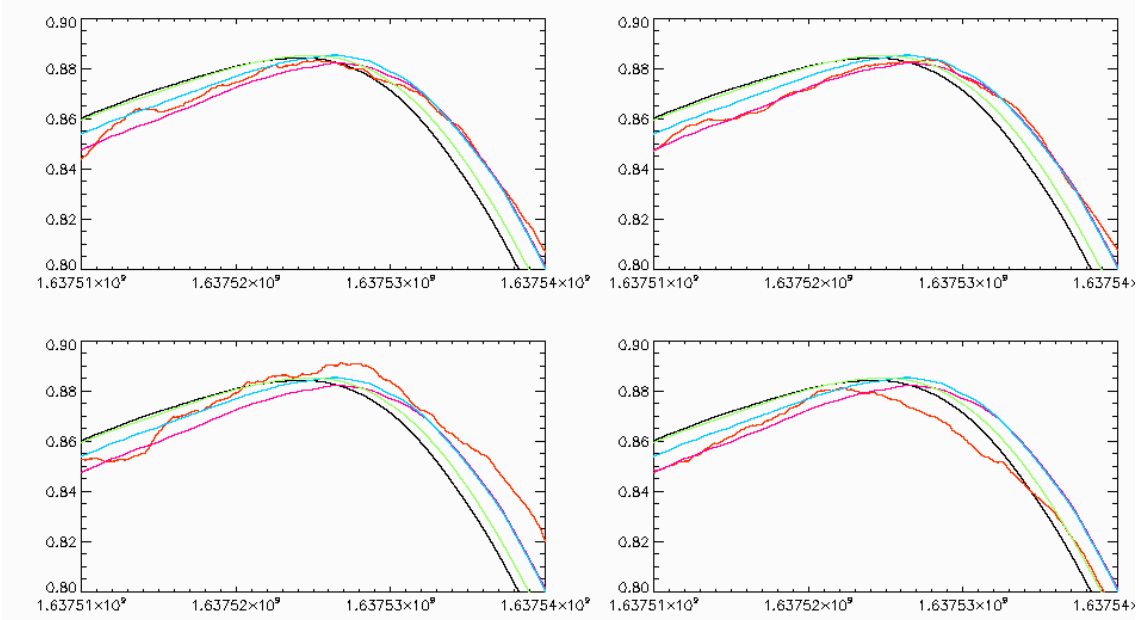

Figure 4 Smoothed sensors (black is R_BEM1, green R_BEM2, purple is L_BEM1, light blue L_BEM2) in the same peaked region than Figure 3 are compared with RCA25 detectors signal output (red). Top left is detector M-00, top right M-01, bottom left is S-10, bottom right S-11.

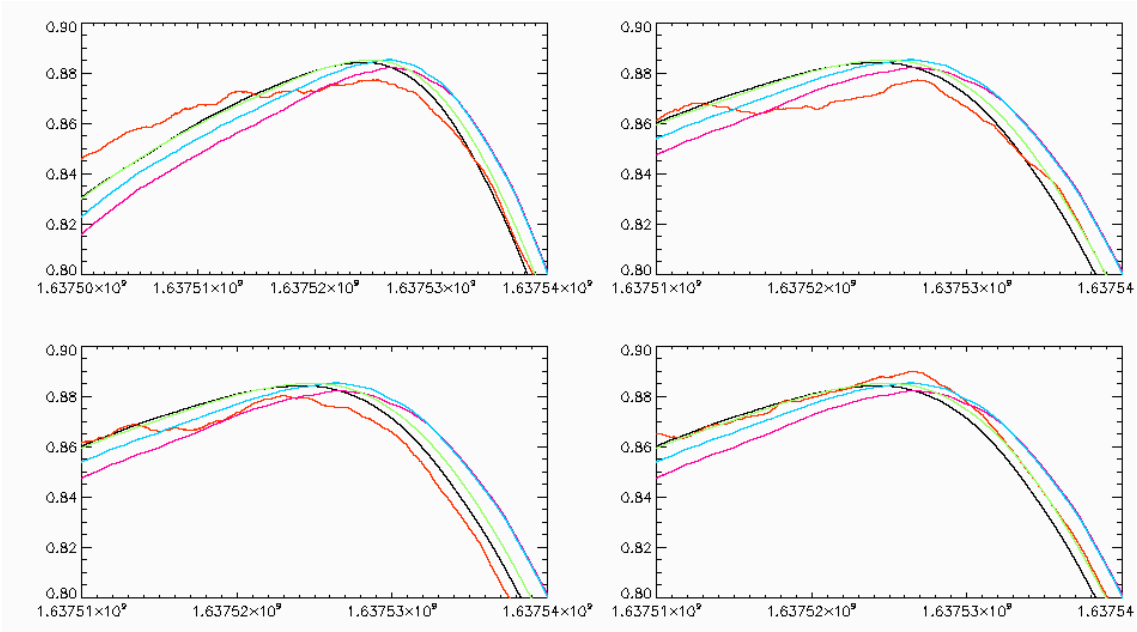

Figure 5 Smoothed sensors (black is R_BEM1, green R_BEM2, purple is L_BEM1, light blue L_BEM2) in the same peaked region than Figure 3 are compared with RCA26 detectors signal output (red). Top left is detector M-00, top right M-01, bottom left is S-10, bottom right S-11.

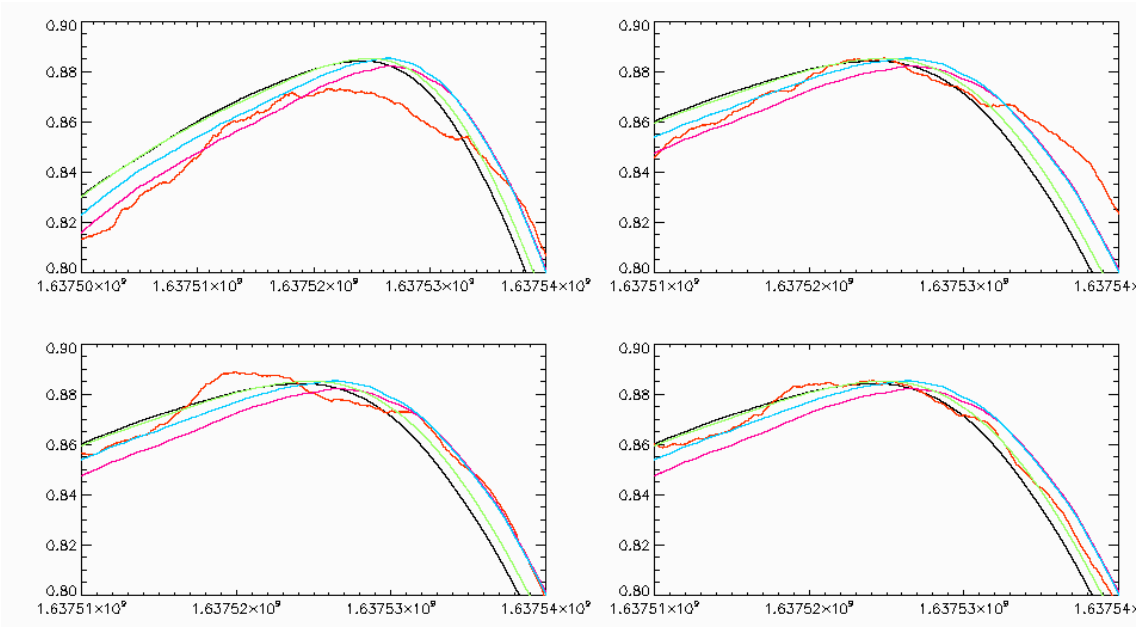

Figure 6 Smoothed sensors (black is R_BEM1, green R_BEM2, purple is L_BEM1, light blue L_BEM2) in the same peaked region than Figure 3 are compared with RCA27 detectors signal output (red). Top left is detector M-00, top right M-01, bottom left is S-10, bottom right S-11.

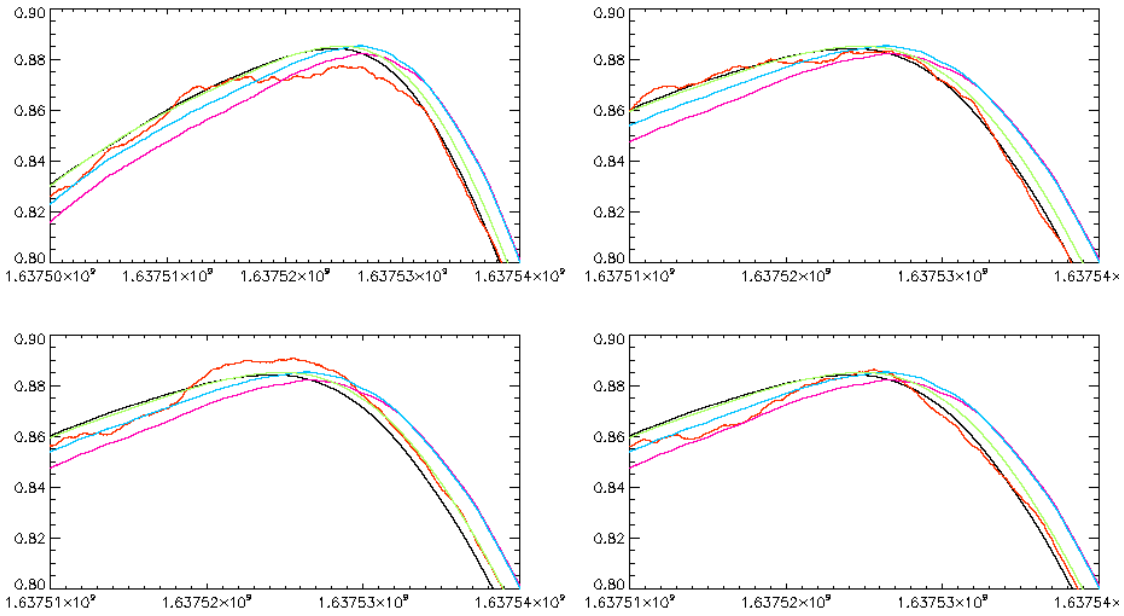

Figure 7 Smoothed sensors (black is R_BEM1, green R_BEM2, purple is L_BEM1, light blue L_BEM2) in the same peaked region than Figure 3 are compared with RCA28 detectors signal output (red). Top left is detector M-00, top right M-01, bottom left is S-10, bottom right S-11.

As also evident in Eq. 2, the choice of a gain modulation factor strongly reduces the effect of the back end fluctuations on the differenced signal as shown in Figure 8, where it is evident that this output does not follow in a well correlated way the temperature drifts.

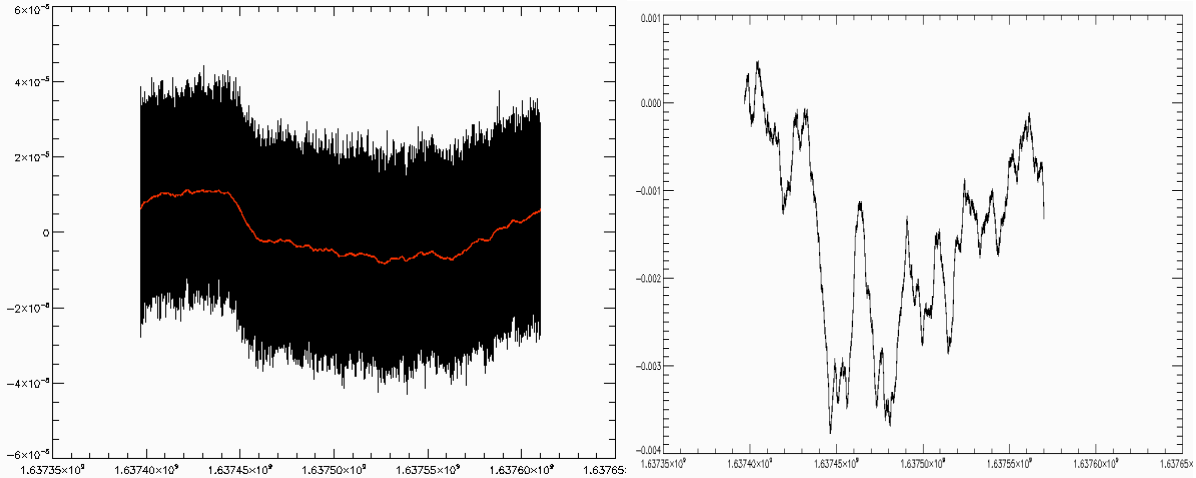

Figure 8 *Left plot: the raw differenced signal of RCA24-01 detector compared with the differenced signal obtained by the filtered total power outputs (red). Right plot: the RCA28-11 differenced output in the same time range of the previous figures; the correlation with the main BEM temperature fluctuation is very low.*

3.2 Strategy and methods for analysis

3.2.1 INTERVALS

We have considered two long duration periods separated by the Transponder status:
OD 150 – OD 250: the transponder was kept OFF and daily switched ON for a time corresponding to the DTCP length.
The radiometers output is characterized by daily periodic fluctuations due to the thermal heating caused by the transponder.

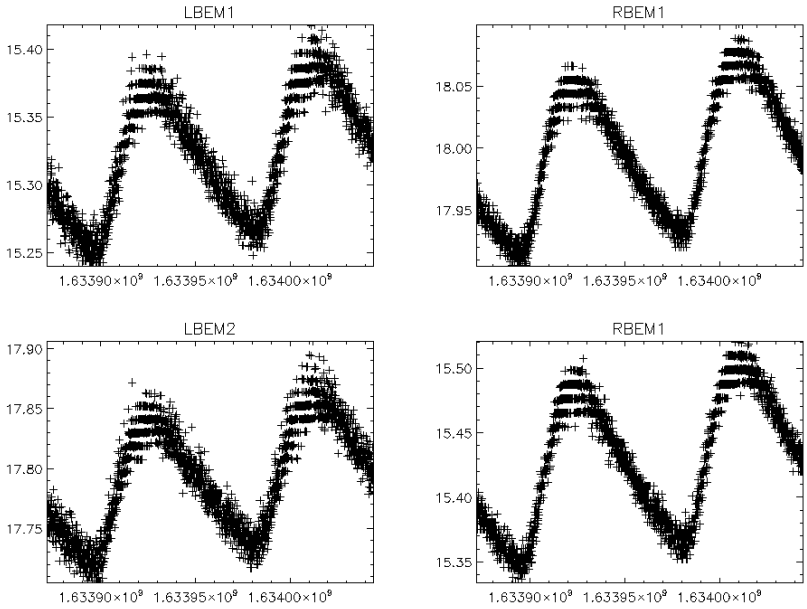

Figure 9 *Daily fluctuation due to Transponder switch ON/OFF during the interval OD 150 -151*

This interval is also characterized by two events , as displayed and highlighted in the pictures below.

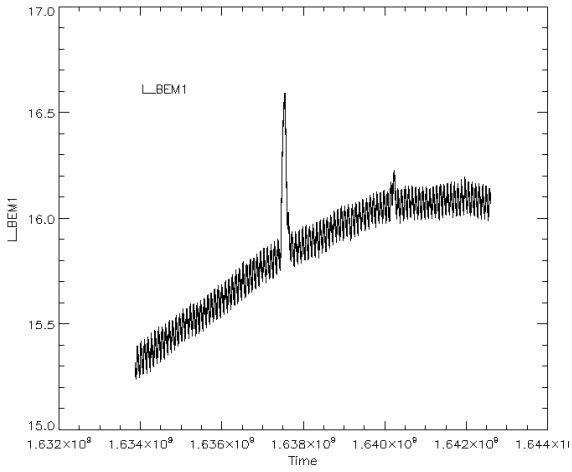

Figure 10 *The two Transponder events during ODs 191-192 and 222-223*

a) The transponder stayed accidentally ON for two ODs
b) The transponder was switched on and off twice in a few hours due to an extra pass

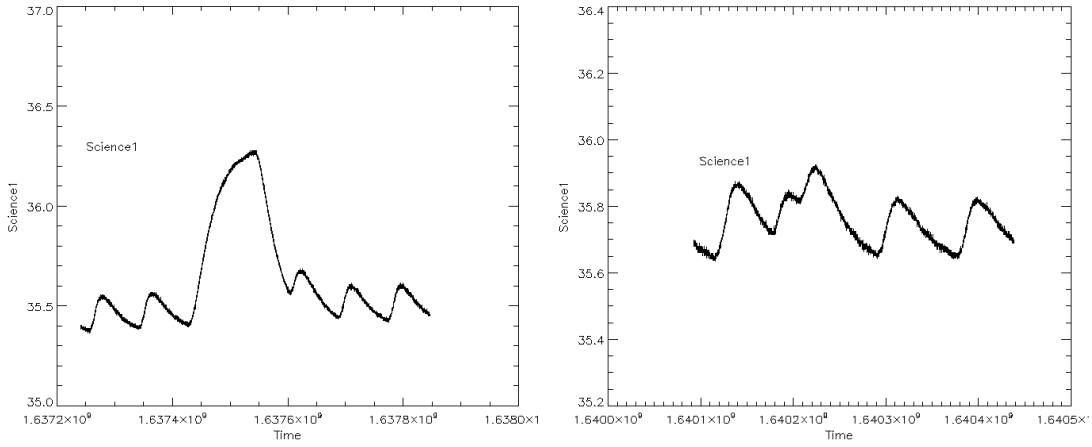

Figure 11 *A zoom view of the two transponder events occurred at ODs 191-192 and 222-223*

Other events are related with FPU temperature changes or with Gain changes in the radiometers: these time intervals have been avoided or discarded when performing analysis. It is however worth noting that the BEU thermal abrupt changes caused a (small) change also in the FPU sensors: this effect is however estimated as being second order, as documented in Section 3.2.2 (***second order effects)*** below.

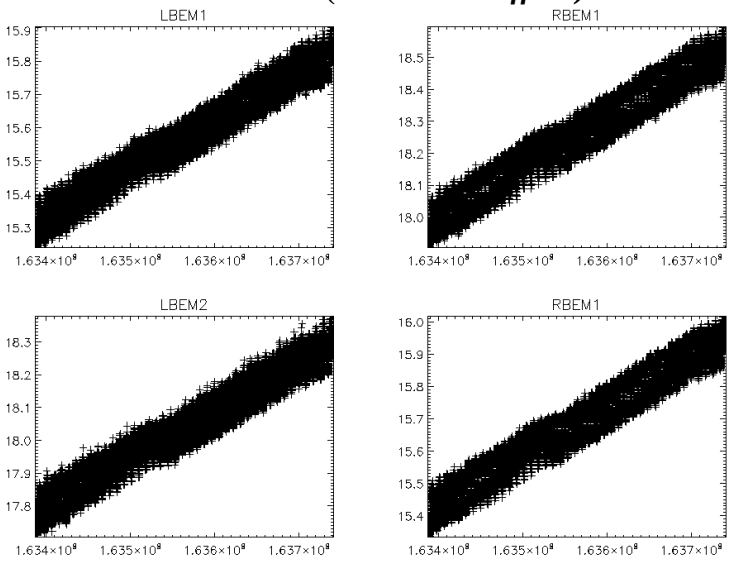

Figure 12 *Long time drift of FPU sensors due to seasonal warming*

OD 255 – OD 350: the transponder was permanently switched ON.
This interval is characterized by an initial large Thermal change in the BEU due to the Transponder permanent switch on; The daily modulation due to the ON/OFF transponder activity is no more evident. The long time thermal drift due to the seasonal warming of the spacecraft is still evident.

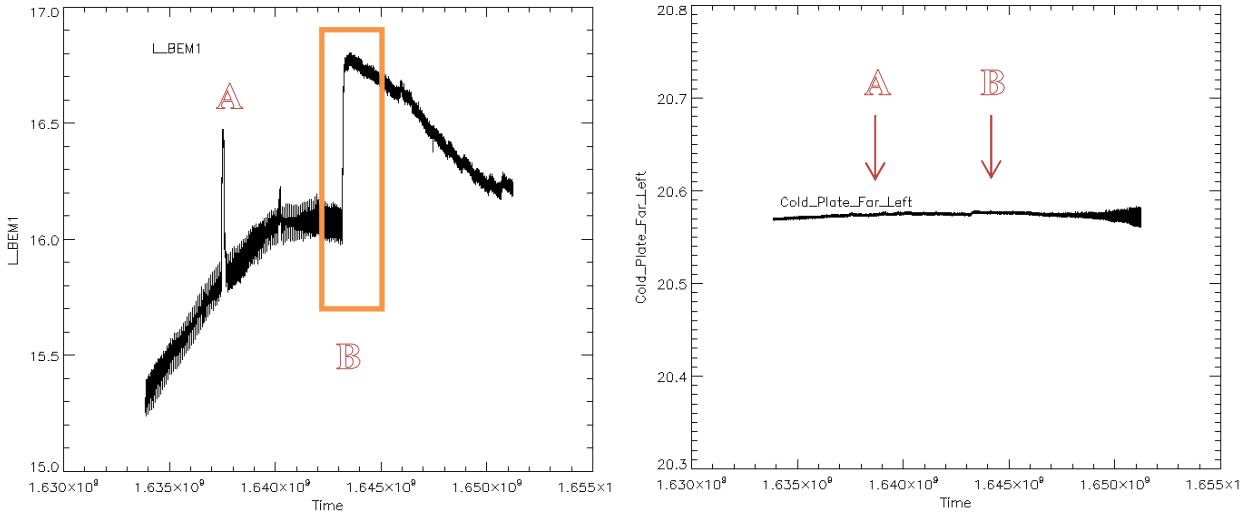

Figure 13 *LBEM1 sensor temperature change (left panel, orange contour) caused by the Transponder permanent switch on occurred during od 258 . The right panel shows the FPU overall stability during the same period (OD150-OD350). To be noted: the p-p increasing fluctuation at the end of the period considered, due to the reduced margin of the SCS TSA active control and the two very small jumps corresponding to the two major Transponder events.*

3.2.2 MODEL

The scientific output form the BEMs is supposed to linearly depend from the BEU temperature. In fact, the effect of changing the BEM temperature is at first order the same of changing the gain in the warm low noise amplifiers. Despite other effects are present, they are expected to be minor.
The video amplifiers offset change with temperature but these changes are expected to be small when compared to gain changes ([9]).

Second order effects

The LNAs Noise, as well as the WGs noise change with temperature. Their relative contribution is, also in this case, small. In fact, each BEM diode accounts for about 0.3-0.7K of the overall noise temperature (REF): assuming that each 1K variation of the BEU temperature causes 1K change in the LNAs noise temperature and 0.2 K in the WGs emission, this contribution is about [5 *1E-4 * 0.5K + 0.2*10E-3K resulting in] 2.5 10^{-4} K. This amounts for less than 1 ppm of the sky and FEU LNAs signals.

Available HK:

To track the BEU thermal behavior we used four representative HK sensors described in Section 3.1:

- Left BEU box LM207332 (LBEM1)
  LM208332 (LBEM2)
- Right BEU box LM307332 (RBEM1)
  LM308332 (RBEM2)

Method:

We divided the two intervals considered in sub intervals, with variable length (detailed in Table 1 and Table 2). The linear correlation between the voltage output and the HK sensors was calculated in each interval.
The sub-division into intervals was aimed at:

- find the interval better describing the thermal dependence
- look for a dependence of the correlation coefficient with the interval duration.
- look for changes in the thermal susceptibility before and after the Transponder activation.

- Find the HK sensor better fitting each voltage output in each interval.

TRANSPONDER ON/OFF			
LARGEST INTERVAL	20 DAYS UNDISTURBED	7 DAYS PERTURBED	20 DAYS PERTURBED
150-190	150-169 170-189		
		189-195	182-201
194-221	194-213		
		219-225	213-232
224-250	231-250 224-243		

Table 1

TRANSPONDER ALWAYS ON			
LARGEST INTERVAL	>16 DAYS UNDISTURBED	7 DAYS PERTURBED	7 DAYS UNPERTURBED
		255-260	
	261-275 296-315		
316-350	316-333 334-350		317-323 324-330 331-337 338-344 345-350

Table 2

Data Analysis

For each of the 44 channels (BEM diodes) we calculated:

- Sensor with the largest correlation in each interval
- Maximum correlation, sensor number, interval
- Recurrence (*R*) of each sensor as the largest correlated HK along the whole set of intervals
- Average correlation of all the *R* best values of each sensor (only the optimal values are hence considered in the average).
- Agreement of the best sensor with the physically expected BEM side (Left, Right) and number (1,2). Sometimes it can happen that although the largest correlated sensor does not correspond to the one physically expected, however the difference of the two correlation coefficients is small. These cases have been flagged and considered.
- For all the above cases, the two linear coefficient are calculated.

	CORR	CH-HK	RANGE	OFFSET	SLOPE	L1	av	L2	av	R1	av	R2	av	SIDE	N
18S	0,32915	LBEM2	213-232	0,9644	0,06513	5	0,08	3	0,25	5	0,27	0	0,00	N	Y
18R	0,32653	LBEM2	213-232	1,01229	0,0673	5	0,08	3	0,24	5	0,25	0	0,00	N	Y
19S	0,9708	RBEM1	189-195	1,06784	0,01701	0	0,00	0	0,00	12	0,74	1	0,97	Y	N
19R	0,97022	RBEM1	189-195	1,10386	0,01739	0	0,00	0	0,00	12	0,73	1	0,97	Y	N
20S	0,9785	RBEM1	189-195	1,28761	0,01832	4	0,79	0	0,00	1	0,98	8	0,70	Y	N
20R	0,97779	RBEM1	189-195	1,349	0,01861	4	0,78	0	0,00	2	0,97	7	0,65	Y	N
21S	0,92	RBEM2	189-195	0,71563	0,00777	1	0,86	5	0,30	2	0,61	5	0,60	N	Y
21R	0,92034	RBEM2	189-195	0,76193	0,00814	1	0,86	5	0,31	2	0,62	5	0,62	N	Y
22S	0,94018	LBEM1	189-195	0,45045	0,00793	6	0,76	2	0,58	1	0,25	4	0,50	Y	N
22R	0,93945	LBEM1	189-195	0,46348	0,00804	6	0,77	2	0,57	1	0,28	4	0,51	Y	N
23S	0,88381	RBEM1	189-195	0,83661	0,0105	9	0,55	0	0,00	1	0,88	3	0,32	N	N
23R	0,88006	RBEM1	189-195	0,85548	0,01048	9	0,57	0	0,00	1	0,88	3	0,32	N	N
24S	-0,99734	LBEM1	189-195	0,10358	-0,00134	2	-1,00	0	0,00	0	0,00	11	-0,95	Y	Y
24R	-0,99723	LBEM1	189-195	0,11297	-0,00143	2	-1,00	0	0,00	1	-0,91	10	-0,95	Y	Y
25S	-0,99801	LBEM1	189-195	0,23122	-0,0027	9	-0,98	1	-0,95	0	0,00	3	-0,91	Y	N
25R	-0,99804	LBEM1	189-195	0,26337	-0,00306	9	-0,98	1	-0,95	0	0,00	3	-0,91	Y	N
26S	-0,99791	RBEM2	189-195	0,16812	-0,00225	0	0,00	0	0,00	11	-0,97	2	-0,97	Y	Y
26R	-0,99809	RBEM2	189-195	0,19936	-0,00267	0	0,00	0	0,00	12	-0,97	1	-1,00	Y	Y
27S	-0,99749	LBEM2	189-195	1,47674	-0,01375	0	0,00	5	-0,88	3	-0,95	5	-0,97	Y	N
27R	-0,99745	LBEM2	189-195	1,69404	-0,01575	0	0,00	5	-0,88	3	-0,95	5	-0,97	Y	N
28S	-0,99874	RBEM2	189-195	1,33046	-0,01332	0	0,00	0	0,00	12	-0,96	1	-1,00	Y	N
28R	-0,9988	RBEM2	189-195	1,3664	-0,01364	0	0,00	0	0,00	12	-0,97	1	-1,00	Y	N

Table 3 *Example of synthetic output of the analysis. From the left column: channel, correlation coefficient, better correlated sensor, range interval where the largest correlation is measured, linear fit coefficients (offset, slope) , recurrence (R) of each sensor as the best correlated and average correlation along the best R values for each of the four sensors, agreement with the physically expected sensor in Side and number (N). Agreement is displayed as Y, disagreement as N.*

All the results were evaluated from the Compact Data Set (CDS), where data are sampled at 1 minute rate, which is enough for studying variations at the daily time scale as those we are considering. The fit was performed considering all the points (but the intervals discarded due to undesired features (such as, for example, gain changes, Front End Unit temperature changes, Sorption Cooler settings, V-grooves thermal adjustments, .. etc) in the whole interval, including the transient.

3.3 Results

Discussion of Results:

Results strongly depend on the channel chosen. As a general rule, 70 GHz channels show a larger variability with the interval considered, often related with poor correlation coefficients. This feature is probably due to the drain current fluctuations in the front end amplifiers, producing common mode fluctuations in each pair of coupled BEM diodes. We will try to model this effect apart in a different work.
In the most cases, the best correlation is tracked by a sensor fixed in the BEM side expected from a physical point of view (from now on, they will be named ‘physical sensors’). The same rule is no longer true for the sensor number, describing the position in the BEM side (see **Figure 2**). Deviations are mostly measured for those channels exhibiting a poor correlation coefficient due to Id current instabilities (for example LFI 18 M and LFI 21, see Figure 14) or to diodes popcorn noise (as LFI 24-10). However, in all the cases, the physical sensors show correlations very close to best values. The correlation coefficient, for each detector and for each interval, is displayed in the histograms from Plot 1 to Plot 6, in Appendix 6.2.

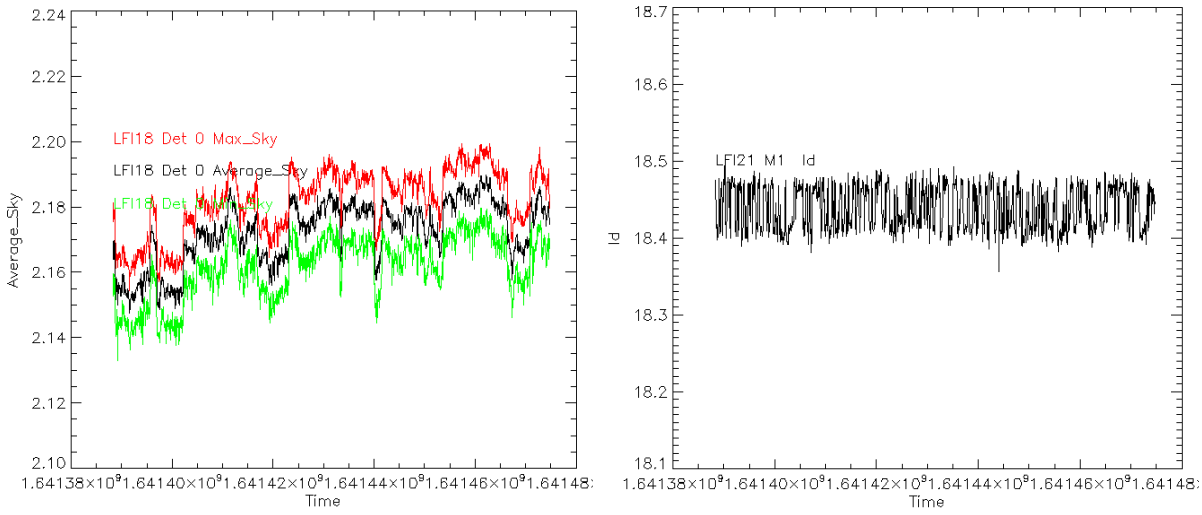

Figure 14 *RCA18-00 sky signal (left plot) typically suffers of Id instabilities; similarly RCA21 main arm detectors are affected by M1 LNA Id fluctuations (pop corn noise on right plot)*

From a qualitative point of view we can conclude that:

70 GHz channels showing large electric instabilities in the front end currents are better described by:

a- The longer intervals : namely intervals 150-250 and 182-201 (the last containing the transponder event labeled as A) in the 'transponder on/off' period

b- Interval 255-260 , labeled as B, in the 'transponder always on' period

Those channels showing a large popcorn noise are better represented when the time interval is longer, due to the increased statistics smoothing the voltage random fluctuations

It is worth noting that the cases described at point a-, in which the correlation increases with the integration time, refer all to intervals before the 'always on' condition: in fact, the permanent transponder switch on cancelled the daily thermal fluctuations in the BEU, while other long time signal drifts due to other thermal effects (FPU and 4K Reference Load drifts) become dominant and their effect is indistinguishable from the BEU driven fluctuations.

Then, in general, we have chosen, in all the cases of good correlation, the linear coefficients calculated from interval 189-195, where the thermal jump is abrupt and short in time, rather than those calculated from interval 255-260, showing a slightly better correlation coefficient: this was done because of the longer duration of the thermal fluctuation in interval 255-260, making the fit possibly influenced by other slow drifts.

44 GHz channels are generally well described in most of the intervals considered. However a particular behaviour is shown by the RCA24-10 detector; in fact the best fit evaluation is strongly dependent on the time interval considered: it had a trend inversion occurred during the two weeks before the long transponder on 'A' event (Figure 13), after that it got back to standard drift. This anomalous behaviour well traced in the Figure 24 in Appendix 6.1 and in the R1D0 plot of Table 21. A further analysis posssibly considering the use of two separate susceptibility models is under discussion.

30 GHz channels are those showing the best correlation coefficients. As expected, both 30 GHz and 44 GHz channels have negative correlations.

The final product delivered is a matrix of 44 linear fit and correlation coefficients, describing the 44 BEM channels. Each diode is usually associated with the BEM sensor, and with the interval, corresponding to the largest correlation coefficient. However, to preserve the physics of the model (reducing errors due to possible phase delay of the more distant sensors), we preferred to provide the final table (Table 7) with the

coefficients referring to the physical sensors rather than to the ones with the highest correlation: this was allowed because of the negligible differences between the correlation coefficients.
In Table 5 and Table 6 results from the 'Transponder ON/OFF' and 'Transponder always ON', shown together with the best choice (final results corresponding to Table 7), are also compared: the comparison is given in terms of the time interval giving the best results, the sensor better correlated, the correlation coefficient.
The final table delivered, showing the chosen coefficients together with the errors associated, is displayed in Table 8

Preliminary estimate of residual after BEU model removal from raw data

To check the goodness of the coefficients found, we attempted a preliminary removal of the BEU effect from raw data. A linear model was drawn for each of the 44 BEU outputs (one for sky and one for ref), combining the susceptibility coefficients found from linear fits to the HK data (the BEU sensor corresponding to those coefficients).

The BEU model was drawn as:

$$V_{out} = b_{hk}(T_{hk}) + a_{hk}$$

Where the subscript *hk* indicates that the linear fit coefficients and the temperature refers to the same HK sensor.
The model was hence removed from total power raw data in time domain, in order to correct data for the BEU thermal changes. It is worth noting that after removal the coincidence of the first point of the two data streams (raw data and model corrected data) is imposed removing the voltage offset $\Delta V = V_{model}(0) - V_{raw}(0)$.
For each channel the model was compared to the raw data, checking the superposition of the two curves in the whole time range considered (OD 91-350). Despite of in the most cases the superposition is good, in others an offset is observed in the second part of the survey (after the Transponder always on): the raw signals show a considerable decrease much faster than the model prediction.

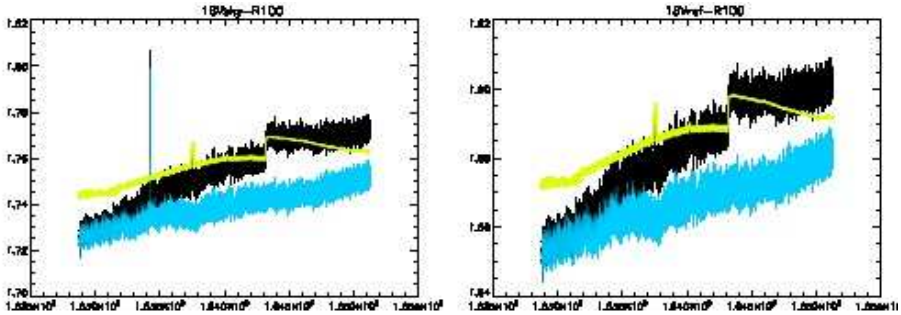

Figure 15 *LFI1810 Sky(left), Ref (right). Raw data(black),model(yellow),corrected (magenta)*

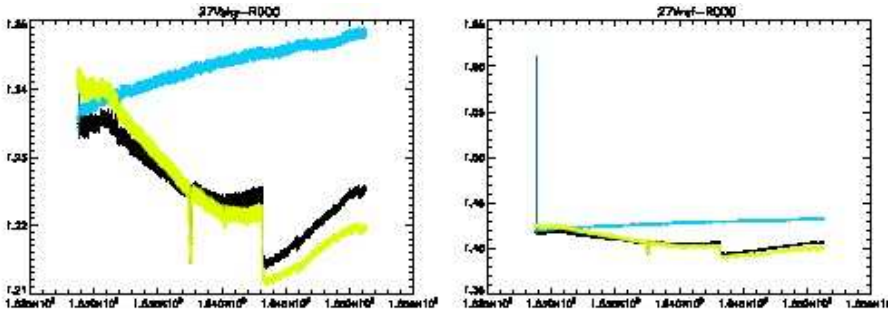

Figure 16 *LFI2700 Sky(left), Ref (right). Raw data(black),model(yellow),corrected (magenta)*

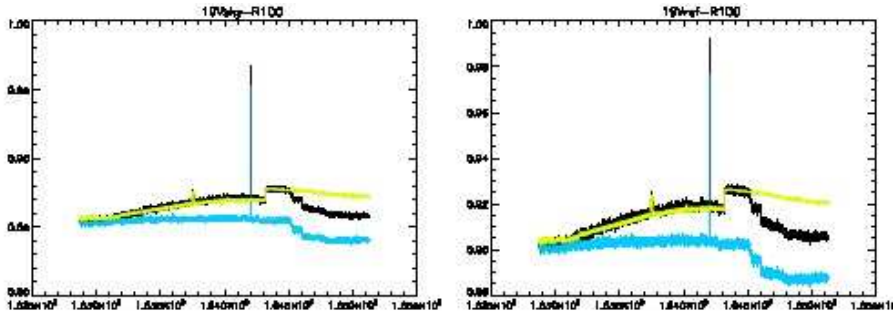

Figure 17 *LFI 1910 Sky(left), Ref (right). Raw data(black),model(yellow),corrected (magenta)*

In particular, the following cases are worth noting: LFI-1910-11 and LFI 1810-11, LFI27 (see Figure 16 and Figure 15). The discrepancy is independent from the model used (old or new coefficients) but seems to be related with some other features (for example susceptibility to Front End fluctuations). Among these channels, Channel LFI-19S is however to be considered as a case apart, showing the strange stepped behavior represented in Figure 17.
Differenced data were calculated from total power corrected data, computing GMF over two different time ranges.

- Single GMF covering the whole interval ($GMF1 = < [Vsky]_{interval} > / < [Vref]_{interval} >$)
- Multiple GMF covering a baseline of 1 day each ($GMF2 = < [Vsky]_{1\text{-}DAY} > / < [Vref]_{1\text{-}DAY} >$). GMF is calculated in the same way as implemented for the CDS differenced data.

Method check in the time domain

Comparison with the 'previous model', obtained using the old coefficients, shows that the new coefficients are able to better represent the raw data, especially in following the discontinuity between the Transponder ON/OFF and Transponder always ON regions. A representative case is shown in Figure 18 while complete results are proposed in 6.4**.**

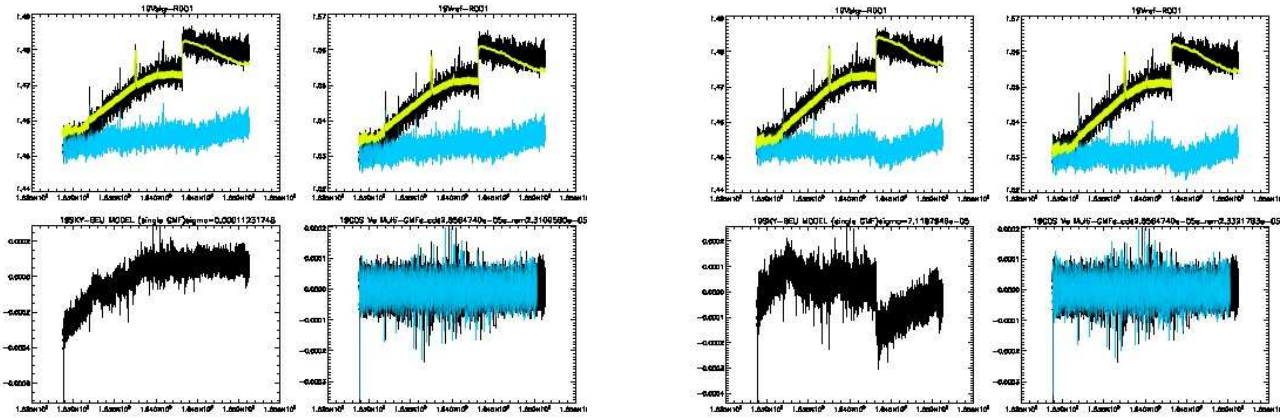

Figure 18 *LFI-1901:BEU drift removal from total power data. Left panel: removal using the new coefficients; Right panel: removal using the old coefficients. Each panel contains: Sky data (top left) Ref data (top right), differenced data using a single GMF (bottom left) and differenced data using multiple GMF (bottom right). Colours represent: raw data from CDS (black) , model (yellow) , corrected data (magenta).*

A first level quantitative comparison between differenced data corrected basing on the two models (new and old coefficients) and on the CDS uncorrected data is possible when comparing RMS . Despite RMS is more sensitive to high frequency changes than to long time drifts , however it is able to track also the largest peak

to peak variations and hence the power of the removal. Corrected differenced data (based on multiple GMF) show in the most cases the best RMS, followed by CDS uncorrected data (based on multiple GMF) and then by corrected data based on single GMF. Corrected differenced data, based on multiple GMF and on the new model show in the most cases improved RMS (also by 20-30%) w.r.t. the corresponding raw CDS data; except few cases, the difference between results obtained using new or old coefficients is marginal (reasonably due to the GMF calculation on 1-day baseline). The full results and comparisons are summarized in 6.3 .

However, it is important to perform again the same analysis on data sampled at the nominal frequency, since the binning performed by the CDS mitigates the differences between the two models.

Method check in the frequency domain

In order to evaluate the accuracy of the modeled susceptibility, a study in the frequency domain was performed in three main steps:

1) we considered the whole set of temperature data for the sensors associated to each detector, from the CDS (ODs from 150 to 350) and low pass filtered them (Figure 19, left);
2) then we modelled the BEU fluctuations induced signal by applying our linear fit parameters to the filtered housekeeping curve (Figure 19, right);

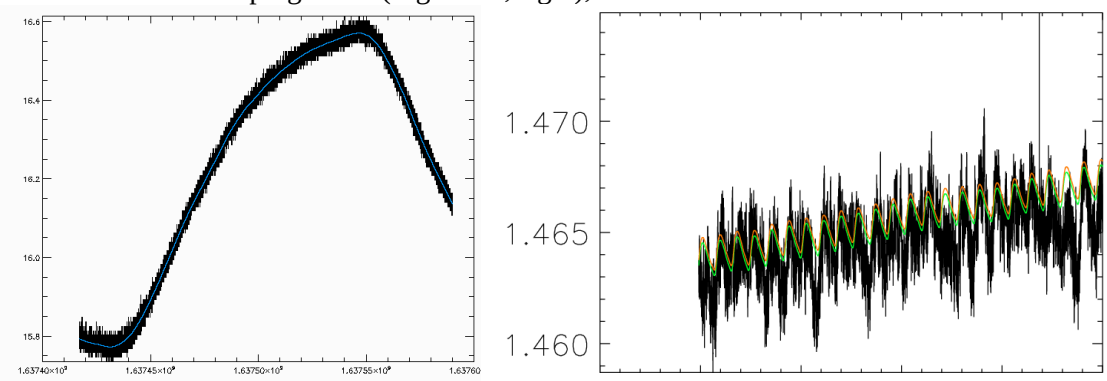

Figure 19 *Left:L-BEM1 sensor raw temperature curve during the change around OD 192 with overplotted (blue line) the filtered curve used in the models. Right: Raw sky output from RCA1901 detector and overplotted the modelled signal with average (green) and starting point normalization (orange)*

3) finally we subtracted the resulting model from the real data and compared the resulting spectrum with the starting raw data spectrum (Figure 20).

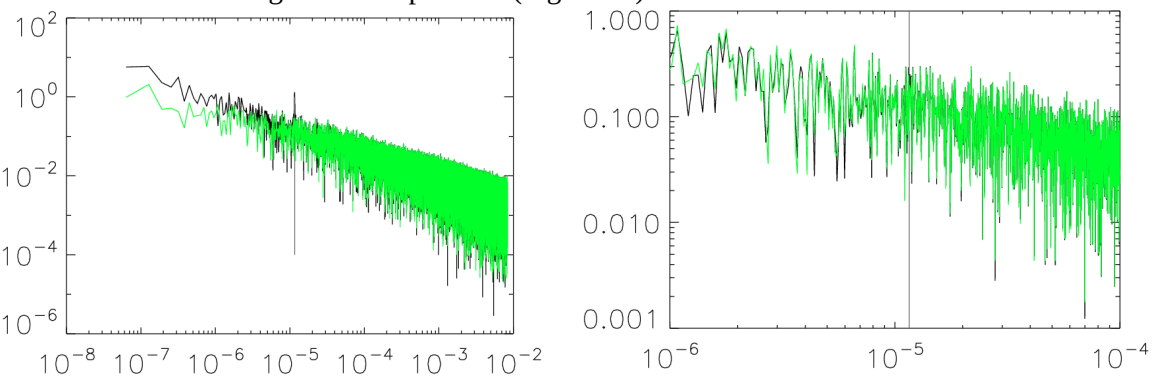

Figure 20 *Left: amplitude spectral density of the raw RCA1901 sky signal (black) and of the signal with the new model removed (green), the vertical grey line marks the daily frequency. Right: a zoom view around the daily frequency (marked by the grey vertical line as well) of the amplitude spectral density of the signal with the new model removed (black line) and with the old simulations model removed (green line). It is evident from the rigth plot how the peak is strongly reduced by subtracting the new model, while if zooming on the residuals the old model has a cleaner effect.*

We applied the same procedure with our fit parameters and with the parameters evaluated during the early phase of mission and used in the systematic maps released up to DX7. A synoptic view of the results is given in the Table 4, where the amplitude of the total power output spectra, at the main oscillation frequency of 1.16 10^{-2} mHz (one day), is given for the different cases and detectors. It is evident how the latest model described in this document has in the most cases the best residual values.

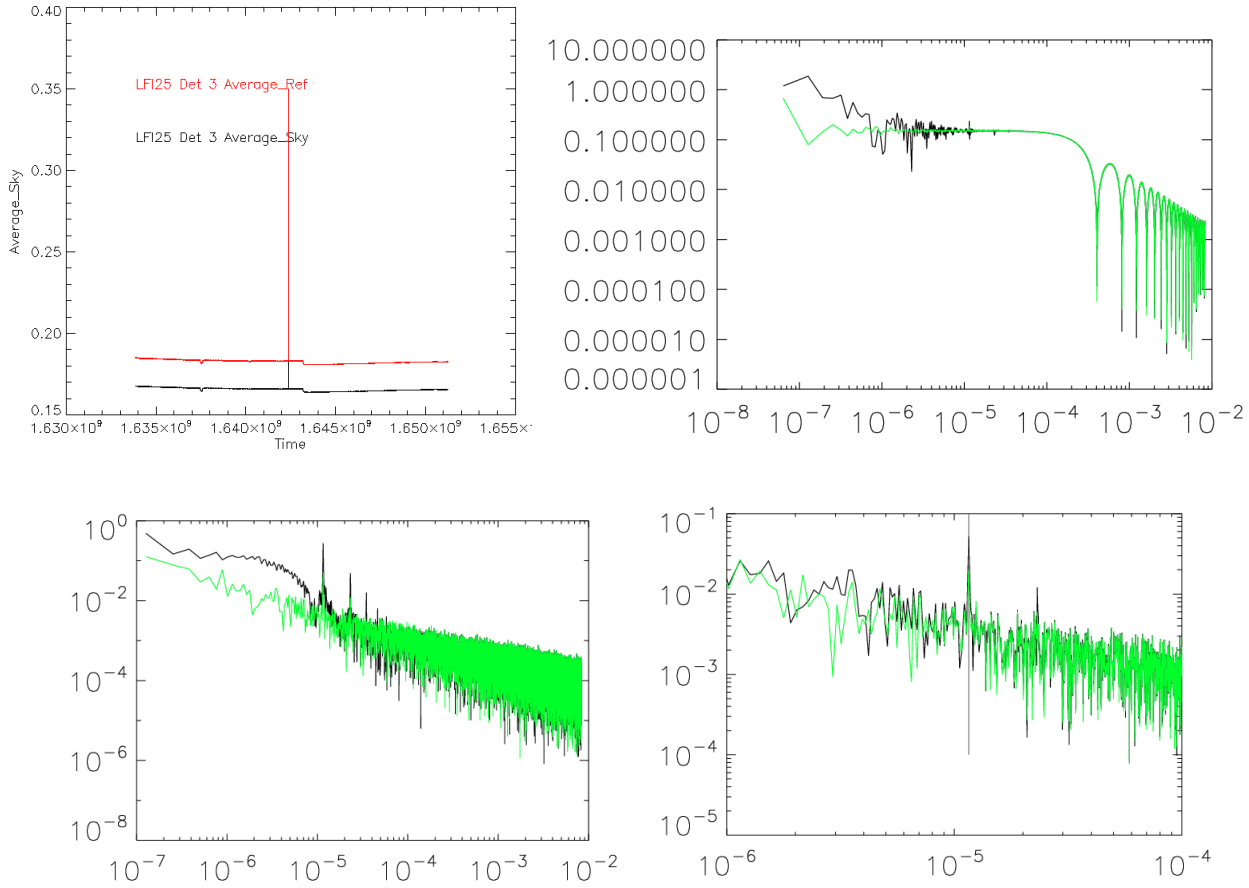

Figure 21 *A large discontinuity in the RCA25-11 total power signals (top left), caused by a gain change, affects the spectrum evaluation (top right) and the peak values reported in the Table 4. Taking into account a clean data range the effectiveness of the model is visible in the frequency space (bottom left compared with raw data spectrum, bottom right with previous model)*

Some relevant exceptions occur in RCA23-11 and 25-11 detectors (Figure 21) that have a strong DAE gain change anomalous event in the period taken into account which affects the spectral information. We then took a subset of data free from anomalies and evaluated the same parameters reported in the second line of double line cells in the Table 4.

Det. Id	Sky peak	Ref peak	Old sky peak	Old ref peak	Raw sky peak	Raw ref peak
RCA1800	1.1916	1.2394	**0.4991**	**0.5109**	2.4496	2.4905
RCA1801	1.2872	1.3489	**0.5061**	**0.5071**	3.1958	3.2763
RCA1810	**0.27998**	**0.30247**	0.9167	0.9232	1.2513	1.3222
RCA1811	**0.20748**	**0.21884**	0.7553	0.7635	1.3846	1.4241
RCA1900	**0.13084**	**0.094818**	0.1778	0.1465	1.7852	1.8138
RCA1901	0.11447	0.12188	**0.07413**	**0.05416**	1.3094	1.3539
RCA1910	**0.12199**	**0.11011**	0.3740	0.3476	0.94663	1.0079
RCA1911	**0.12044**	**0.12934**	0.2678	0.2748	0.94216	0.96283
RCA2000	**0.16063**	**0.16667**	0.3805	0.2940	1.9601	1.9945
RCA2001	**0.11807**	**0.12518**	0.1813	0.2028	1.2795	1.2946
RCA2010	**0.17067**	**0.15755**	0.5623	0.5657	1.1026	1.0925
RCA2011	**0.38707**	**0.40379**	0.4980	0.5380	1.1900	1.2147
RCA2100	**0.044369**	0.039367	0.06495	**0.03520**	0.88235	0.93307
RCA2101	0.11285	0.092320	**0.08377**	**0.06805**	1.0450	1.0565
RCA2110	**0.33646**	**0.34900**	0.6999	0.7175	1.1849	1.2158
RCA2111	**0.36901**	**0.37584**	0.7552	0.7617	1.1516	1.1709
RCA2200	**0.072010**	**0.069086**	0.1226	0.1182	0.83279	0.84282
RCA2201	**0.076613**	**0.082041**	0.1923	0.1848	0.86583	0.87960
RCA2210	**0.13354**	**0.13715**	0.3945	0.3861	0.83002	0.83633
RCA2211	**0.20427**	**0.20302**	0.4081	0.3997	0.86823	0.86229
RCA2300	**0.11645**	**0.12014**	0.5169	0.5252	0.94593	0.94829
RCA2301	**0.42061**	**0.23521**	0.9826	0.8120	0.54160	0.74965
RCA2310	**0.045407**	**0.050738**	0.7710	0.7759	0.94159	0.96308
RCA2311 (OD150-245)	0.66430 *(0.60569)*	0.68859 *(0.62372)*	0.4645 ***(0.35887)***	0.5073 ***(0.39933)***	0.32017 *(0.61126)*	0.31972 *(0.62087)*
RCA2400	**0.009936**	**0.011039**	0.01427	0.01624	0.11065	0.11768
RCA2401	**0.003620**	**0.004238**	0.008772	0.01382	0.11595	0.12072
RCA2410	**0.016935**	**0.019259**	0.09464	0.1022	0.19611	0.21622
RCA2411	0.009824	0.009259	**0.003779**	**0.004170**	0.21407	0.22922
RCA2500	0.012123	0.014631	**0.01095**	**0.01242**	0.23911	0.27036
RCA2501	0.018012	**0.012560**	**0.01230**	0.01278	0.24492	0.26046
RCA2510	**0.10950**	**0.12476**	0.1126	0.1305	0.26576	0.29747
RCA2511 (OD91-245)	0.18986 *(0.02582)*	0.20627 *(0.02165)*	0.1642 ***(0.00753)***	0.1882 ***(0.01012)***	0.10136 *(0.1789)*	0.10724 *(0.19988)*
RCA2600	**0.020691**	**0.025823**	0.03751	0.04367	0.21393	0.25235
RCA2601	0.014542	0.016736	**0.007268**	**0.003264**	0.30561	0.33895
RCA2610	0.064977	0.046039	**0.05470**	**0.03483**	0.31616	0.33563
RCA2611	**0.003445**	**0.000829**	0.01225	0.006483	0.26588	0.29443
RCA2700	**0.016156**	**0.031807**	0.3569	0.3728	1.2281	1.3919
RCA2701	**0.040506**	**0.045062**	0.3877	0.4093	1.3753	1.5776
RCA2710	**0.046993**	**0.050077**	0.3564	0.3996	1.2486	1.4212
RCA2711	**0.058893**	**0.049603**	0.3034	0.3463	0.98162	1.1306
RCA2800	**0.052480**	**0.051807**	0.2368	0.2211	1.3251	1.3613
RCA2801	**0.10752**	**0.12102**	0.4160	0.4333	1.5645	1.6288
RCA2810	**0.059898**	**0.060849**	0.1695	0.1149	1.1923	1.2857
RCA2811	**0.056282**	**0.066485**	1.011	0.5083	0.96845	1.0580

Table 4 *Amplitude of the peak at the 1-day frequency for the total power output of all the LFI detectors. Data with the model, described in this document, removed are in the column 2-3, removed model with values from the early analysis are column 4-5 while the original peak values in raw data are reported in column 6-7. Bold values evidence are the minimum values for each line. For the double line detectors, see text.*

Spectrograms

Results from BEU effect removal were also checked by comparing spectrograms (from differenced data) calculated before and after removal. We calculated spectra for each detector, keeping 1-day as baseline. Spectrograms show the evolution of 1-day spectra along the whole period considered. It comes out that the largest differences between corrected and uncorrected data are condensed in the low frequency part of the spectrum and in the time range before the Transponder always ON time. As for comparisons in the time domain, clearer results are expected from the next step, using as source data the data sampled at nominal frequency instead of the binned data from CDS.
An example is shown in the following panels (Figure 22); full results are displayed in 6.5.

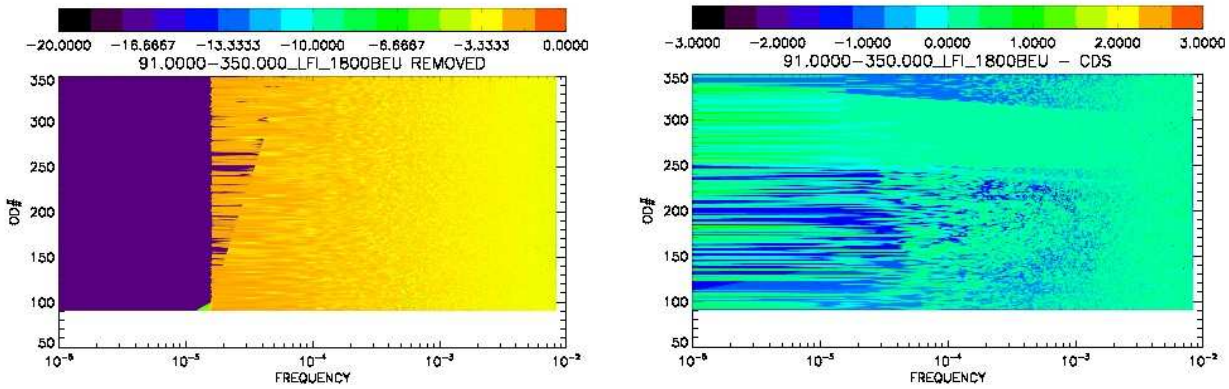

Figure 22 *LFI1800 Spectrograms : the log colour scale shows the frequency behaviour against OD in the whole interval OD 91- OD 350. Spectrogram from data corrected for the new model on the left panel; Spectrogram difference between the left panel and the same obtained from CDS uncorrected data (right panel)*

Differenced Data Spectra
We calculated also frequency spectra along the whole interval OD91- OD350, in the following cases (see the example given in Figure 23) :

- data diff with the BEU effect removed calculated basing on single GMF (GMF1)
- data diff uncorrected for the BEU effect, calculated basing on single GMF (GMF1)
- data diff with the BEU effect removed calculated basing on multiple GMF (GMF2)
- data diff from CDS uncorrected for the BEU effect, calculated basing on multiple GMF (GMF2)

All results are presented in Appendix, section 6.6 . The plots show the frequency part of the spectrum comprised between 10^{-7} and 10^{-4}. This is to focus on the main effect of the BEU effect removal, expected in the low frequency region. In the most cases the benefit from removal, as from the new set of susceptibility coefficients, are evident. The same analysis is planned to be performed on nominally sampled data instead on the 1 minute binned data.

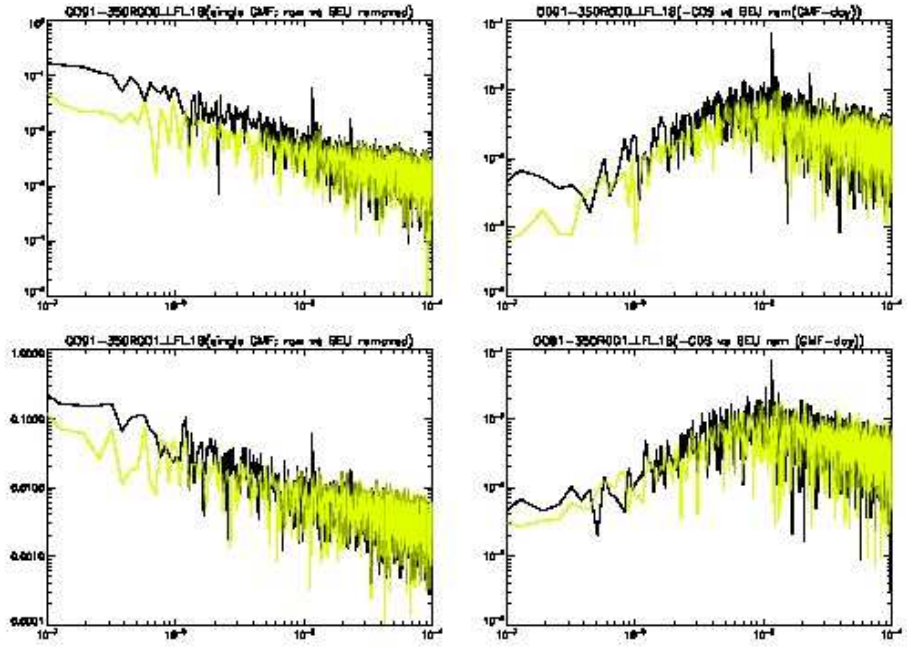

Figure 23 Amplitude spectral density for LFI-1800 (top panels) and LFI-1801(bottom panels) in the interval OD91-OD350. The two left plots refer to differenced data calculated using single GMF (black line are uncorrected data, yellow are corrected data), the two right panels represent differenced data calculated using multiple GMF (as before, black line are uncorrected data, yellow are corrected data).

4. In flight front end modules thermal susceptibility

TBW

4.1 Strategy and methods for analysis

TBW

4.2 Results

TBW

5. Conclusions

Thermal effects are part of the most relevant sources of instrumental systematic effects for the Planck LFI radiometers. Due to in-flight bias optimization and different environmental conditions, an evaluation of the susceptibility of LFI signals to temperature fluctuations at the level of the main instrument thermal interfaces is performed using adequate flight data ranges.
The first temperature stage taken into account is the warm back end unit, which, at the beginning of the flight routine phase, suffered of a daily large temperature fluctuation.
A preliminary estimation of the BEU thermal susceptibility was obtained using a large interval of data from the early phase of the mission and the parameters derived from that early study [10] was used to produce maps of predicted systematic effects released from DPC.
In this document we have described a further extensive analysis, performed over several periods of the operational days from 91 to 350, deriving our best estimation (with corresponding uncertainties) of the model which describes the dependence of the total power outputs to the back end temperature.
Methods and results of our analysis are reported and also compared to the previous results, proposing different estimators to quantify the model accuracy.
In general, the results indicate a better quality of the latest parameters produced.
We then suggest to update the back end susceptibility parameters database for systematic effects simulation code with the values contained in Table 8. An Issue still open for further analysis is related with LFI-2410, showing a temporary period of anamalous (not yet understood) behaviour, as described in 3.3.

Next step (currently in progress) will be:

- to perform a more accurate attempt of removal of such effect working with full sampled data, instead of binned CDS data:
- starting from data cleaned from the BEU effect, to perform the same analysis to estimate the radiometers susceptibility to Front End Unit thermal instabilities.

Finally results will be used to investigate and remove 4K temperature fluctuation effects.

6. APPENDIX

6.1 BEST FIT PLOTS

Plots contained in this section refer to the HK sensor (displayed in the title of each plot) and time range interval chosen to produce the delivered Table 8. Different plots are produced for each detector and for sky and ref.

LFI 18

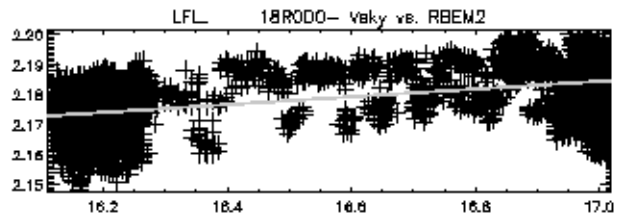

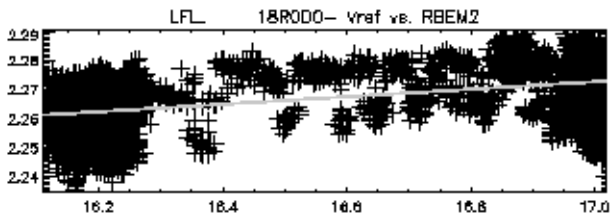

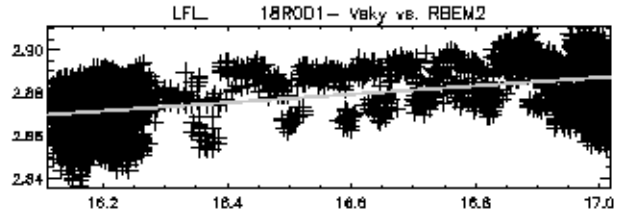

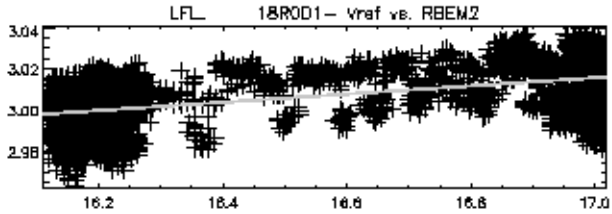

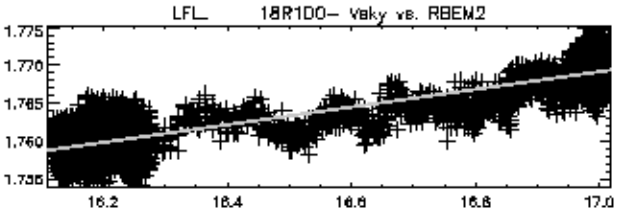

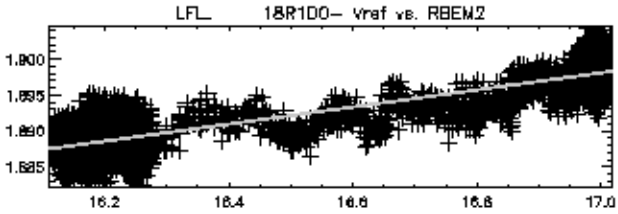

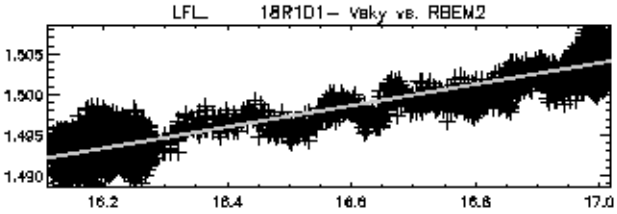

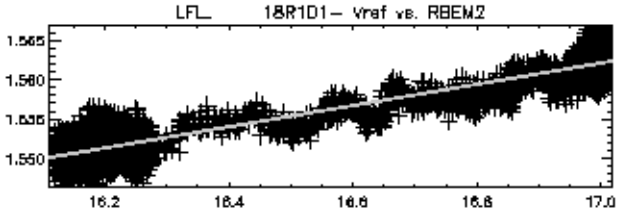

LFI 19

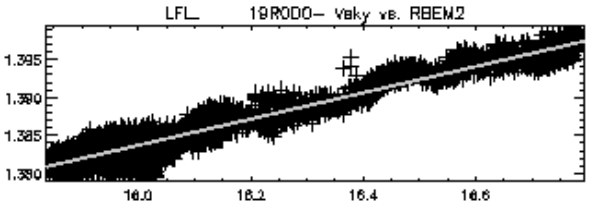
LFI_ 19R0D0– Vsky vs. RBEM2
1.395
1.390
1.385
1.380
16.0
16.2
16.4
16.6

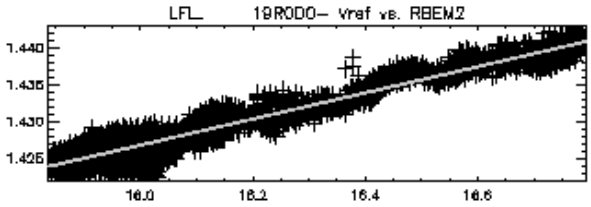
LFI_ 19R0D0– Vref vs. RBEM2
1.440
1.435
1.430
1.425
16.0
16.2
16.4
16.6

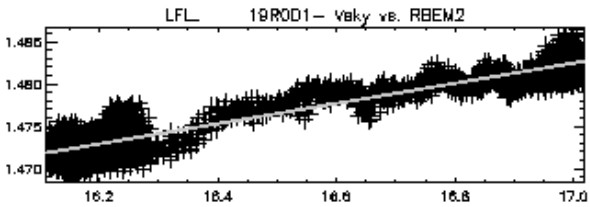
LFI_ 19R0D1– Vsky vs. RBEM2
1.485
1.480
1.475
1.470
16.2
16.4
16.6
16.8
17.0

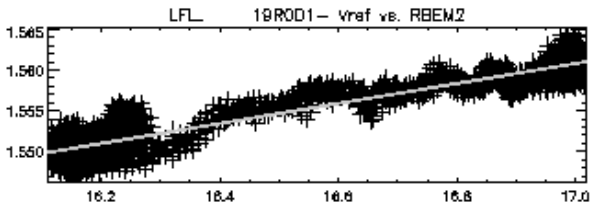
LFI_ 19R0D1– Vref vs. RBEM2
1.565
1.560
1.555
1.550
16.2
16.4
16.6
16.8
17.0

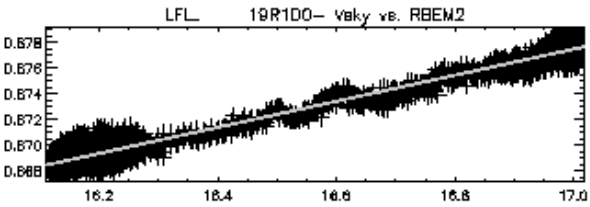
LFI_ 19R1D0– Vsky vs. RBEM2
0.878
0.876
0.874
0.872
0.870
0.868
16.2
16.4
16.6
16.8
17.0

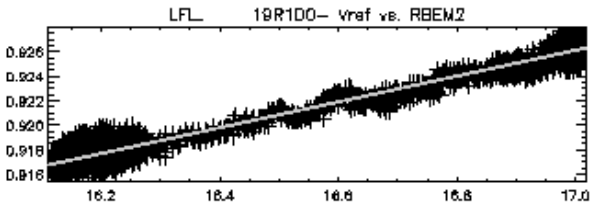
LFI_ 19R1D0– Vref vs. RBEM2
0.926
0.924
0.922
0.920
0.918
0.916
16.2
16.4
16.6
16.8
17.0

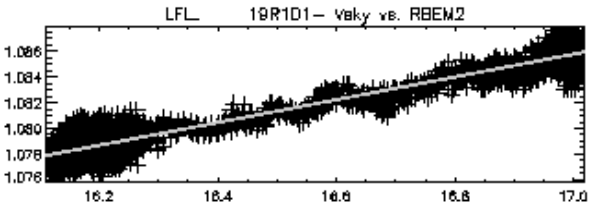
LFI_ 19R1D1– Vsky vs. RBEM2
1.086
1.084
1.082
1.080
1.078
1.076
16.2
16.4
16.6
16.8
17.0

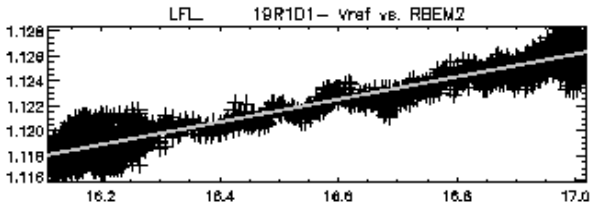
LFI_ 19R1D1– Vref vs. RBEM2
1.128
1.126
1.124
1.122
1.120
1.118
1.116
16.2
16.4
16.6
16.8
17.0

LFI 20

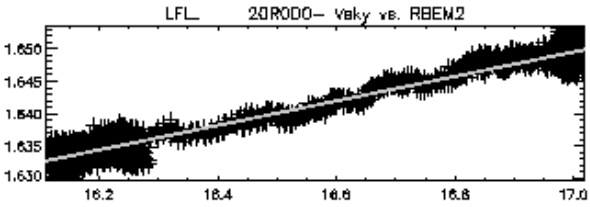
LFI_ 20R0D0– Vsky vs. RBEM2
1.650
1.645
1.640
1.635
1.630
16.2
16.4
16.6
16.8
17.0

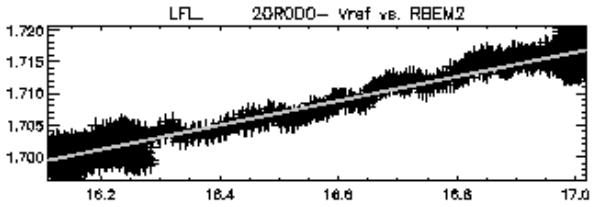
LFI_ 20R0D0– Vref vs. RBEM2
1.720
1.715
1.710
1.705
1.700
16.2
16.4
16.6
16.8
17.0

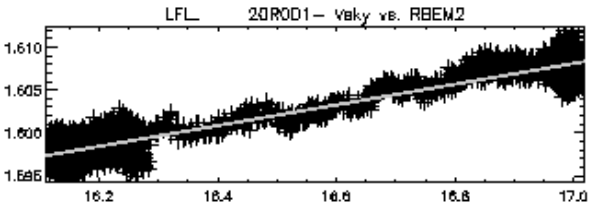
LFI_ 20R0D1– Vsky vs. RBEM2
1.610
1.605
1.600
1.595
16.2
16.4
16.6
16.8
17.0

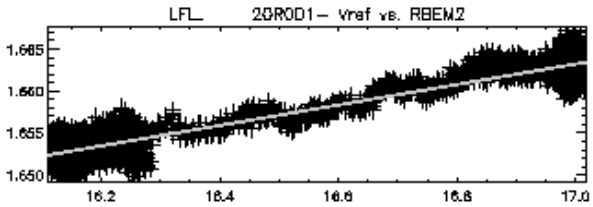
LFI_ 20R0D1– Vref vs. RBEM2
1.665
1.660
1.655
1.650
16.2
16.4
16.6
16.8
17.0

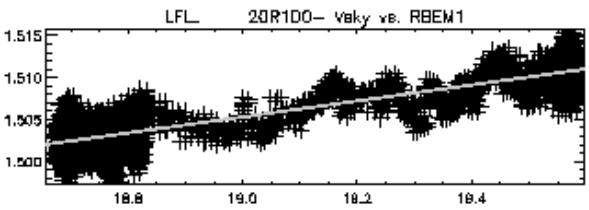
LFI_ 20R1D0– Vsky vs. RBEM1
1.515
1.510
1.505
1.500
18.8
19.0
19.2
19.4

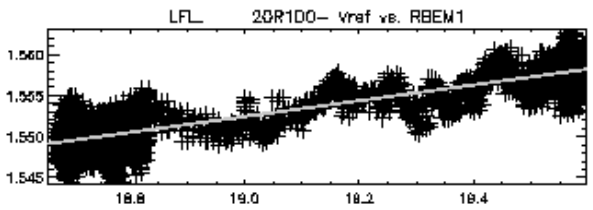
LFI_ 20R1D0– Vref vs. RBEM1
1.560
1.555
1.550
1.545
18.8
19.0
19.2
19.4

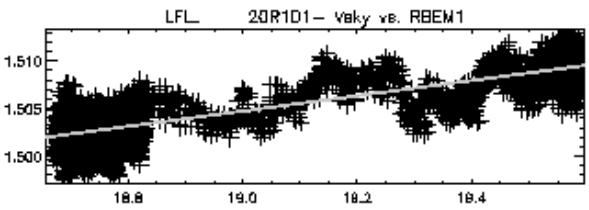
LFI_ 20R1D1– Vsky vs. RBEM1
1.510
1.505
1.500
18.8
19.0
19.2
19.4

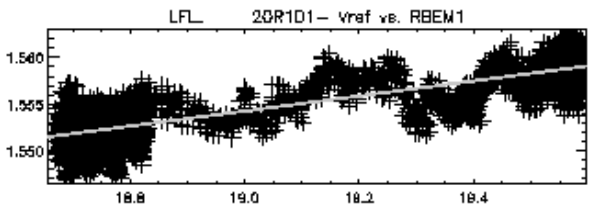
LFI_ 20R1D1– Vref vs. RBEM1
1.560
1.555
1.550
18.8
19.0
19.2
19.4

LFI 21

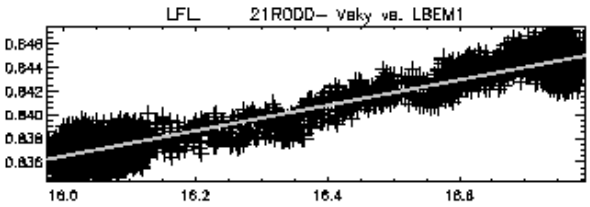
LFI 21R0DD– Vsky vs. LBEM1
0.846
0.844
0.842
0.840
0.838
0.836
16.0
16.2
16.4
16.6

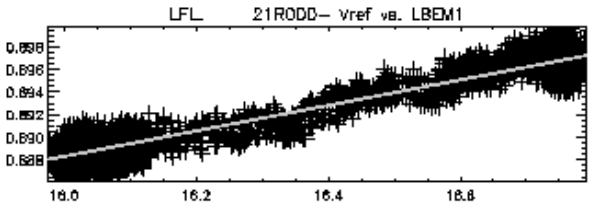
LFI 21R0DD– Vref vs. LBEM1
0.898
0.896
0.894
0.892
0.890
0.888
16.0
16.2
16.4
16.6

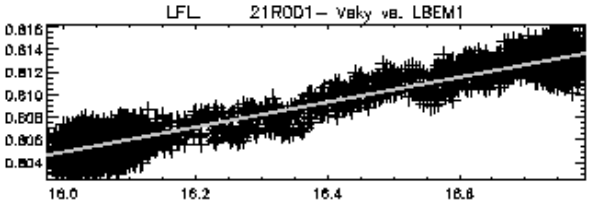
LFI 21R0D1– Vsky vs. LBEM1
0.816
0.814
0.812
0.810
0.808
0.806
0.804
16.0
16.2
16.4
16.6

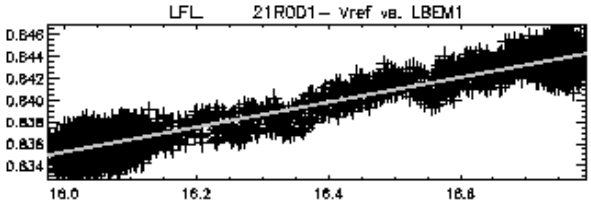
LFI 21R0D1– Vref vs. LBEM1
0.846
0.844
0.842
0.840
0.838
0.836
0.834
16.0
16.2
16.4
16.6

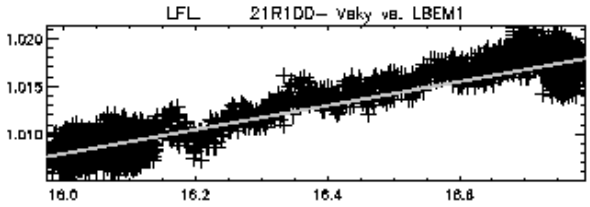
LFI 21R1DD– Vsky vs. LBEM1
1.020
1.015
1.010
16.0
16.2
16.4
16.6

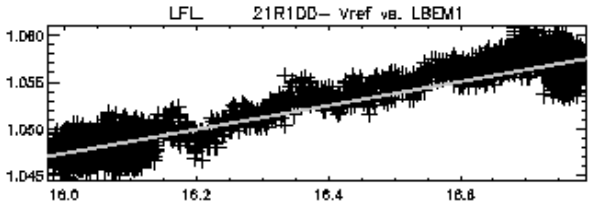
LFI 21R1DD– Vref vs. LBEM1
1.060
1.055
1.050
1.045
16.0
16.2
16.4
16.6

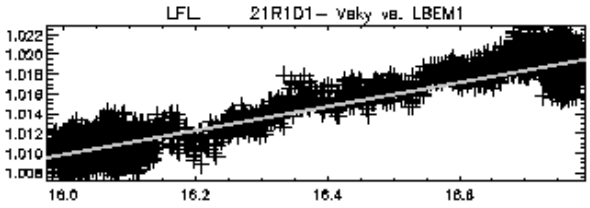
LFI 21R1D1– Vsky vs. LBEM1
1.022
1.020
1.018
1.016
1.014
1.012
1.010
1.008
16.0
16.2
16.4
16.6

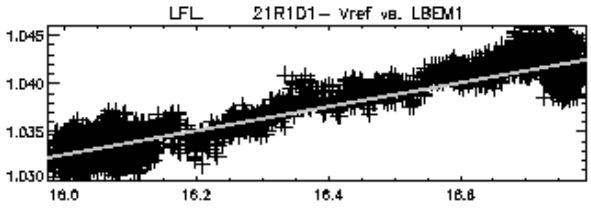
LFI 21R1D1– Vref vs. LBEM1
1.045
1.040
1.035
1.030
16.0
16.2
16.4
16.6

LFI 22

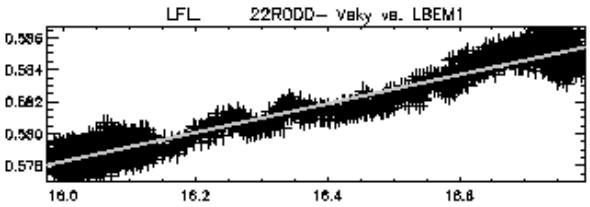
LFI 22R0D0– Vsky vs. LBEM1
0.586
0.584
0.582
0.580
0.578
16.0
16.2
16.4
16.6

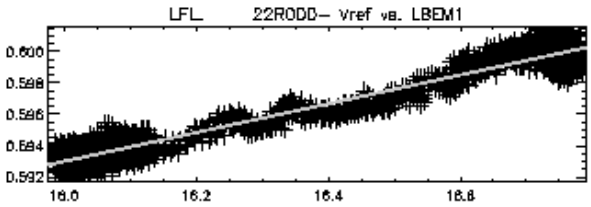
LFI 22R0D0– Vref vs. LBEM1
0.600
0.598
0.596
0.594
0.592
16.0
16.2
16.4
16.6

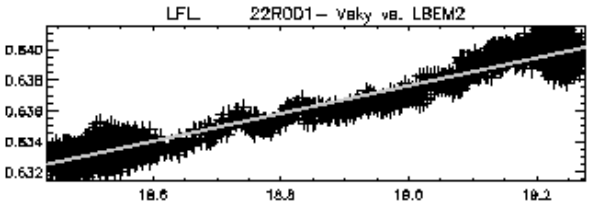
LFI 22R0D1– Vsky vs. LBEM2
0.640
0.638
0.636
0.634
0.632
16.6
16.8
18.0
18.2

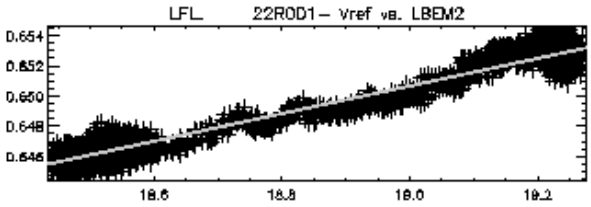
LFI 22R0D1– Vref vs. LBEM2
0.654
0.652
0.650
0.648
0.646
16.6
16.8
18.0
18.2

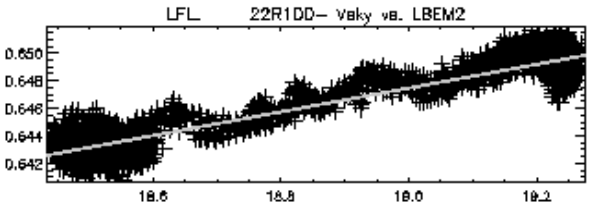
LFI 22R1D0– Vsky vs. LBEM2
0.650
0.648
0.646
0.644
0.642
16.6
16.8
18.0
18.2

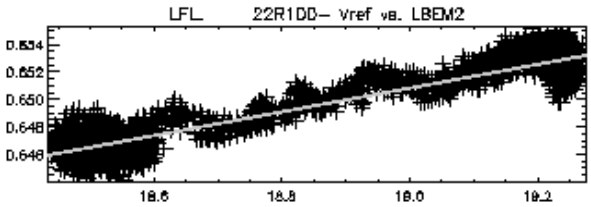
LFI 22R1D0– Vref vs. LBEM2
0.654
0.652
0.650
0.648
0.646
16.6
16.8
18.0
18.2

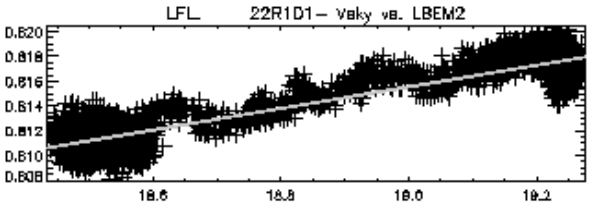
LFI 22R1D1– Vsky vs. LBEM2
0.820
0.818
0.816
0.814
0.812
0.810
0.808
16.6
16.8
18.0
18.2

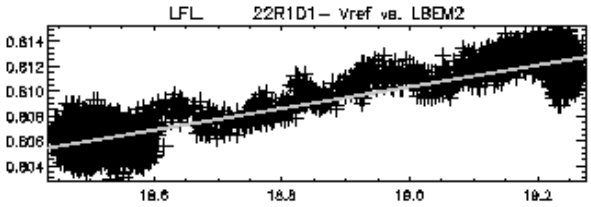
LFI 22R1D1– Vref vs. LBEM2
0.814
0.812
0.810
0.808
0.806
0.804
16.6
16.8
18.0
18.2

LFI 23

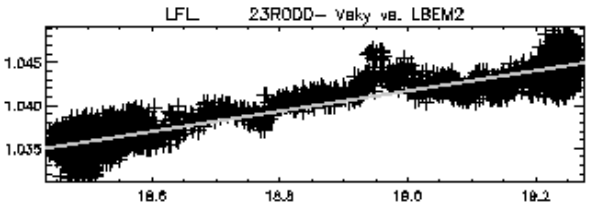
LFI_ 23R0DD– Vsky vs. LBEM2
1.045
1.040
1.035
18.6
18.8
19.0
19.2

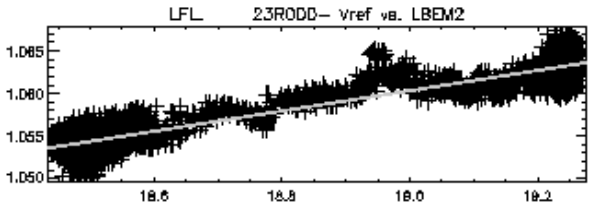
LFI_ 23R0DD– Vref vs. LBEM2
1.065
1.060
1.055
1.050
18.6
18.8
19.0
19.2

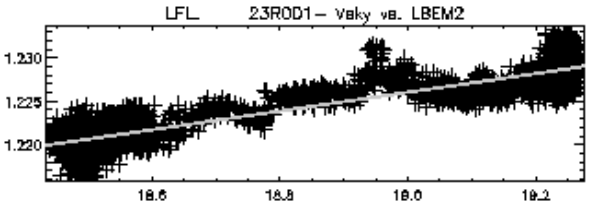
LFI_ 23R0D1– Vsky vs. LBEM2
1.230
1.225
1.220
18.6
18.8
19.0
19.2

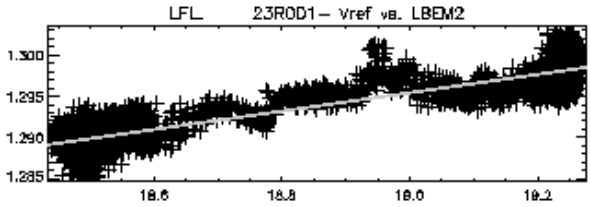
LFI_ 23R0D1– Vref vs. LBEM2
1.300
1.295
1.290
1.285
18.6
18.8
19.0
19.2

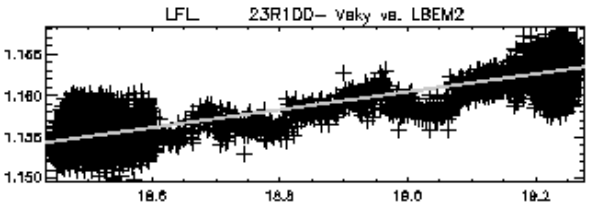
LFI_ 23R1DD– Vsky vs. LBEM2
1.165
1.160
1.155
1.150
18.6
18.8
19.0
19.2

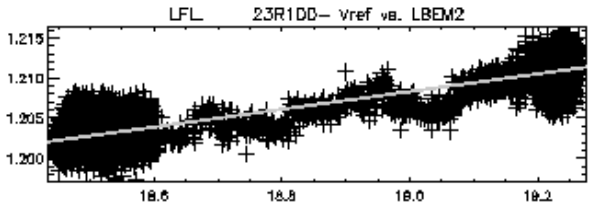
LFI_ 23R1DD– Vref vs. LBEM2
1.215
1.210
1.205
1.200
18.6
18.8
19.0
19.2

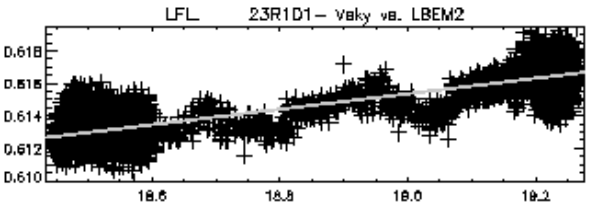
LFI_ 23R1D1– Vsky vs. LBEM2
0.618
0.616
0.614
0.612
0.610
18.6
18.8
19.0
19.2

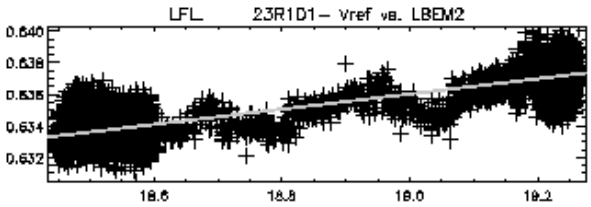
LFI_ 23R1D1– Vref vs. LBEM2
0.640
0.638
0.636
0.634
0.632
18.6
18.8
19.0
19.2

LFI 24

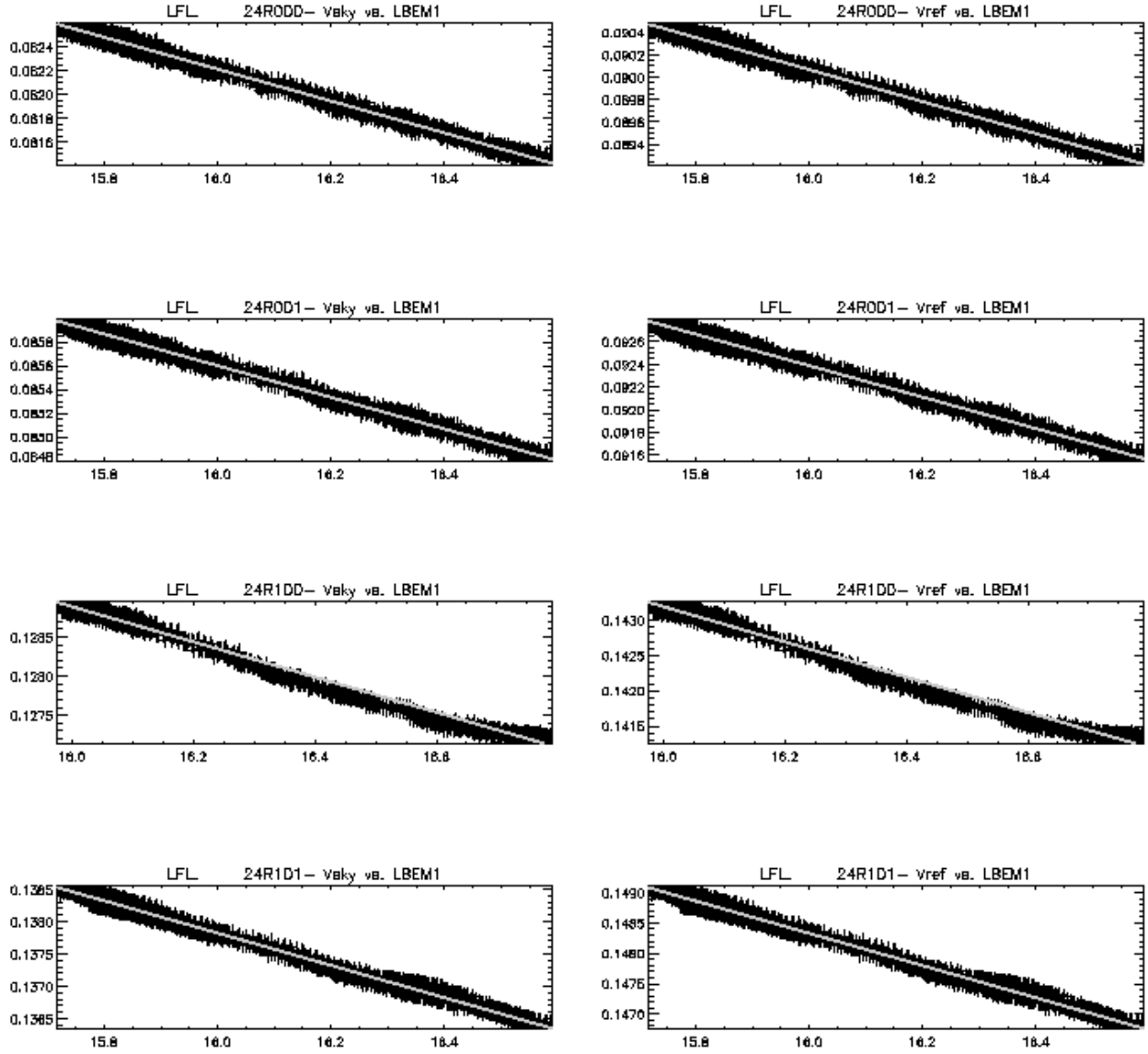

To be noticed that for detector 3 interval 255-261 was preferred to interval 189-195 due to the feature shown below.

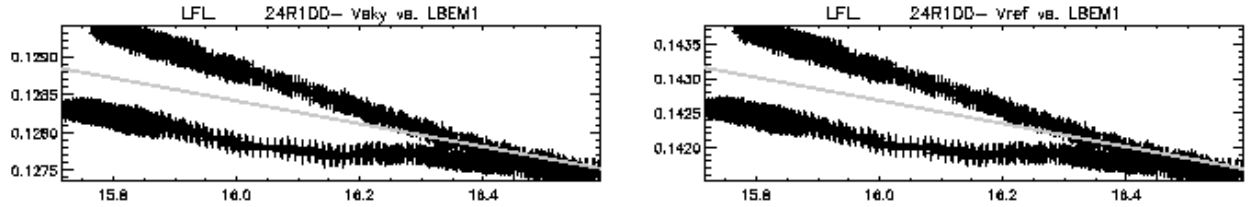

Figure 24

LFI 25

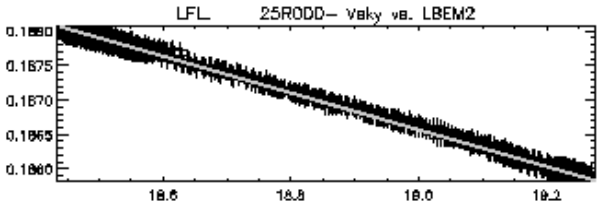
LFI 25R0D0– Vsky vs. LBEM2

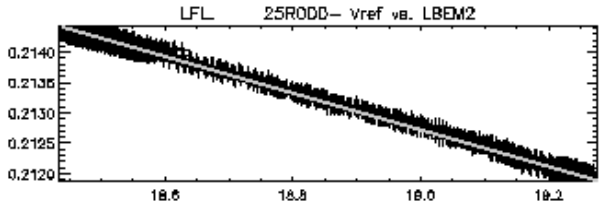
LFI 25R0D0– Vref vs. LBEM2

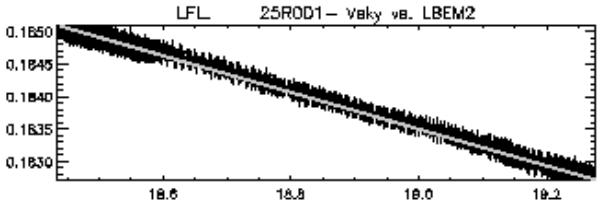
LFI 25R0D1– Vsky vs. LBEM2

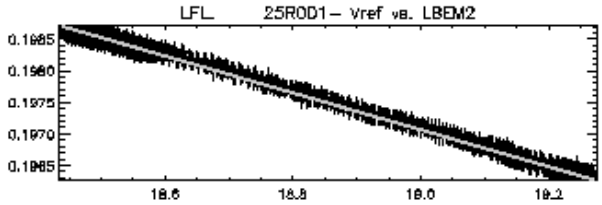
LFI 25R0D1– Vref vs. LBEM2

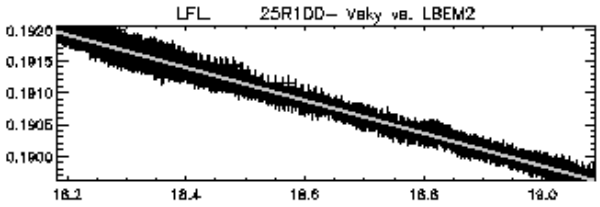
LFI 25R1D0– Vsky vs. LBEM2

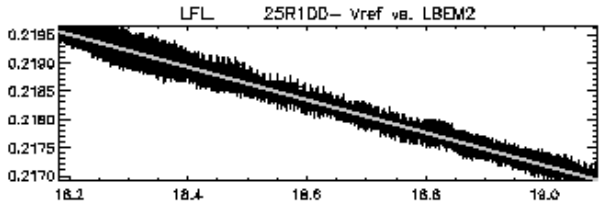
LFI 25R1D0– Vref vs. LBEM2

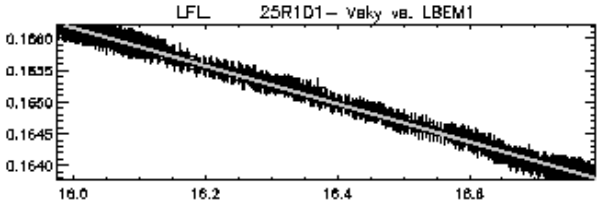
LFI 25R1D1– Vsky vs. LBEM1

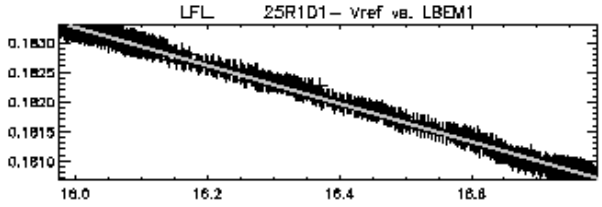
LFI 25R1D1– Vref vs. LBEM1

LFI 26

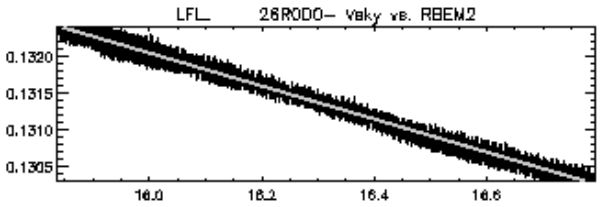
LFI_ 26R0D0– Vsky vs. RBEM2
0.1320
0.1315
0.1310
0.1305
16.0
16.2
16.4
16.6

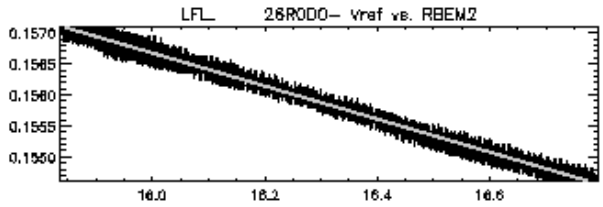
LFI_ 26R0D0– Vref vs. RBEM2
0.1570
0.1565
0.1560
0.1555
0.1550
16.0
16.2
16.4
16.6

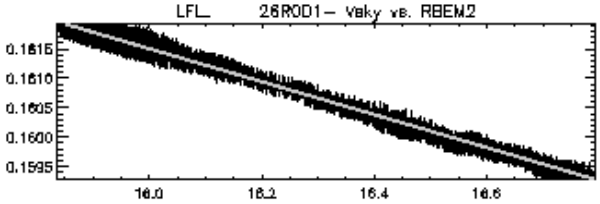
LFI_ 26R0D1– Vsky vs. RBEM2
0.1615
0.1610
0.1605
0.1600
0.1595
16.0
16.2
16.4
16.6

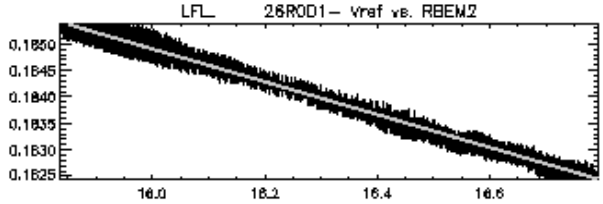
LFI_ 26R0D1– Vref vs. RBEM2
0.1850
0.1845
0.1840
0.1835
0.1830
0.1825
16.0
16.2
16.4
16.6

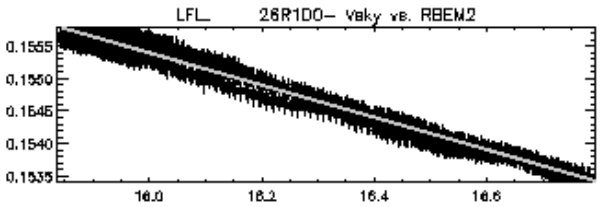
LFI_ 26R1D0– Vsky vs. RBEM2
0.1555
0.1550
0.1545
0.1540
0.1535
16.0
16.2
16.4
16.6

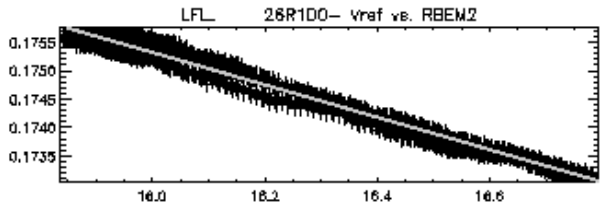
LFI_ 26R1D0– Vref vs. RBEM2
0.1755
0.1750
0.1745
0.1740
0.1735
16.0
16.2
16.4
16.6

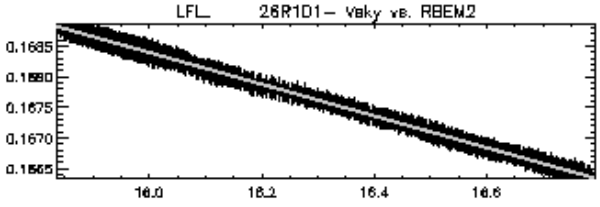
LFI_ 26R1D1– Vsky vs. RBEM2
0.1685
0.1680
0.1675
0.1670
0.1665
16.0
16.2
16.4
16.6

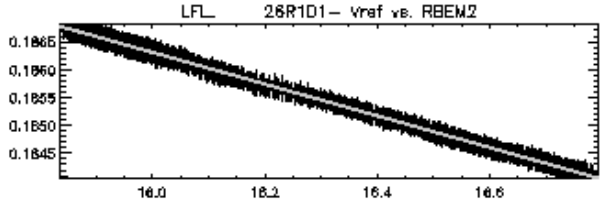
LFI_ 26R1D1– Vref vs. RBEM2
0.1865
0.1860
0.1855
0.1850
0.1845
16.0
16.2
16.4
16.6

LFI 27

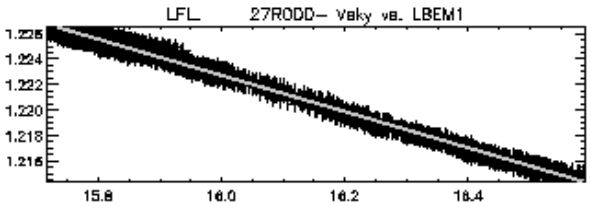
LFI 27RODD– Vsky vs. LBEM1
1.226
1.224
1.222
1.220
1.218
1.216
15.8
16.0
16.2
16.4

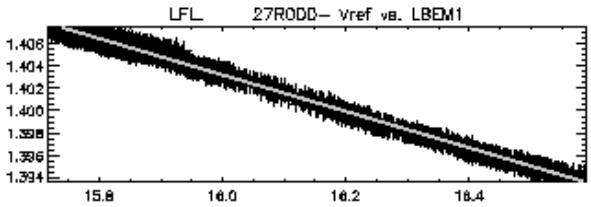
LFI 27RODD– Vref vs. LBEM1
1.406
1.404
1.402
1.400
1.398
1.396
1.394
15.8
16.0
16.2
16.4

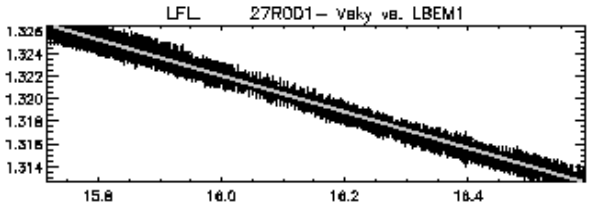
LFI 27ROD1– Vsky vs. LBEM1
1.326
1.324
1.322
1.320
1.318
1.316
1.314
15.8
16.0
16.2
16.4

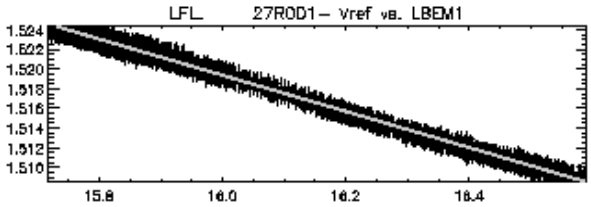
LFI 27ROD1– Vref vs. LBEM1
1.524
1.522
1.520
1.518
1.516
1.514
1.512
1.510
15.8
16.0
16.2
16.4

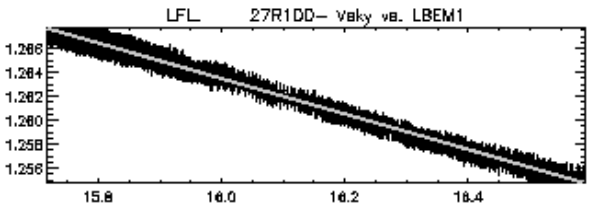
LFI 27R1DD– Vsky vs. LBEM1
1.266
1.264
1.262
1.260
1.258
1.256
15.8
16.0
16.2
16.4

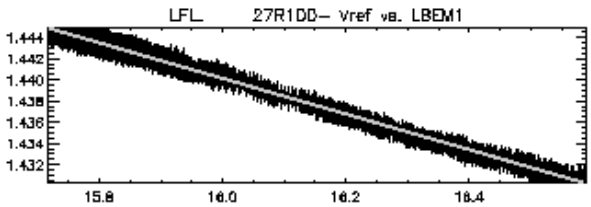
LFI 27R1DD– Vref vs. LBEM1
1.444
1.442
1.440
1.438
1.436
1.434
1.432
15.8
16.0
16.2
16.4

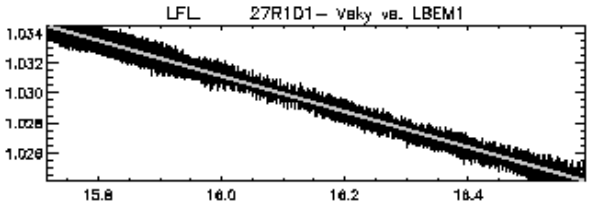
LFI 27R1D1– Vsky vs. LBEM1
1.034
1.032
1.030
1.028
1.026
15.8
16.0
16.2
16.4

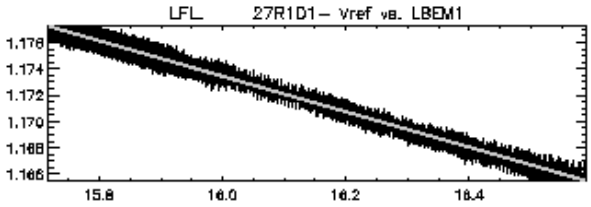
LFI 27R1D1– Vref vs. LBEM1
1.176
1.174
1.172
1.170
1.168
1.166
15.8
16.0
16.2
16.4

LFI 28

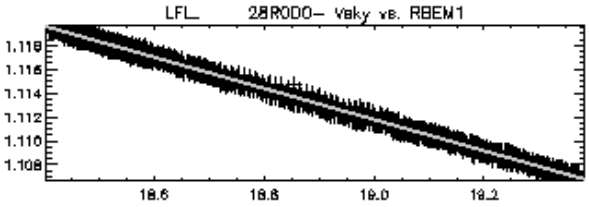
LFI_ 28R0D0– Vsky vs. RBEM1
1.118
1.116
1.114
1.112
1.110
1.108
18.6
18.8
19.0
19.2

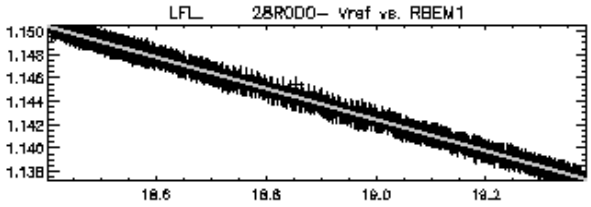
LFI_ 28R0D0– Vref vs. RBEM1
1.150
1.148
1.146
1.144
1.142
1.140
1.138
18.6
18.8
19.0
19.2

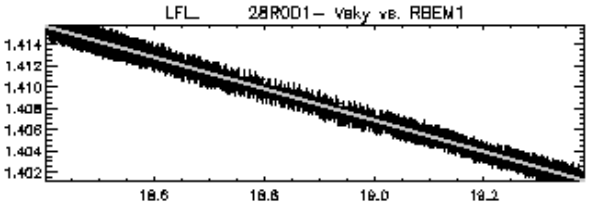
LFI_ 28R0D1– Vsky vs. RBEM1
1.414
1.412
1.410
1.408
1.406
1.404
1.402
18.6
18.8
19.0
19.2

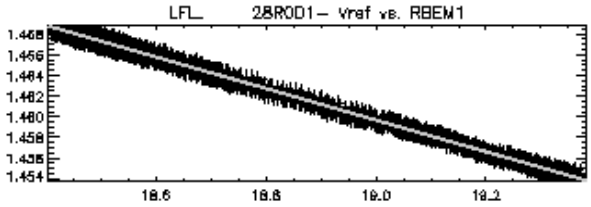
LFI_ 28R0D1– Vref vs. RBEM1
1.468
1.466
1.464
1.462
1.460
1.458
1.456
1.454
18.6
18.8
19.0
19.2

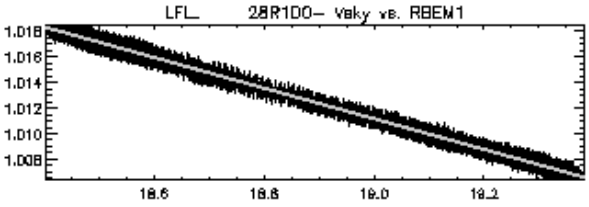
LFI_ 28R1D0– Vsky vs. RBEM1
1.018
1.016
1.014
1.012
1.010
1.008
18.6
18.8
19.0
19.2

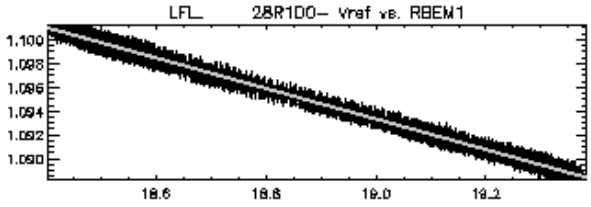
LFI_ 28R1D0– Vref vs. RBEM1
1.100
1.098
1.096
1.094
1.092
1.090
18.6
18.8
19.0
19.2

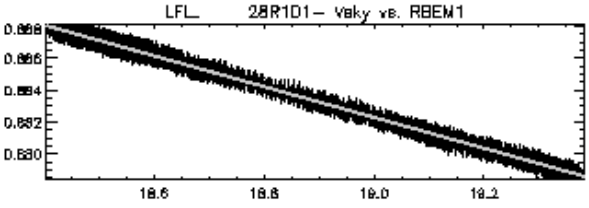
LFI_ 28R1D1– Vsky vs. RBEM1
0.888
0.886
0.884
0.882
0.880
18.6
18.8
19.0
19.2

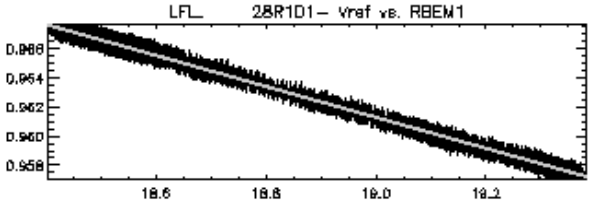
LFI_ 28R1D1– Vref vs. RBEM1
0.968
0.964
0.962
0.960
0.958
18.6
18.8
19.0
19.2

6.2 Correlation Plots

Each plot (one for each detector) displays how the correlation coefficient varies with the time interval considered. Sky and Ref are differently represented in each plot (sky in dark grey, in light grey).

70 GHz

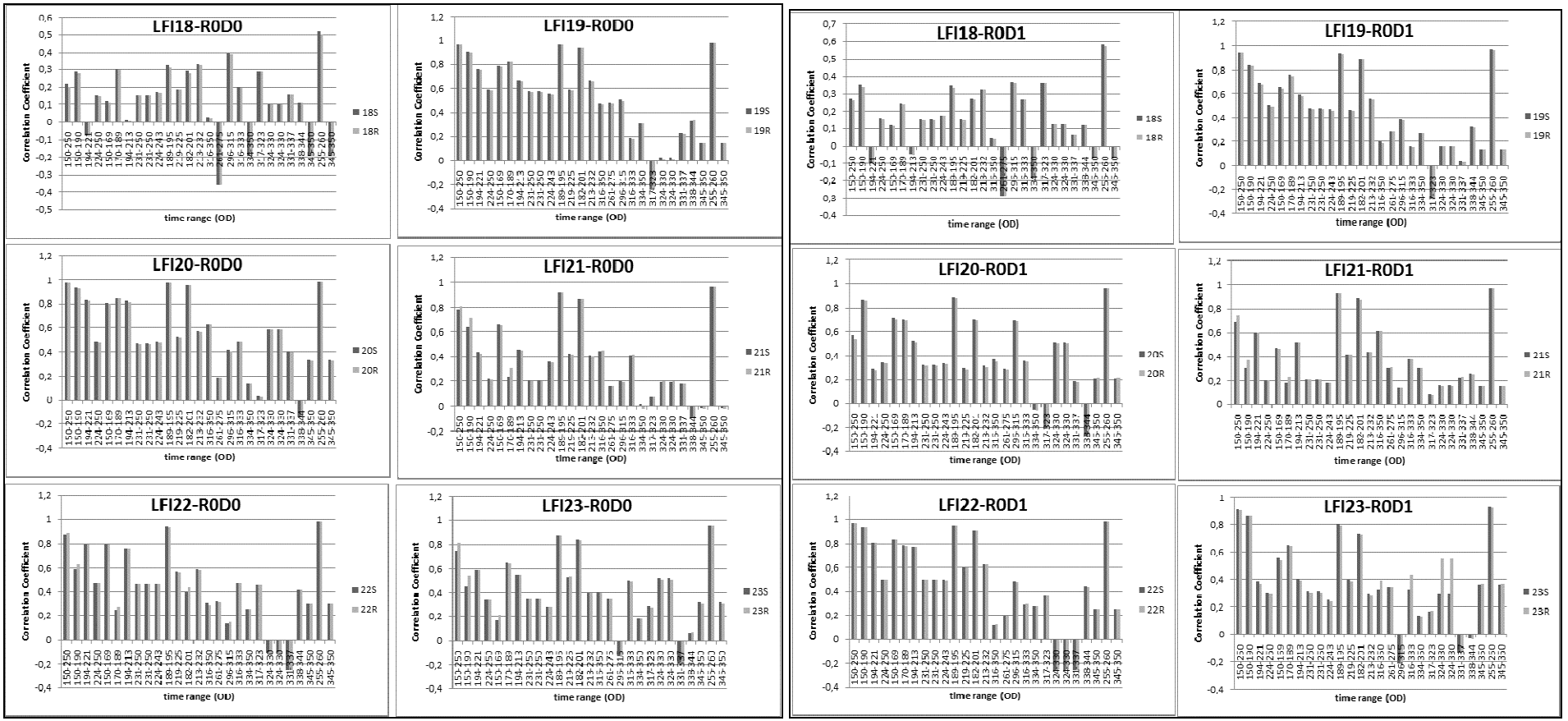

Plot 1 70 GHz Channels Main Arm: Correlation coefficient calculated for each detector in each of the intervals considered.

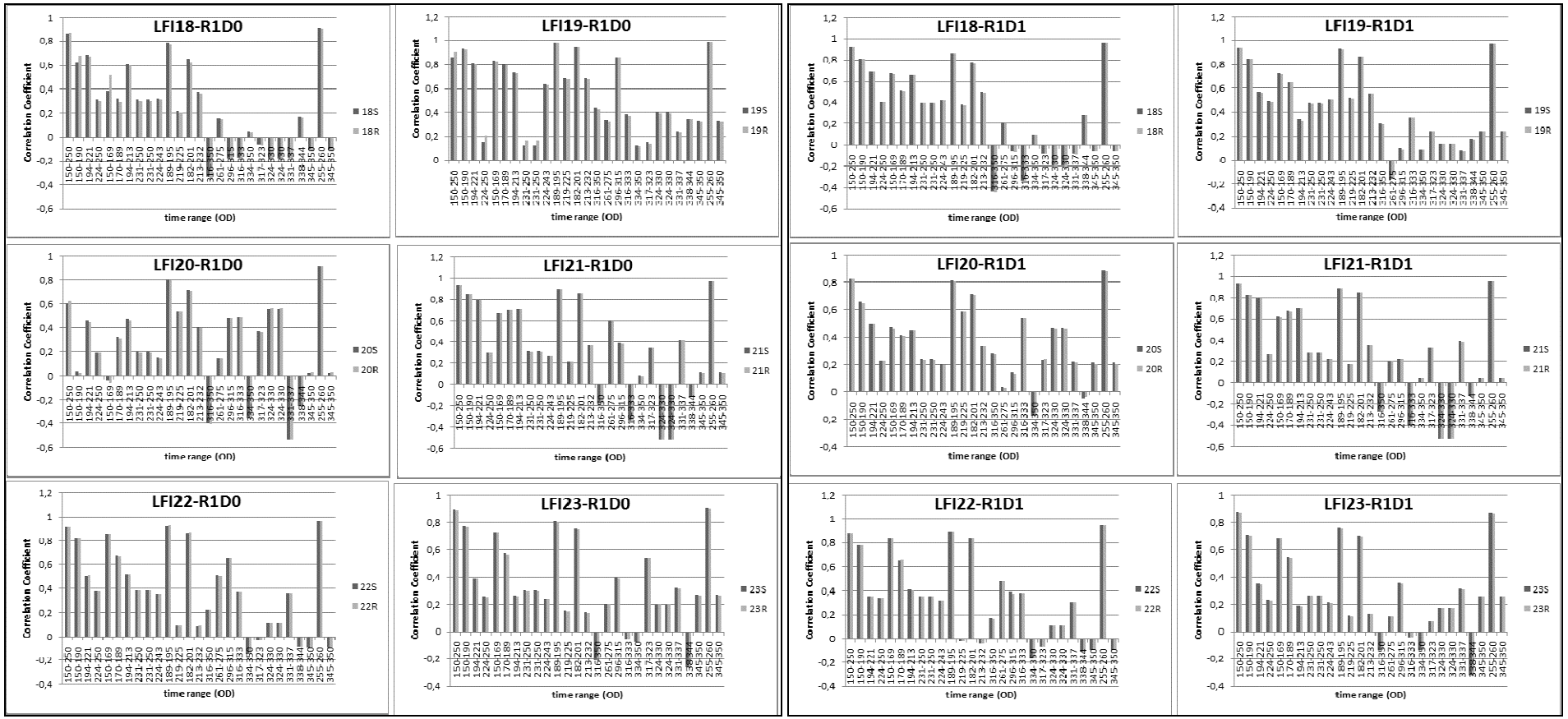

Plot 2 70 GHz Channels Side Arm. Correlation coefficient calculated for each detector in each of the intervals considered.

44 GHz

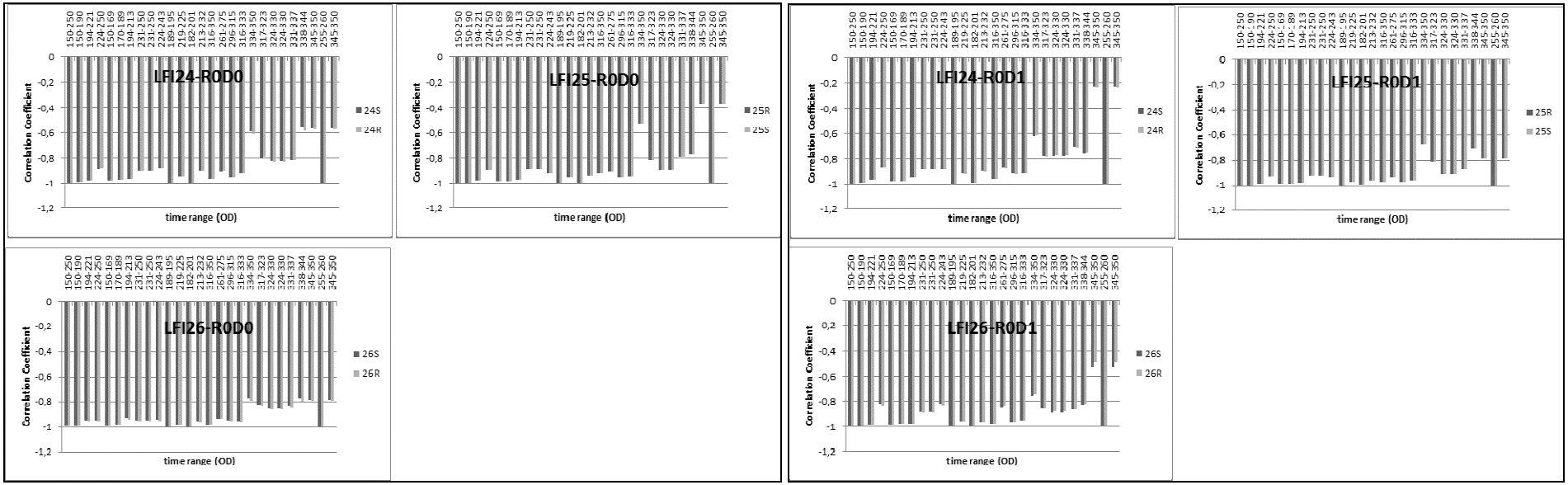

Plot 3 44 GHz Channels, Main Arm. Correlation coefficient calculated for each detector in each of the intervals considered.

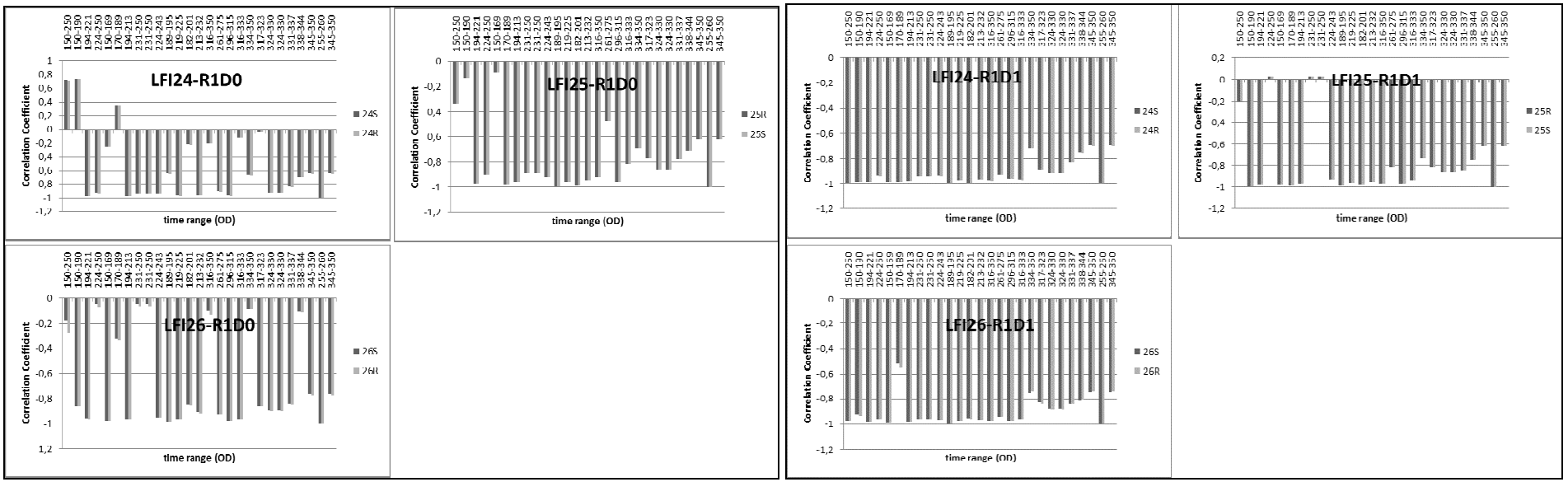

Plot 4 44 GHz Channels, Side Arm. Correlation coefficient calculated for each detector in each of the intervals considered.

30 GHz

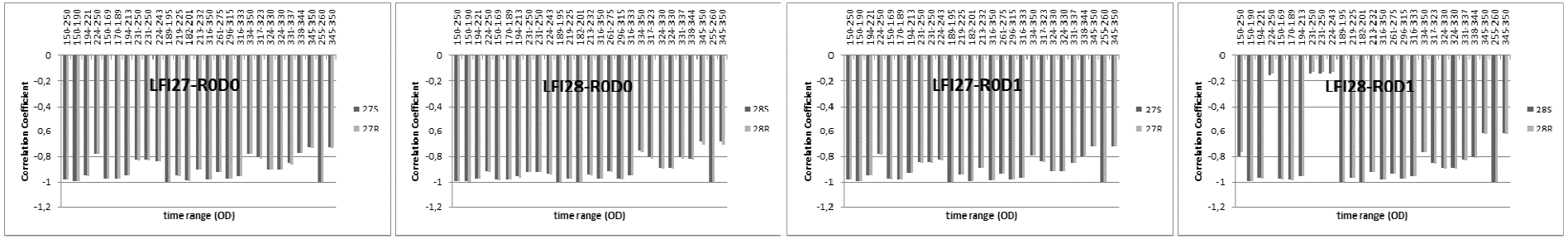

Plot 5 30 GHz Channels, Main Arm . correlation coefficient calculated for each detector in each of the intervals considered.

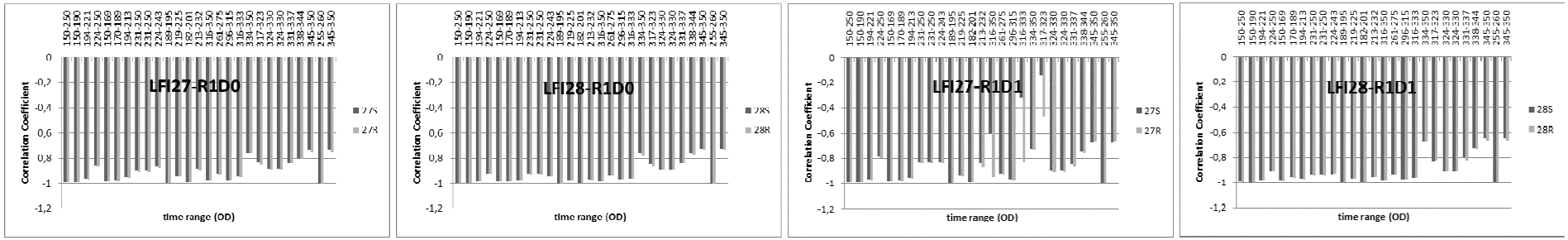

Plot 6 30 GHz Channels, Side Arm . correlation coefficient calculated for each detector in each of the intervals considered.

6.3 TABLES

	R0D0									R0D1								
	INTERVAL			SENSOR			CORRELATION			INTERVAL			SENSOR			CORRELATION		
	on/off	alw on	final	on/off	alw on	final	on/off	alw on	final	on/off	alw on	final	on/off	alw on	final	on/off	alw on	final
18S	213-232	255-260	255-260	L2	R1	R2	0,32915	0,51981	0,5193	150-190	255-260	255-260	R2	R1	R2	0,35007	0,58442	0,5841
18R	213-232	255-260	255-260	L2	R1	R2	0,32653	0,50227	0,5017	150-190	255-260	255-260	R2	R1	R2	0,3395	0,57262	0,5723
19S	189-195	255-260	189-195	R1	L1	R2	0,9708	0,98194	0,9700	150-250	255-260	255-260	R2	L2	R2	0,94554	0,96792	0,9677
19R	189-195	255-260	189-195	R1	L1	R2	0,97022	0,98155	0,9694	150-250	255-260	255-260	R2	L2	R2	0,94177	0,96629	0,9661
20S	189-195	255-260	255-260	R1	R2	R2	0,9785	0,9853	0,9853	189-195	255-260	255-260	R2	R2	R2	0,88744	0,96429	0,9643
20R	189-195	255-260	255-260	R1	R2	R2	0,97779	0,98463	0,9846	189-195	255-260	255-260	R2	R2	R2	0,88218	0,96221	0,9622
21S	189-195	255-260	255-260	R2	L1	L1	0,92	0,96584	0,9658	189-195	255-260	255-260	L2	R1	L1	0,93028	0,96827	0,9681
21R	189-195	255-260	255-260	R2	L1	L1	0,92034	0,96587	0,9659	189-195	255-260	255-260	L2	R1	L2	0,9298	0,96809	0,9679
22S	189-195	255-260	255-260	L1	L1	L1	0,94018	0,98259	0,9826	150-250	255-260	255-260	L2	L1	L2	0,96753	0,98265	0,9824
22R	189-195	255-260	255-260	L1	L1	L1	0,93945	0,98224	0,9822	150-250	255-260	255-260	L2	L1	L2	0,96708	0,98226	0,9820
23S	189-195	255-260	255-260	R1	R1	L2	0,88381	0,95434	0,9535	150-250	255-260	255-260	L2	R1	L2	0,91356	0,93278	0,9319
23R	189-195	255-260	255-260	R1	R1	L2	0,88006	0,95385	0,9530	150-250	255-260	255-260	L2	R1	L2	0,90906	0,92884	0,9279
24S	189-195	255-260	189-195	L1	L1	L1	-0,99734	-0,99901	-0,9973	189-195	255-260	189-195	L1	R2	L1	-0,9973	-0,99877	-0,9973
24R	189-195	255-260	189-195	L1	L1	L1	-0,99723	-0,999	-0,9972	189-195	255-260	189-195	L1	L2	L1	-0,9973	-0,99877	-0,9973
25S	189-195	255-260	255-260	L1	L1	L2	-0,99801	-0,99914	-0,9991	150-250	255-260	255-260	L2	L1	L2	-0,99723	-0,99925	-0,9991
25R	189-195	255-260	255-260	L1	L1	L2	-0,99804	-0,99912	-0,9991	150-250	255-260	255-260	L2	L1	L2	-0,99722	-0,9993	-0,9992
26S	189-195	255-260	189-195	R2	R2	R2	-0,99791	-0,99933	-0,9979	189-195	255-260	189-195	R2	L1	R2	-0,99746	-0,99876	-0,9972
26R	189-195	255-260	189-195	R2	R2	R2	-0,99809	-0,99936	-0,9981	189-195	255-260	189-195	R2	L1	R2	-0,99714	-0,99866	-0,9968
27S	189-195	255-260	189-195	L2	L1	L1	-0,99749	-0,99903	-0,9972	189-195	255-260	189-195	L1	L1	L1	-0,9977	-0,99901	-0,9977
27R	189-195	255-260	189-195	L2	L1	L1	-0,99745	-0,99907	-0,9971	189-195	255-260	189-195	L1	L1	L1	-0,99787	-0,99905	-0,9978
28S	189-195	255-260	189-195	R2	R1	R1	-0,99874	-0,99944	-0,9985	189-195	255-260	189-195	R1	R1	R1	-0,9983	-0,99936	-0,9983
28R	189-195	255-260	189-195	R2	R1	R1	-0,9988	-0,99946	-0,9986	189-195	255-260	189-195	R1	R1	R1	-0,99846	-0,9994	-0,9985

Table 5 Main Arm: comparison of results. Correlation coefficients, best sensors and time intervals are compared for the three data sets: 'transponder ON/OFF' period, 'transponder always on' period, final choices relative to results in Table 7

	R1D0								
	INTERVAL			SENSOR			CORRELATION		
	on/off	alw on	final	on/off	alw on	final	on/off	alw on	final
18S	150-250	255-260	255-260	L1	L1	R2	0,8662	0,91203	0,9112
18R	150-250	255-260	255-260	L1	L1	R2	0,87116	0,90237	0,9015
19S	189-195	255-260	255-260	R2	L2	R2	0,97543	0,98946	0,9894
19R	189-195	255-260	255-260	R2	L2	R2	0,97398	0,98896	0,9889
20S	189-195	255-260	255-260	R1	R1	R1	0,80196	0,91153	0,9115
20R	189-195	255-260	255-260	R1	R1	R1	0,79452	0,90901	0,9090
21S	150-250	255-260	255-260	L1	R1	L1	0,93364	0,96336	0,9613
21R	150-250	255-260	255-260	L1	R1	L1	0,93264	0,9624	0,9603
22S	189-195	255-260	255-260	R2	R1	L2	0,92505	0,96524	0,9638
22R	189-195	255-260	255-260	R2	R1	L2	0,92637	0,96464	0,9631
23S	150-250	255-260	255-260	L1	L1	L2	0,89148	0,90578	0,9042
23R	150-250	255-260	255-260	L1	L1	L2	0,88824	0,90146	0,8998
24S	194-221	255-260	255-260	R2	R1	L1	-0,97867	-0,99854	-0,9978
24R	194-221	255-260	255-260	R2	R1	L1	-0,9791	-0,99853	-0,9977
25S	189-195	255-260	189-195	L1	L1	L2	-0,99363	-0,99873	-0,9929
25R	189-195	255-260	189-195	L1	L1	L2	-0,99342	-0,99881	-0,9926
26S	189-195	255-260	189-195	R1	R2	R2	-0,98738	-0,99917	-0,9859
26R	189-195	255-260	189-195	R1	R2	R2	-0,98832	-0,99917	-0,9869
27S	189-195	255-260	189-195	L2	L1	L1	-0,99772	-0,99903	-0,9975
27R	189-195	255-260	189-195	L2	L1	L1	-0,99773	-0,9991	-0,9974
28S	189-195	255-260	189-195	R2	R1	R1	-0,99884	-0,99946	-0,9988
28R	189-195	255-260	189-195	R2	R1	R1	-0,99884	-0,99946	-0,9987

	R1D1								
	INTERVAL			SENSOR			CORRELATION		
	on/off	alw on	final	on/off	alw on	final	on/off	alw on	final
18S	150-250	255-260	255-260	L1	L1	R2	0,92167	0,95493	0,9547
18R	150-250	255-260	255-260	L1	L1	R2	0,92024	0,95431	0,9541
19S	150-250	255-260	255-260	R2	R1	R2	0,93903	0,97319	0,9731
19R	150-250	255-260	255-260	R2	R1	R2	0,93683	0,97256	0,9725
20S	150-250	255-260	255-260	R1	R1	R1	0,8308	0,88784	0,8878
20R	150-250	255-260	255-260	R1	R1	R1	0,82556	0,88354	0,8835
21S	150-250	255-260	255-260	L1	R1	L1	0,93118	0,95939	0,9579
21R	150-250	255-260	255-260	L1	R1	L1	0,92989	0,95891	0,9574
22S	189-195	255-260	255-260	R1	R1	L2	0,89897	0,94909	0,6502
22R	189-195	255-260	255-260	R1	R1	L2	0,8987	0,94985	0,6454
23S	150-250	150-250	255-260	L1	L1	L2	0,87524	0,87524	0,8688
23R	150-250	150-250	255-260	L1	L1	L2	0,8718	0,8718	0,8627
24S	189-195	255-260	189-195	L1	L1	L1	-0,99692	-0,9993	-0,9969
24R	189-195	255-260	189-195	L1	L2	L1	-0,99675	-0,99931	-0,9968
25S	150-190	255-260	255-260	R2	L1	L1	-0,99405	-0,99911	-0,9991
25R	150-190	255-260	255-260	R2	L1	L1	-0,99448	-0,9991	-0,9991
26S	189-195	255-260	189-195	R2	R2	R2	-0,99899	-0,99954	-0,9990
26R	189-195	255-260	189-195	R2	R2	R2	-0,99904	-0,99954	-0,9990
27S	189-195	255-260	189-195	L2	L1	L1	-0,99801	-0,99898	-0,9979
27R	189-195	255-260	189-195	L2	L1	L1	-0,99814	-0,99906	-0,9981
28S	189-195	255-260	189-195	R1	R1	R1	-0,99866	-0,99935	-0,9987
28R	189-195	255-260	189-195	R1	R1	R1	-0,99875	-0,99937	-0,9988

Table 6 Side Arm: comparison of results. Correlation coefficients, best sensors and time intervals are compared for the three data sets: 'transponder ON/OFF' period, 'transponder always on' period, final choices relative to results in Table 7

	R0D0					R0D1					R1D0					R1D1				
18S	**255-260**	R2	0,51927	1,9639	0,01297	**255-260**	R2	0,58411	2,55422	0,01958	**255-260**	R2	0,91124	1,57042	0,01169	**255-260**	R2	0,95472	1,28004	0,01317
18R	**255-260**	R2	0,50172	2,05314	0,01291	**255-260**	R2	0,57231	2,67967	0,01977	**255-260**	R2	0,9015	1,69587	0,01189	**255-260**	R2	0,9541	1,3327	0,01349
19S	**189-195**	R2	0,96995	1,10648	0,01733	**255-260**	R2	0,96772	1,27944	0,01194	**255-260**	R2	0,98944	0,70446	0,01018	**255-260**	R2	0,97311	0,93448	0,0089
19R	**189-195**	R2	0,96935	1,14336	0,01771	**255-260**	R2	0,96609	1,35163	0,01231	**255-260**	R2	0,98893	0,74712	0,01053	**255-260**	R2	0,97249	0,97165	0,00909
20S	**255-260**	R2	0,9853	1,32857	0,01888	**255-260**	R2	0,96429	1,40212	0,01212	**255-260**	R1	0,91153	1,32419	0,00953	**255-260**	R1	0,88784	1,3529	0,00799
20R	**255-260**	R2	0,98463	1,39096	0,01915	**255-260**	R2	0,96221	1,45576	0,0122	**255-260**	R1	0,90901	1,36912	0,00965	**255-260**	R1	0,88354	1,40108	0,00806
21S	**255-260**	L1	0,96584	0,66483	0,01073	**255-260**	L1	0,96808	0,62842	0,01103	**255-260**	L1	0,96129	0,80671	0,01258	**255-260**	L1	0,95791	0,8145	0,01221
21R	**255-260**	L1	0,96587	0,70832	0,01125	**255-260**	L2	0,96789	0,65321	0,01138	**255-260**	L1	0,9603	0,8417	0,01285	**255-260**	L1	0,95739	0,8337	0,01243
22S	**255-260**	L1	0,98259	0,43349	0,00905	**255-260**	L2	0,9824	0,46576	0,00905	**255-260**	L2	0,96376	0,48336	0,00864	**255-260**	L2	0,65021	0,0087	0,94693
22R	**255-260**	L1	0,98224	0,44644	0,00916	**255-260**	L2	0,98203	0,47686	0,00915	**255-260**	L2	0,96313	0,48678	0,00863	**255-260**	L2	0,64538	0,00868	0,94771
23S	**255-260**	L2	0,95354	0,81686	0,01183	**255-260**	L2	0,93188	1,02142	0,01077	**255-260**	L2	0,90421	0,9556	0,01078	**255-260**	L2	0,86884	0,52486	0,00476
23R	**255-260**	L2	0,95301	0,83428	0,0119	**255-260**	L2	0,92793	1,08439	0,01111	**255-260**	L2	0,89984	0,99933	0,011	**255-260**	L2	0,86265	0,5445	0,00482
24S	**189-195**	L1	-0,99734	0,10358	-0,00134	**189-195**	L1	-0,9973	0,10691	-0,00133	**255-260**	L1	-0,99778	0,1649	-0,00225	**189-195**	L1	-0,99692	0,17768	-0,00249
24R	**189-195**	L1	-0,99723	0,11297	-0,00143	**189-195**	L1	-0,9973	0,11456	-0,00139	**255-260**	L1	-0,99774	0,18314	-0,0025	**189-195**	L1	-0,99675	0,19079	-0,00265
25S	**255-260**	L2	-0,99909	0,23708	-0,00266	**255-260**	L2	-0,99913	0,23706	-0,00282	**189-195**	L2	-0,99288	0,23896	-0,00258	**255-260**	L1	-0,99911	0,21405	-0,00299
25R	**255-260**	L2	-0,99908	0,27015	-0,00302	**255-260**	L2	-0,9992	0,25254	-0,00292	**189-195**	L2	-0,99263	0,27226	-0,0029	**255-260**	L1	-0,9991	0,23479	-0,00322
26S	**189-195**	R2	-0,99791	0,16812	-0,00225	**189-195**	R2	-0,99715	0,20633	-0,0028	**189-195**	R2	-0,98588	0,1952	-0,00249	**189-195**	R2	-0,99899	0,20991	-0,00259
26R	**189-195**	R2	-0,99809	0,19936	-0,00267	**189-195**	R2	-0,99679	0,2345	-0,0031	**189-195**	R2	-0,98689	0,22095	-0,00285	**189-195**	R2	-0,99904	0,23178	-0,00284
27S	**189-195**	L1	-0,99717	1,44992	-0,0142	**189-195**	L1	-0,99769	1,57821	-0,01601	**189-195**	L1	-0,99747	1,50031	-0,0148	**189-195**	L1	-0,99794	1,22046	-0,01183
27R	**189-195**	L1	-0,99711	1,66332	-0,01626	**189-195**	L1	-0,9978	1,81236	-0,01831	**189-195**	L1	-0,99744	1,70878	-0,01679	**189-195**	L1	-0,99806	1,38858	-0,01345
28S	**189-195**	R1	-0,99854	1,3599	-0,01306	**189-195**	R1	-0,9983	1,68732	-0,01476	**189-195**	R1	-0,99879	1,23778	-0,01193	**189-195**	R1	-0,99866	1,06623	-0,00968
28R	**189-195**	R1	-0,99859	1,39655	-0,01337	**189-195**	R1	-0,99846	1,74974	-0,01527	**189-195**	R1	-0,99873	1,33734	-0,01284	**189-195**	R1	-0,99875	1,16243	-0,01059

Table 7 Final BEU Thermal susceptibility values. For each channel (Sky and Ref) and for each detector ((RiDj, i,j=1,2) are reported from left to right: the interval chosen, the correlation coefficient, the linear fit coefficients a and b (Vout=a + b T).

	R0D0					R0D1					R1D0					R1D1				
	HK	a	sigma_a	b	sigma_b	HK	a	sigma_a	b	sigma_b	HK	a	sigma_a	b	sigma_b	HK	a	sigma_a	b	sigma_b
LFI18S	R2	1,9639	3,81E-03	0,01297	2,30E-04	R2	2,55422	4,86E-03	0,01958	2,93E-04	R2	1,57042	9,44E-04	0,01169	5,68E-05	R2	1,28004	7,33E-04	0,01317	4,41E-05
LFI18R	R2	2,0531	3,97E-03	0,01291	2,39E-04	R2	2,67967	5,06E-03	0,01977	3,05E-04	R2	1,69587	1,02E-03	0,01189	6,14E-05	R2	1,3327	7,57E-04	0,01349	4,56E-05
LFI19S	R2	1,1065	6,97E-04	0,01733	4,33E-05	R2	1,27944	5,56E-04	0,01194	3,35E-05	R2	0,70446	2,66E-04	0,01018	1,60E-05	R2	0,93448	3,76E-04	0,0089	2,27E-05
LFI19R	R2	1,1434	7,20E-04	0,01771	4,47E-05	R2	1,35163	5,87E-04	0,01231	3,54E-05	R2	0,74712	2,82E-04	0,01053	1,70E-05	R2	0,97165	3,89E-04	0,00909	2,34E-05
LFI20S	R2	1,3286	5,85E-04	0,01888	3,52E-05	R2	1,40212	5,94E-04	0,01212	3,58E-05	R1	1,32419	8,87E-04	0,00953	4,63E-05	R1	1,3529	8,54E-04	0,00799	4,46E-05
LFI20R	R2	1,391	6,07E-04	0,01915	3,65E-05	R2	1,45576	6,17E-04	0,01220	3,71E-05	R1	1,36912	9,12E-04	0,00965	4,76E-05	R1	1,40108	8,81E-04	0,00806	4,60E-05
LFI21S	L1	0,6648	5,08E-04	0,01073	3,10E-05	L1	0,62842	5,04E-04	0,01103	3,07E-05	L1	0,80671	6,36E-04	0,01258	3,88E-05	L1	0,8145	6,46E-04	0,01221	3,94E-05
LFI21R	L1	0,7083	5,33E-04	0,01125	3,24E-05	L2	0,63189	5,82E-04	0,01102	3,08E-05	L1	0,8417	6,59E-04	0,01285	4,02E-05	L1	0,8337	6,62E-04	0,01243	4,03E-05
LFI22S	L1	0,4335	3,02E-04	0,00905	1,84E-05	L2	0,46576	3,49E-04	0,00905	1,85E-05	L2	0,48336	4,86E-04	0,00864	2,57E-05	L2	0,65021	6,00E-04	0,0087	3,18E-05
LFI22R	L1	0,4464	3,09E-04	0,00916	1,88E-05	L2	0,47686	3,18E-04	0,00915	1,94E-05	L2	0,48678	4,44E-04	0,00863	2,71E-05	L2	0,64538	5,39E-04	0,00868	3,28E-05
LFI23S	L2	0,8169	7,60E-04	0,01183	4,02E-05	L2	1,02142	8,52E-04	0,01077	4,51E-05	L2	0,9556	1,03E-03	0,01078	5,48E-05	L2	0,52486	5,51E-04	0,00476	2,92E-05
LFI23R	L2	0,8343	7,68E-04	0,0119	4,07E-05	L2	1,08439	9,06E-04	0,01111	4,80E-05	L2	0,99933	1,08E-03	0,011	5,73E-05	L2	0,5445	5,74E-04	0,00482	3,04E-05
LFI24S	L1	0,1036	1,55E-05	-0,0013	9,72E-07	L1	0,10691	1,56E-05	-0,00133	9,76E-07	L1	0,1649	2,66E-05	-0,0023	1,62E-06	L1	0,17768	3,12E-05	-0,0025	1,95E-06
LFI24R	L1	0,113	1,70E-05	-0,0014	1,06E-06	L1	0,11456	1,62E-05	-0,00139	1,02E-06	L1	0,18314	2,97E-05	-0,0025	1,47E-06	L1	0,19079	3,41E-05	-0,0027	2,14E-06
LFI25S	L2	0,2371	2,31E-05	-0,0027	1,22E-06	L2	0,23706	2,39E-05	-0,00282	1,26E-06	L2	0,23896	5,70E-05	-0,0026	3,09E-06	L1	0,21405	2,23E-05	-0,003	1,36E-06
LFI25R	L2	0,2702	2,64E-05	-0,003	1,40E-06	L2	0,25254	2,37E-05	-0,00292	1,26E-06	L2	0,27226	6,50E-05	-0,0029	3,52E-06	L1	0,23479	2,42E-05	-0,0032	1,48E-06
LFI26S	R2	0,1681	2,34E-05	-0,0023	1,45E-06	R2	0,20633	3,40E-05	-0,00280	2,11E-06	R2	0,1952	6,78E-05	-0,0025	4,21E-06	R2	0,20991	1,88E-05	-0,0026	1,16E-06
LFI26R	R2	0,1994	2,65E-05	-0,0027	1,65E-06	R2	0,2345	3,99E-05	-0,00310	2,48E-06	R2	0,22095	7,49E-05	-0,0029	4,65E-06	R2	0,23178	2,00E-05	-0,0028	1,24E-06
LFI27S	L1	1,4499	1,70E-04	-0,0142	1,07E-05	L1	1,57821	1,73E-04	-0,01601	1,09E-05	L1	1,50031	1,68E-04	-0,0148	1,05E-05	L1	1,22046	1,21E-04	-0,0118	7,58E-06
LFI27R	L1	1,6633	1,97E-04	-0,0163	1,23E-05	L1	1,81236	1,93E-04	-0,01831	1,21E-05	L1	1,70878	1,92E-04	-0,0168	1,20E-05	L1	1,38858	1,33E-04	-0,0135	8,34E-06
LFI28S	R1	1,3599	1,32E-04	-0,0131	7,05E-06	R1	1,68732	1,60E-04	-0,01476	8,58E-06	R1	1,23778	1,09E-04	-0,0119	5,85E-06	R1	1,06623	9,33E-05	-0,0097	5,00E-06
LFI28R	R1	1,3966	1,32E-04	-0,0134	7,08E-06	R1	1,74974	1,58E-04	-0,01527	8,44E-06	R1	1,33734	1,21E-04	-0,0128	6,46E-06	R1	1,16243	9,86E-05	-0,0106	5,28E-06

Table 8 BEU Thermal susceptibility: Delivered Table. For each channel (Sky and Ref) and for each detector ((RiDj, i,j=1,2) are reported from left to right: the sensor used, the linear fit coefficients a and b (Vout = a + bT) together with the respective uncertainties

CH#	REMOVED (GMF1)	CDS (GMF2)	OLD REMOVED (GMF2)	NEW REMOVED (GMF2)	GMF2-GMF1	NEW - CDS	NEW-OLD
18R0D0	8,10E-05	4,54E-05	4,31E-05	4,33E-05	-46,5	-4,6	0,5
18R0D1	1,69E-04	6,88E-05	7,20E-05	7,02E-05	-58,4	2,0	-2,5
18R1D0	5,78E-04	5,68E-04	3,26E-05	3,25E-05	-94,4	-94,3	-0,3
18R1D1	4,19E-04	4,11E-04	2,42E-05	2,39E-05	-94,3	-94,2	-1,2
19R0D0	4,42E-04	4,30E-04	2,27E-05	2,25E-05	-94,9	-94,8	-0,9
19R0D1	1,12E-04	2,66E-05	2,33E-05	2,31E-05	-79,4	-13,2	-0,9
19R1D0	2,95E-04	2,85E-04	2,45E-05	2,44E-05	-91,7	-91,4	-0,4
19R1D1	5,22E-05	3,18E-05	3,25E-05	3,24E-05	-37,9	1,9	-0,3
20R0D0	3,88E-03	3,70E-03	2,79E-05	2,49E-05	-99,4	-99,3	-10,8
20R0D1	5,08E-05	2,11E-05	2,22E-05	2,21E-05	-56,5	4,7	-0,5
20R1D0	3,32E-04	3,16E-04	2,52E-05	2,51E-05	-92,4	-92,1	-0,4
20R1D1	6,46E-05	2,35E-05	2,38E-05	2,38E-05	-63,2	1,3	0,0
21R0D0	2,35E-04	1,97E-04	2,02E-05	1,97E-05	-91,6	-90,0	-2,5
21R0D1	2,90E-04	2,85E-04	1,88E-05	1,87E-05	-93,5	-93,4	-0,5
21R1D0	3,82E-05	1,83E-05	1,47E-05	1,46E-05	-61,8	-20,2	-0,7
21R1D1	7,20E-05	1,28E-05	1,43E-05	1,42E-05	-80,3	10,9	-0,7
22R0D0	1,67E-04	1,63E-04	1,08E-05	1,07E-05	-93,6	-93,4	-0,9
22R0D1	4,62E-05	1,01E-05	1,34E-05	1,32E-05	-71,4	30,7	-1,5
22R1D0	2,23E-05	1,07E-05	1,20E-05	1,19E-05	-46,6	11,2	-0,8
22R1D1	5,85E-05	3,14E-05	1,32E-05	1,28E-05	-78,1	-59,2	-3,0
23R0D0	5,68E-04	5,60E-04	3,20E-05	3,20E-05	-94,4	-94,3	0,0
23R0D1	2,50E-03	2,47E-03	2,49E-05	2,46E-05	-99,0	-99,0	-1,2
23R1D0	9,16E-05	2,47E-05	2,05E-05	2,00E-05	-78,2	-19,0	-2,4
23R1D1	1,35E-03	5,74E-04	1,29E-05	1,26E-05	-99,1	-97,8	-2,3
24R0D0	4,40E-06	2,80E-06	2,10E-06	2,10E-06	-52,3	-25,0	0,0
24R0D1	1,78E-05	3,10E-06	2,10E-06	2,20E-06	-87,6	-29,0	4,8
24R1D0	4,67E-05	4,39E-05	2,70E-06	2,70E-06	-94,2	-93,8	0,0
24R1D1	1,04E-03	1,66E-04	2,00E-06	2,00E-06	-99,8	-98,8	0,0
25R0D0	6,10E-06	3,00E-06	2,40E-06	2,40E-06	-60,7	-20,0	0,0
25R0D1	5,70E-05	4,30E-06	2,50E-06	2,70E-06	-95,3	-37,2	8,0
25R1D0	2,41E-05	1,29E-05	4,00E-06	4,00E-06	-83,4	-69,0	0,0
25R1D1	5,53E-05	4,70E-06	2,90E-06	3,10E-06	-94,4	-34,0	6,9
26R0D0	9,70E-06	5,20E-06	4,80E-06	4,80E-06	-50,5	-7,7	0,0
26R0D1	3,18E-05	6,90E-06	5,40E-06	5,30E-06	-83,3	-23,2	-1,9
26R1D0	3,75E-04	3,66E-04	6,00E-06	6,00E-06	-98,4	-98,4	0,0
26R1D1	4,32E-05	5,40E-06	5,30E-06	5,20E-06	-88,0	-3,7	-1,9
27R0D0	2,85E-04	2,68E-04	2,65E-05	2,67E-05	-90,6	-90,0	0,8
27R0D1	2,19E-04	1,21E-04	2,88E-05	2,90E-05	-86,8	-76,1	0,7
27R1D0	3,91E-04	3,57E-04	2,74E-05	2,75E-05	-93,0	-92,3	0,4
27R1D1	4,74E-04	4,35E-04	1,82E-05	1,82E-05	-96,2	-95,8	0,0
28R0D0	2,14E-04	1,28E-04	2,91E-05	2,90E-05	-86,5	-77,4	-0,3
28R0D1	2,44E-04	2,04E-04	2,94E-05	2,93E-05	-88,0	-85,6	-0,3
28R1D0	2,68E-04	5,09E-05	2,86E-05	2,80E-05	-89,6	-45,0	-2,1
28R1D1	1,43E-02	7,59E-03	4,47E-05	2,42E-05	-99,8	-99,7	-45,9

Figure 25 RMS comparison between the different models applied. Values refer to the plots in the next section 6.4. From the left: diff data corrected for the model, using a single GMF (GMF1). Differenced uncorrected data from CDS. Corrected data based on the OLD coefficients: differences are calculated using multiple GMF (GMF2) with 1-day baseline. Corrected data based on the NEW coefficients: differences are calculated using multiple GMF (GMF2) with 1-day baseline. Comparison between new model corrected data and the remaining three models given in percent.

6.4 Total Power correction

LFI18

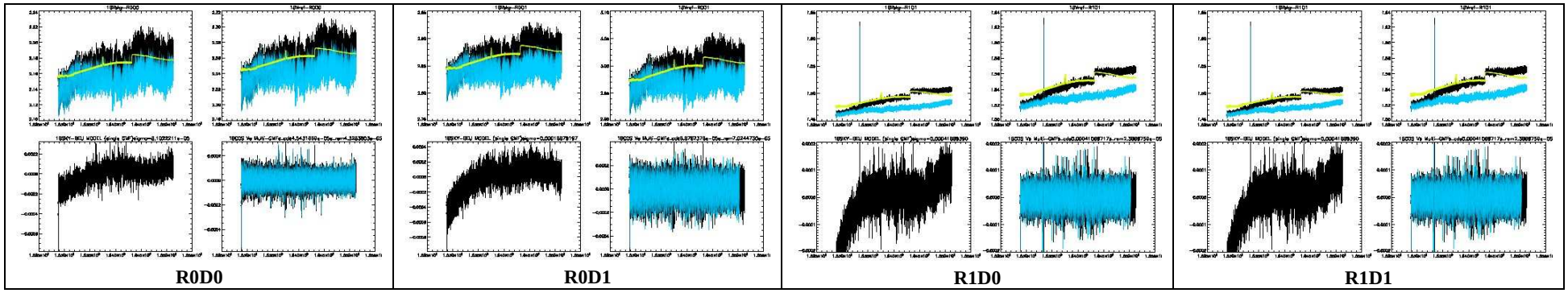

Table 9 BEU drift removal from total power data, using the new coefficients; Each panel contains: Sky data (top left) Ref data (top right), differenced data using a single GMF (bottom left) and differenced data using multiple GMF (bottom right). Colours represent: raw data from: CDS (black) , model (yellow) , corrected data (magenta).

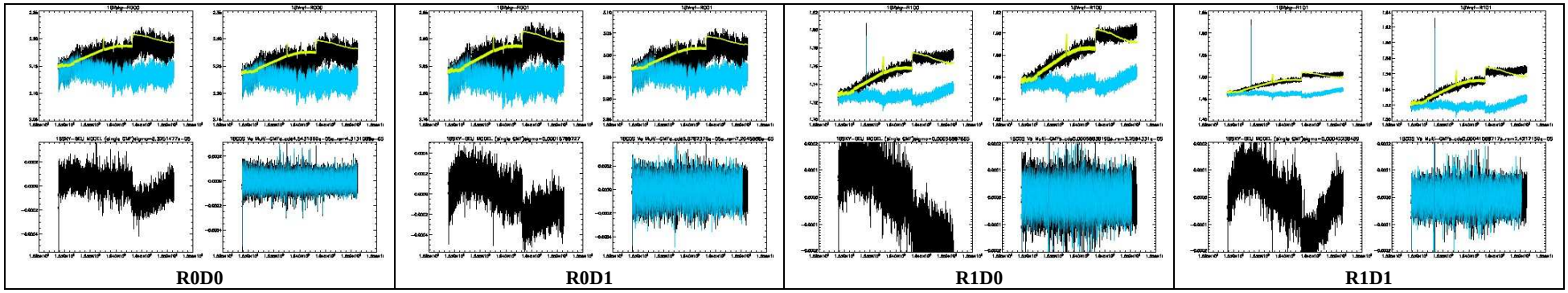

Table 10 BEU drift removal from total power data, using the OLD coefficients; Each panel contains: Sky data (top left) Ref data (top right), differenced data using a single GMF (bottom left) and differenced data using multiple GMF (bottom right). Colours represent: raw data from: CDS (black) , model (yellow) , corrected data (magenta).

LFI19

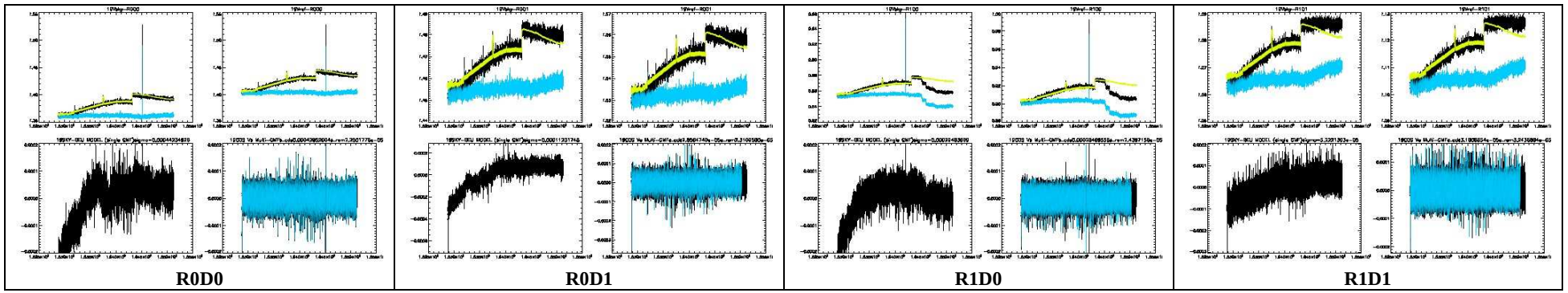

Table 11 BEU drift removal from total power data, using the new coefficients; Each panel contains: Sky data (top left) Ref data (top right), differenced data using a single GMF (bottom left) and differenced data using multiple GMF (bottom right). Colours represent: raw data from: CDS (black) , model (yellow) , corrected data (magenta).

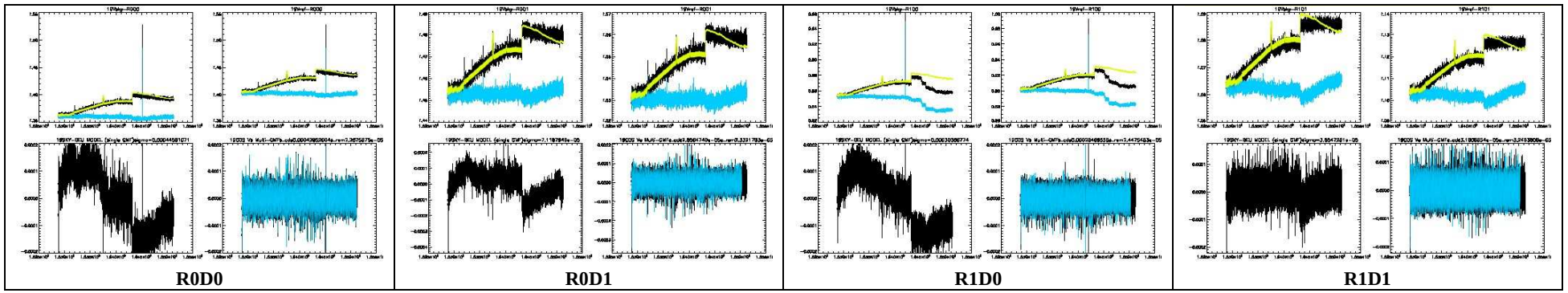

Table 12 BEU drift removal from total power data, using the OLD coefficients; Each panel contains: Sky data (top left) Ref data (top right), differenced data using a single GMF (bottom left) and differenced data using multiple GMF (bottom right). Colours represent: raw data from: CDS (black) , model (yellow) , corrected data (magenta).

LFI20

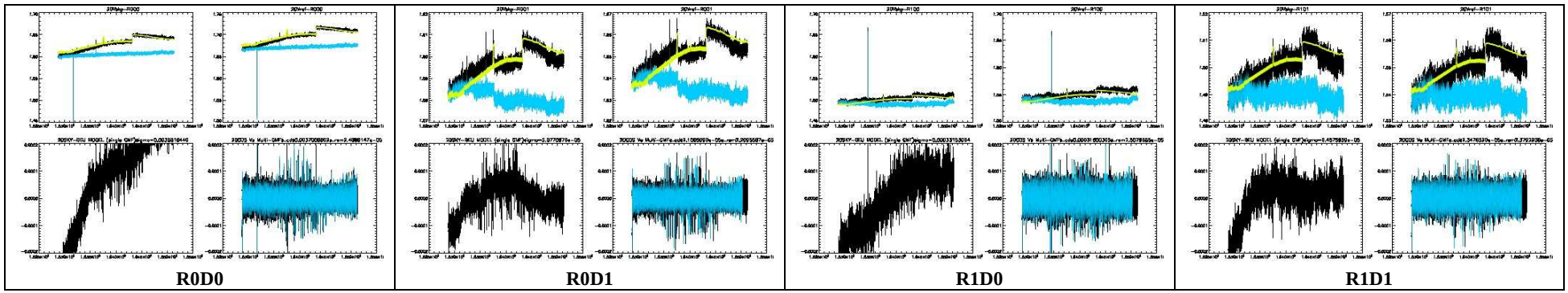

Table 13 BEU drift removal from total power data, using the new coefficients; Each panel contains: Sky data (top left) Ref data (top right), differenced data using a single GMF (bottom left) and differenced data using multiple GMF (bottom right). Colours represent: raw data from: CDS (black) , model (yellow) , corrected data (magenta).

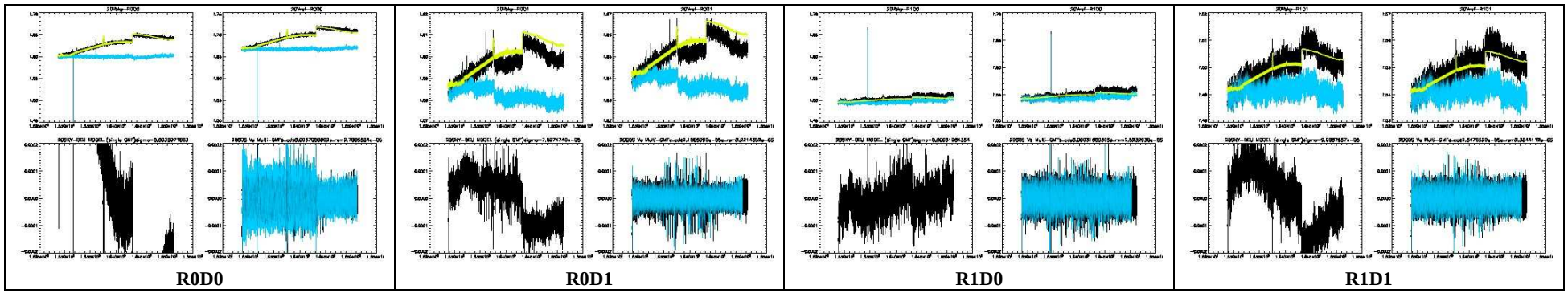

Table 14 BEU drift removal from total power data, using the OLD coefficients; Each panel contains: Sky data (top left) Ref data (top right), differenced data using a single GMF (bottom left) and differenced data using multiple GMF (bottom right). Colours represent: raw data from: CDS (black) , model (yellow) , corrected data (magenta).

INAF – IASF Bologna

LFI Project System Team

LFI21

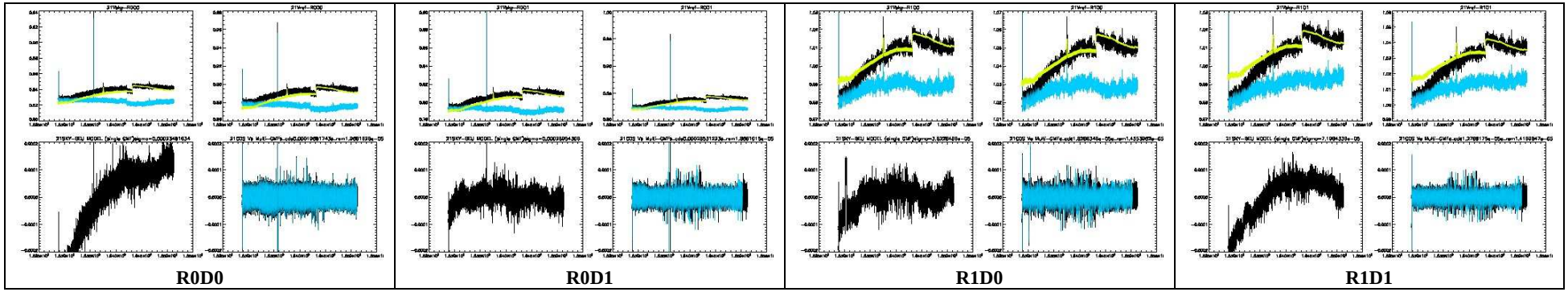

Table 15 BEU drift removal from total power data, using the new coefficients; Each panel contains: Sky data (top left) Ref data (top right), differenced data using a single GMF (bottom left) and differenced data using multiple GMF (bottom right). Colours represent: raw data from: CDS (black) , model (yellow) , corrected data (magenta).

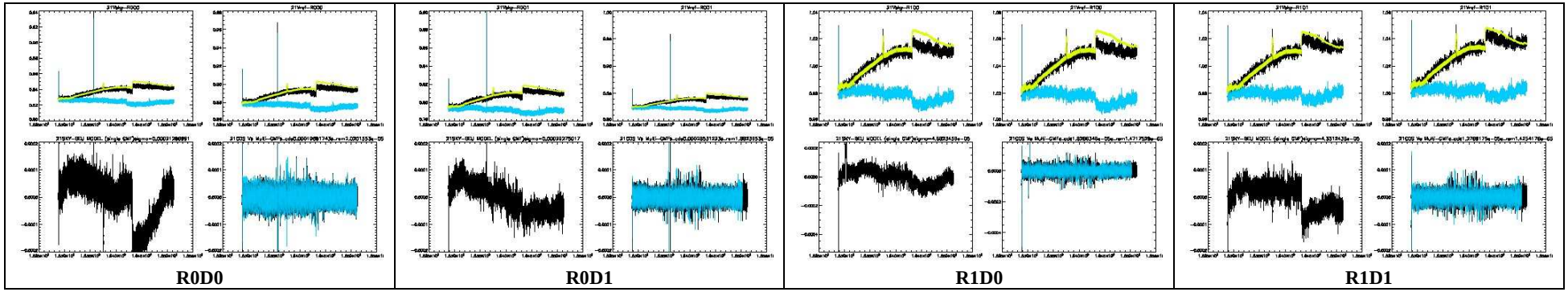

Table 16 BEU drift removal from total power data, using the OLD coefficients; Each panel contains: Sky data (top left) Ref data (top right), differenced data using a single GMF (bottom left) and differenced data using multiple GMF (bottom right). Colours represent: raw data from: CDS (black) , model (yellow) , corrected data (magenta).

INAF – IASF Bologna

LFI Project System Team

LFI22

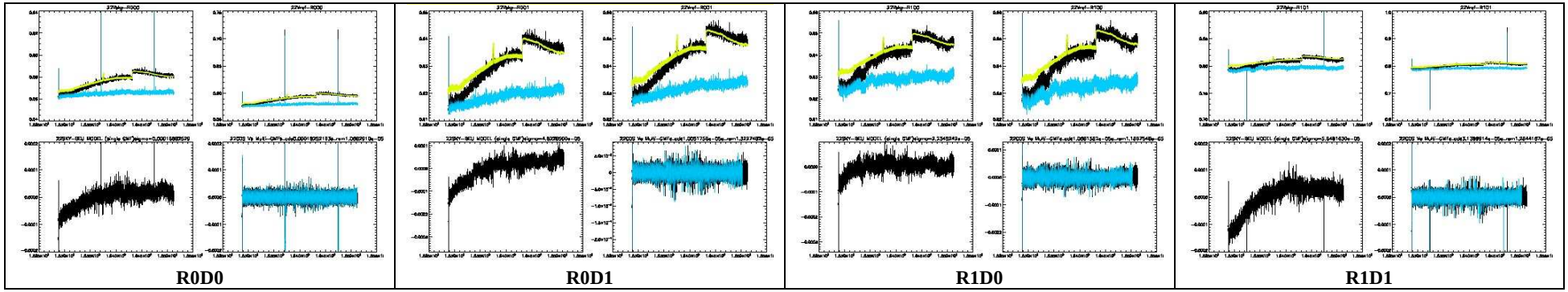

R0D0 **R0D1** **R1D0** **R1D1**

Table 17 BEU drift removal from total power data, using the new coefficients; Each panel contains: Sky data (top left) Ref data (top right), differenced data using a single GMF (bottom left) and differenced data using multiple GMF (bottom right). Colours represent: raw data from: CDS (black) , model (yellow) , corrected data (magenta).

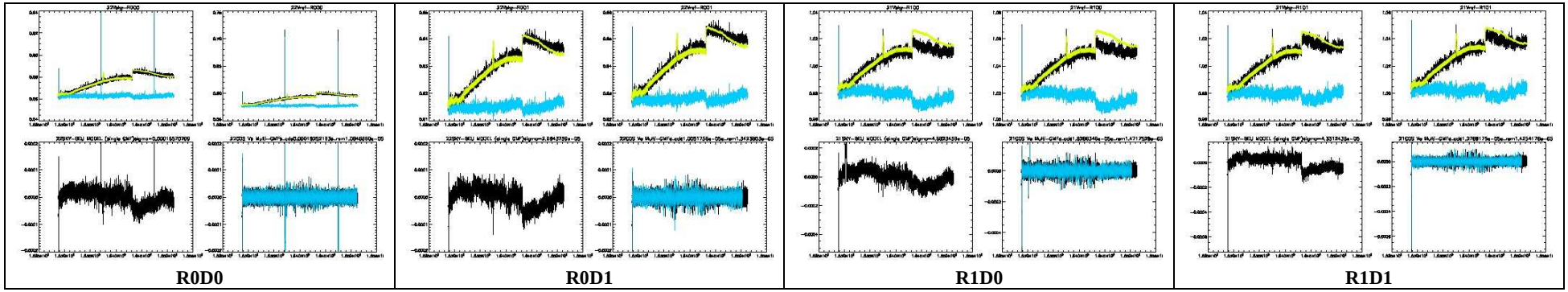

R0D0 **R0D1** **R1D0** **R1D1**

Table 18 BEU drift removal from total power data, using the OLD coefficients; Each panel contains: Sky data (top left) Ref data (top right), differenced data using a single GMF (bottom left) and differenced data using multiple GMF (bottom right). Colours represent: raw data from: CDS (black) , model (yellow) , corrected data (magenta).

INAF – IASF Bologna

LFI Project System Team

LFI23

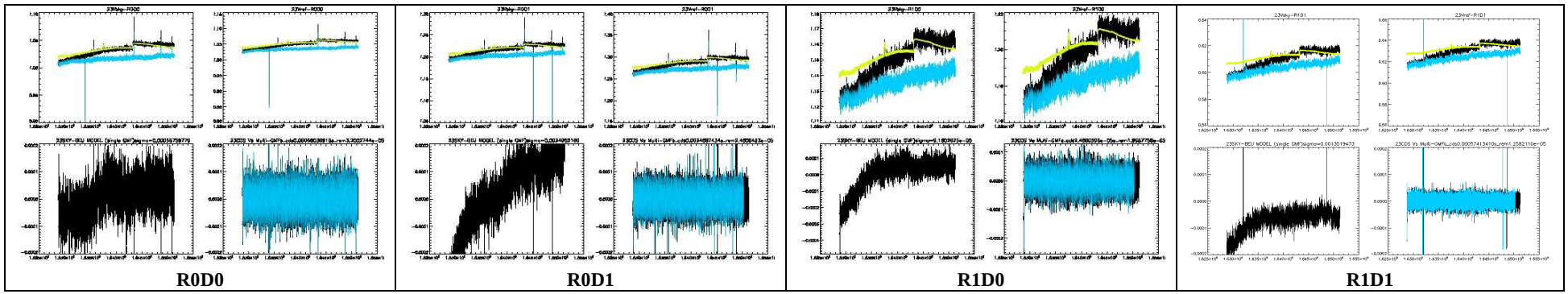

Table 19 BEU drift removal from total power data, using the new coefficients; Each panel contains: Sky data (top left) Ref data (top right), differenced data using a single GMF (bottom left) and differenced data using multiple GMF (bottom right). Colours represent: raw data from: CDS (black) , model (yellow) , corrected data (magenta).

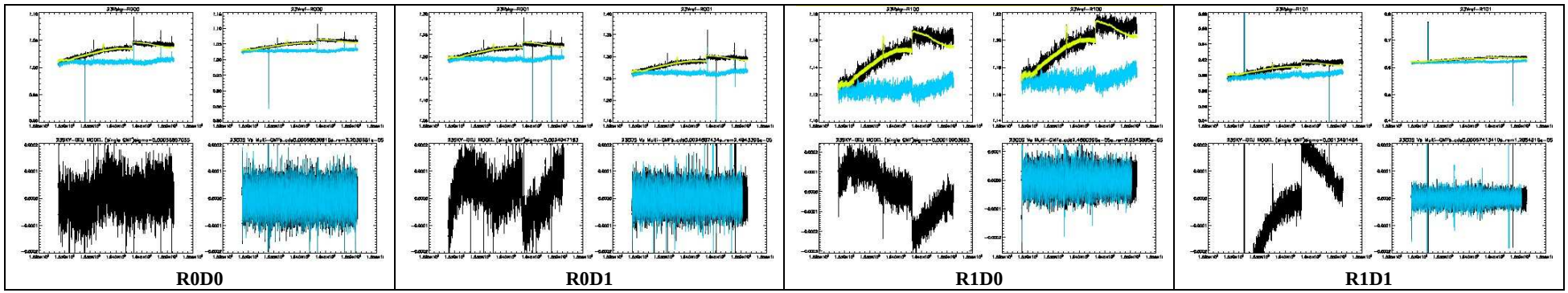

Table 20 BEU drift removal from total power data, using the OLD coefficients; Each panel contains: Sky data (top left) Ref data (top right), differenced data using a single GMF (bottom left) and differenced data using multiple GMF (bottom right). Colours represent: raw data from: CDS (black) , model (yellow) , corrected data (magenta).

LFI24

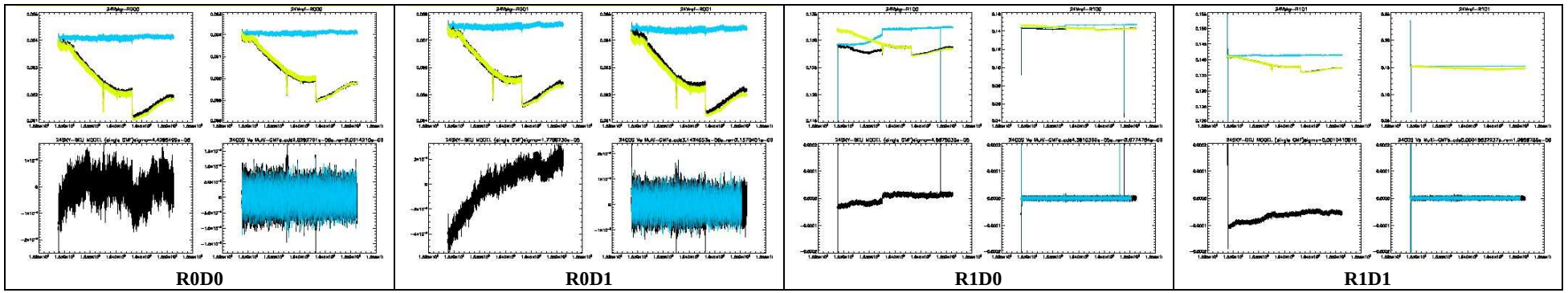

Table 21 BEU drift removal from total power data, using the new coefficients; Each panel contains: Sky data (top left) Ref data (top right), differenced data using a single GMF (bottom left) and differenced data using multiple GMF (bottom right). Colours represent: raw data from: CDS (black) , model (yellow) , corrected data (magenta).

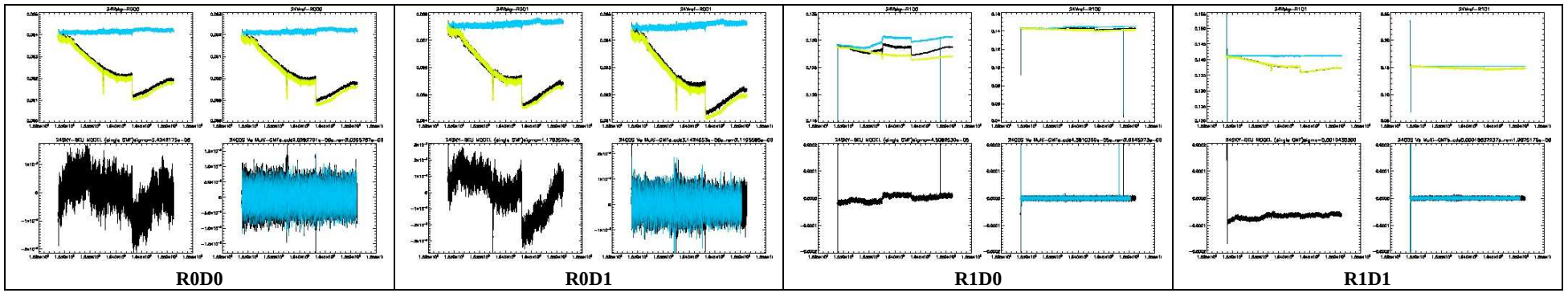

Table 22 BEU drift removal from total power data, using the OLD coefficients; Each panel contains: Sky data (top left) Ref data (top right), differenced data using a single GMF (bottom left) and differenced data using multiple GMF (bottom right). Colours represent: raw data from: CDS (black) , model (yellow) , corrected data (magenta).

LFI25

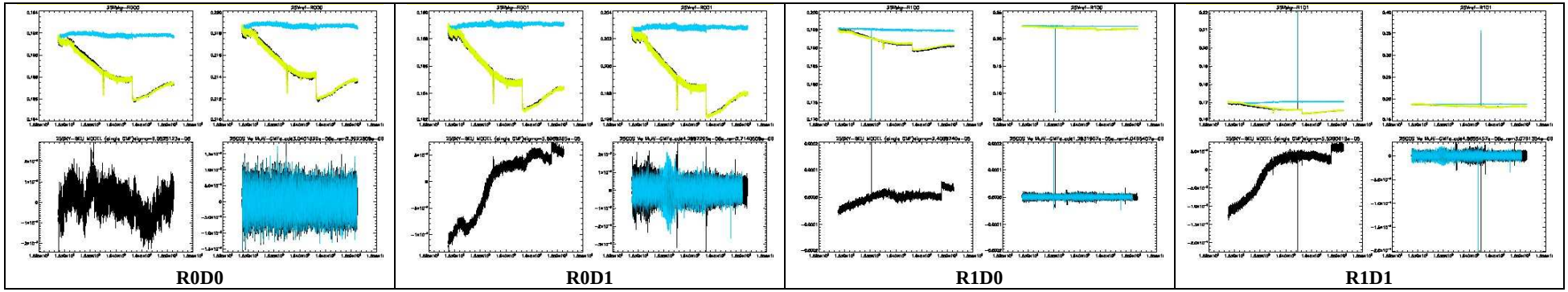

Table 23 BEU drift removal from total power data, using the new coefficients; Each panel contains: Sky data (top left) Ref data (top right), differenced data using a single GMF (bottom left) and differenced data using multiple GMF (bottom right). Colours represent: raw data from: CDS (black) , model (yellow) , corrected data (magenta).

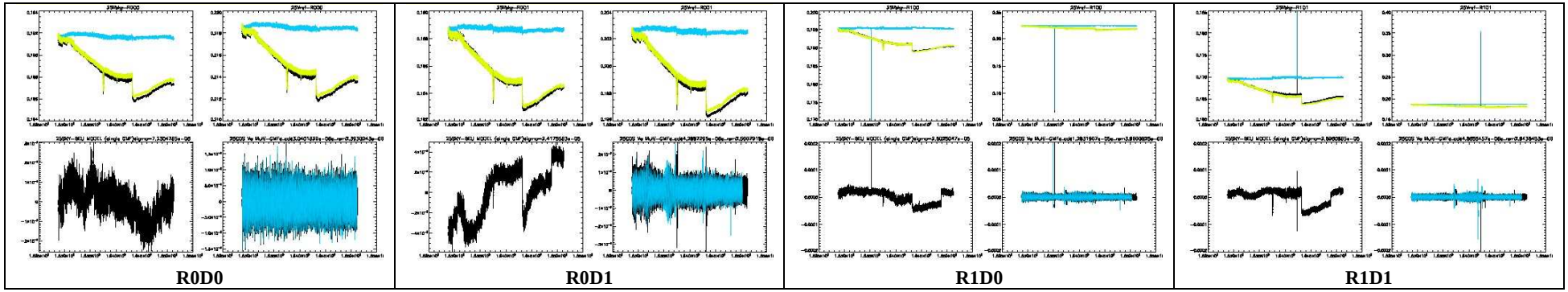

Table 24 BEU drift removal from total power data, using the OLD coefficients; Each panel contains: Sky data (top left) Ref data (top right), differenced data using a single GMF (bottom left) and differenced data using multiple GMF (bottom right). Colours represent: raw data from: CDS (black) , model (yellow) , corrected data (magenta).

LFI26

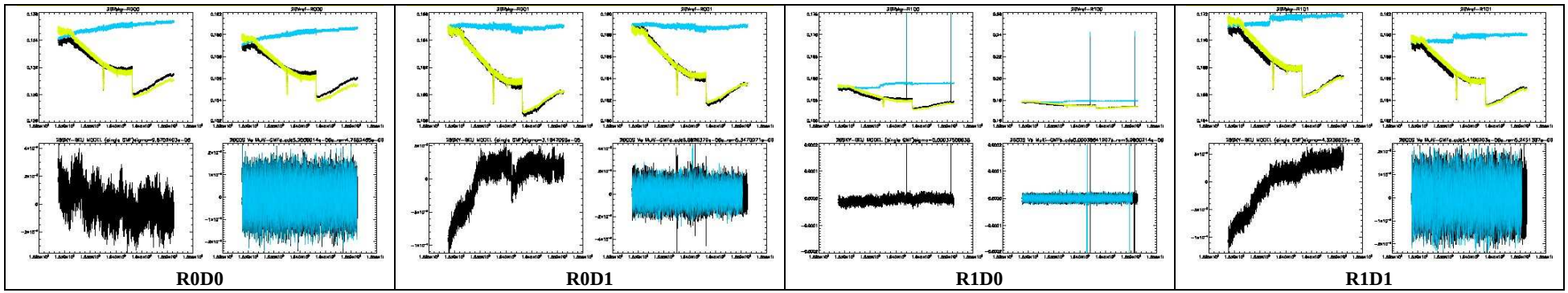

Table 25 BEU drift removal from total power data, using the new coefficients; Each panel contains: Sky data (top left) Ref data (top right), differenced data using a single GMF (bottom left) and differenced data using multiple GMF (bottom right). Colours represent: raw data from: CDS (black) , model (yellow) , corrected data (magenta).

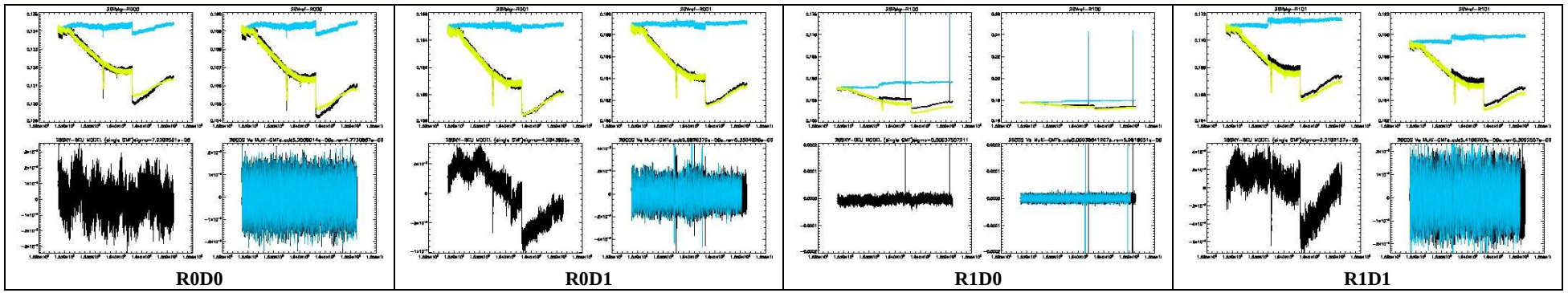

Table 26 BEU drift removal from total power data, using the OLD coefficients; Each panel contains: Sky data (top left) Ref data (top right), differenced data using a single GMF (bottom left) and differenced data using multiple GMF (bottom right). Colours represent: raw data from: CDS (black) , model (yellow) , corrected data (magenta).

INAF – IASF Bologna

LFI Project System Team

LFI27

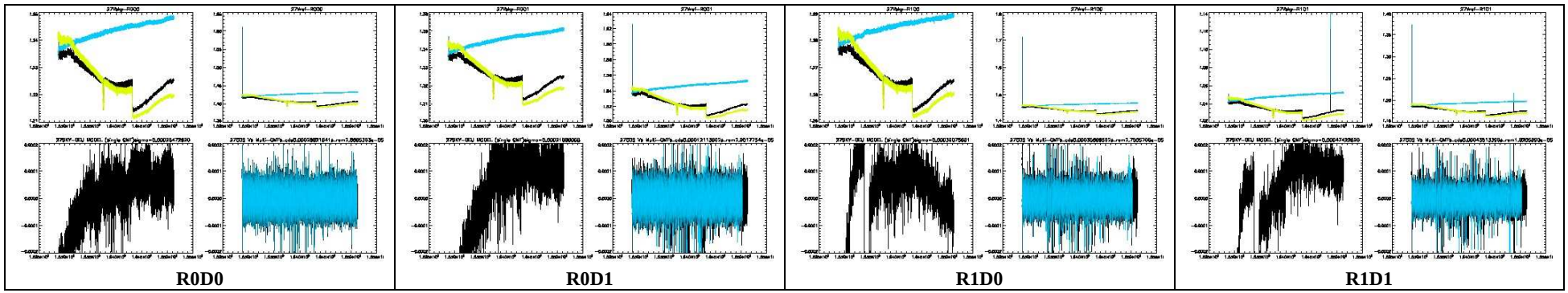

R0D0 **R0D1** **R1D0** **R1D1**

Table 27 BEU drift removal from total power data, using the new coefficients; Each panel contains: Sky data (top left) Ref data (top right), differenced data using a single GMF (bottom left) and differenced data using multiple GMF (bottom right). Colours represent: raw data from: CDS (black) , model (yellow) , corrected data (magenta).

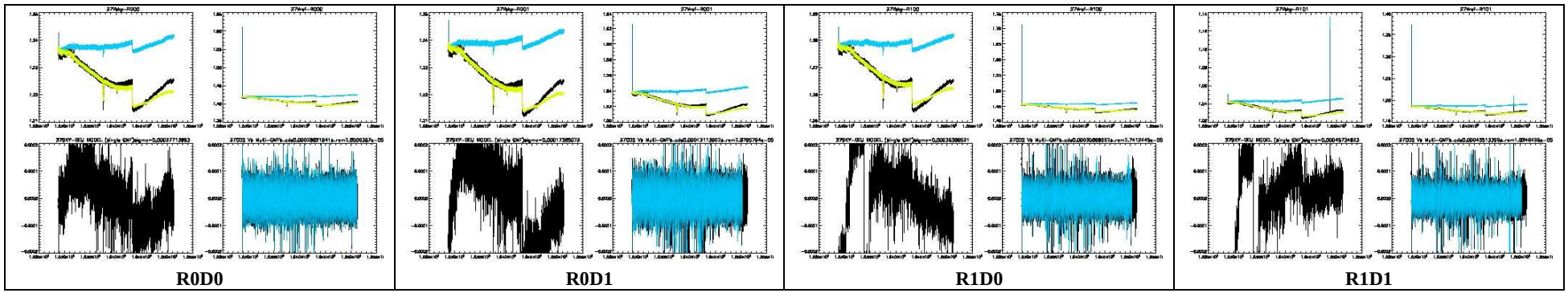

R0D0 **R0D1** **R1D0** **R1D1**

Table 28 BEU drift removal from total power data, using the OLD coefficients; Each panel contains: Sky data (top left) Ref data (top right), differenced data using a single GMF (bottom left) and differenced data using multiple GMF (bottom right). Colours represent: raw data from: CDS (black) , model (yellow) , corrected data (magenta).

LFI28

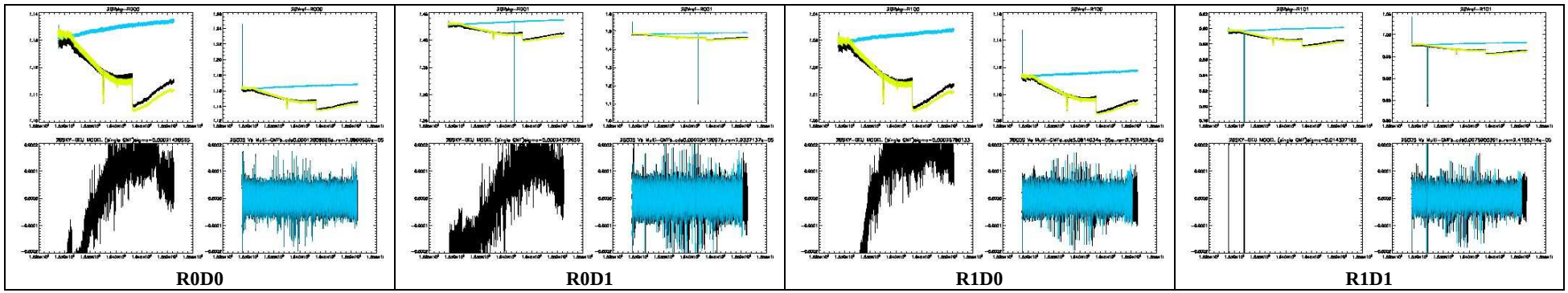

Table 29 BEU drift removal from total power data, using the new coefficients; Each panel contains: Sky data (top left) Ref data (top right), differenced data using a single GMF (bottom left) and differenced data using multiple GMF (bottom right). Colours represent: raw data from: CDS (black) , model (yellow) , corrected data (magenta).

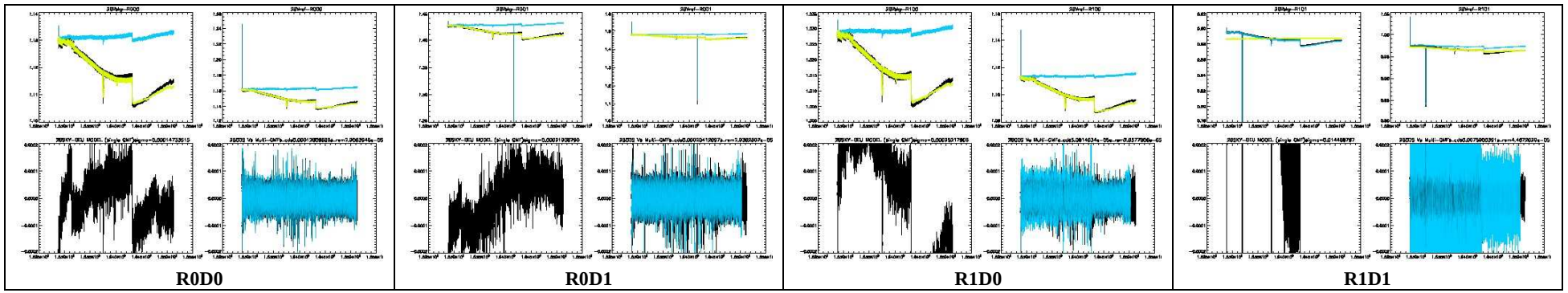

Table 30 BEU drift removal from total power data, using the OLD coefficients; Each panel contains: Sky data (top left) Ref data (top right), differenced data using a single GMF (bottom left) and differenced data using multiple GMF (bottom right). Colours represent: raw data from: CDS (black) , model (yellow) , corrected data (magenta).

6.5 Spectrograms

Section containing the spectral behaviour of each detector with time. Spectrograms display in log color scales the amplitude spectral density versus OD. Each channel is represented by four rows (one for each detector). Each row contains two panels. The left panel shows the spectral behavior of differenced data, calculated using multiple GMF2 (one GMF per day) after the BEM effect removal. The right panel shows at first level the result of removal: they are obtained as difference between the plot in the left panel and the corresponding one calculated from CDS uncorrected differenced data. It is evident that the major effect of removal appears in the low frequency region, and especially roughly before day 250, when the Transponder was permanently switched ON (strongly reducing the daily thermal fluctuations).

LFI-18

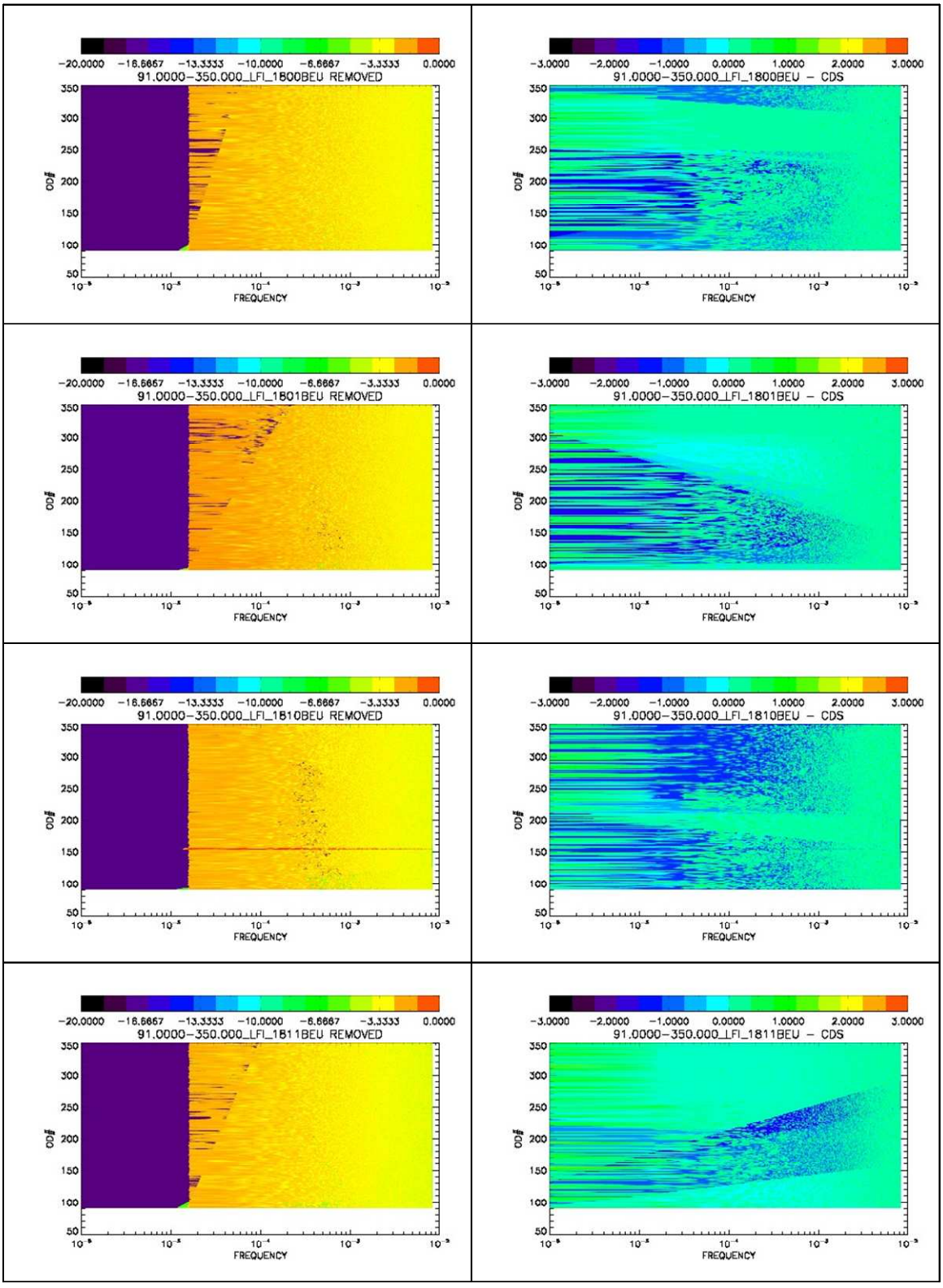

Figure 26

LFI-19

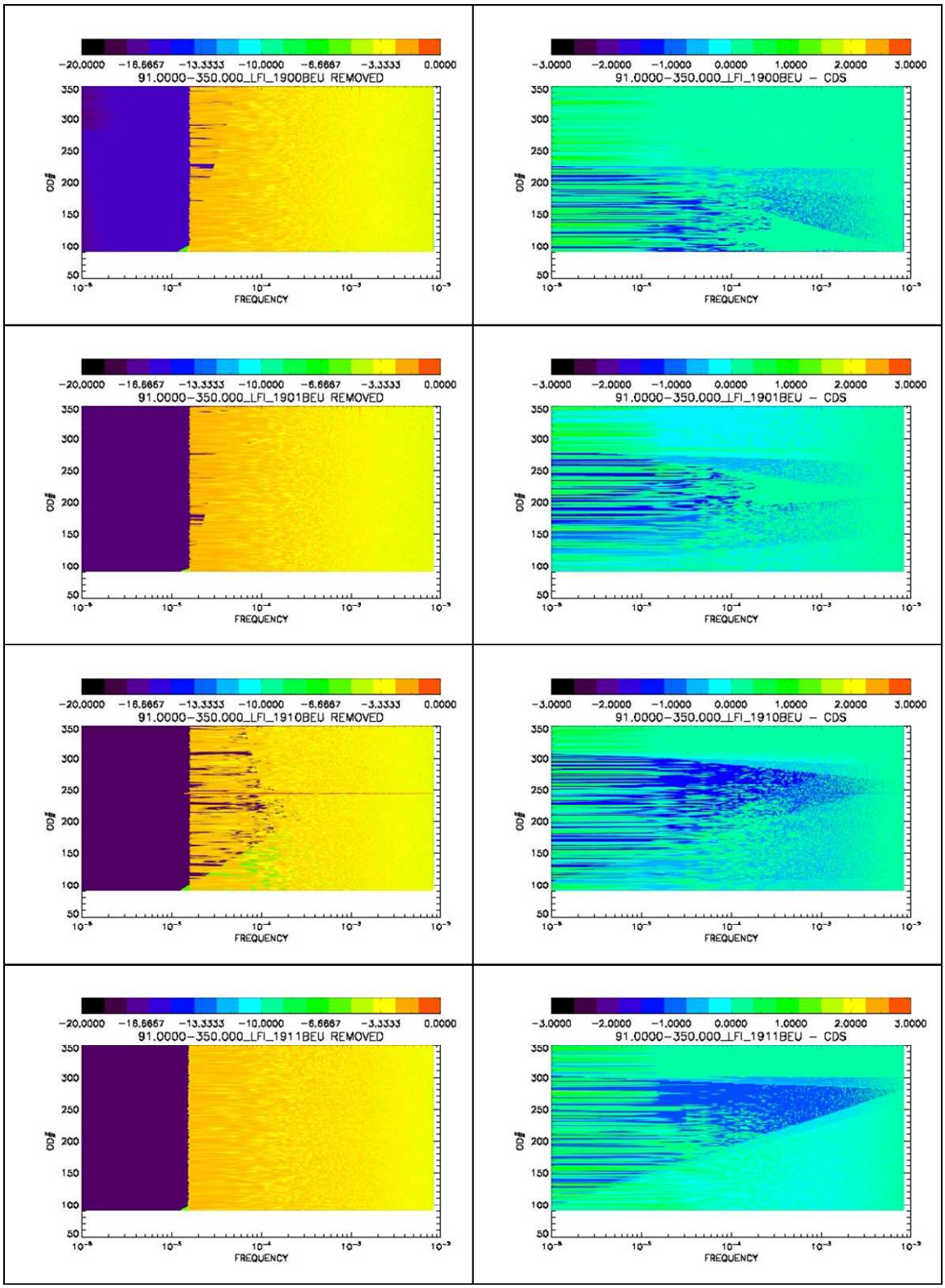

Figure 27

LFI-20

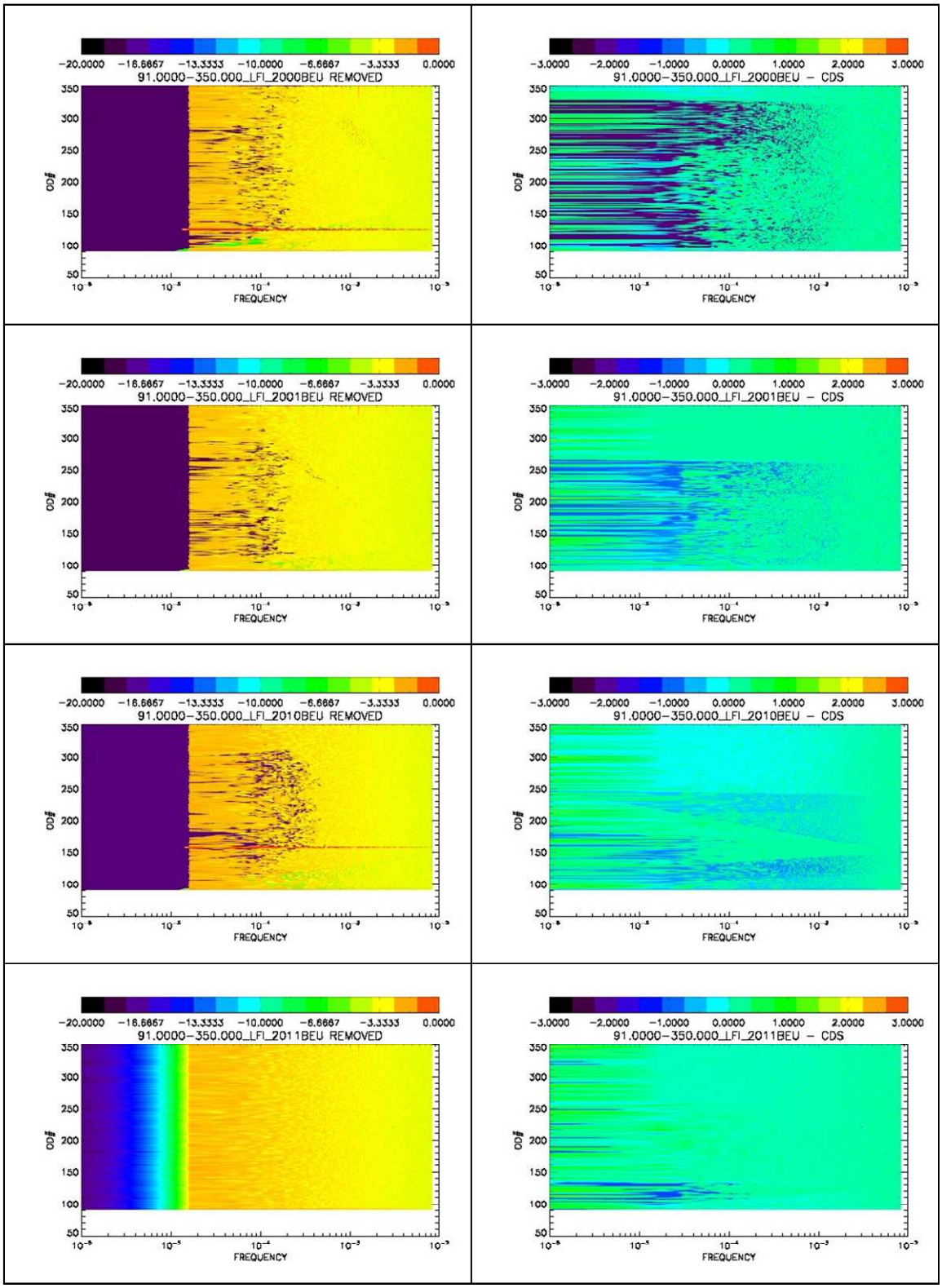

Figure 28

LFI-21

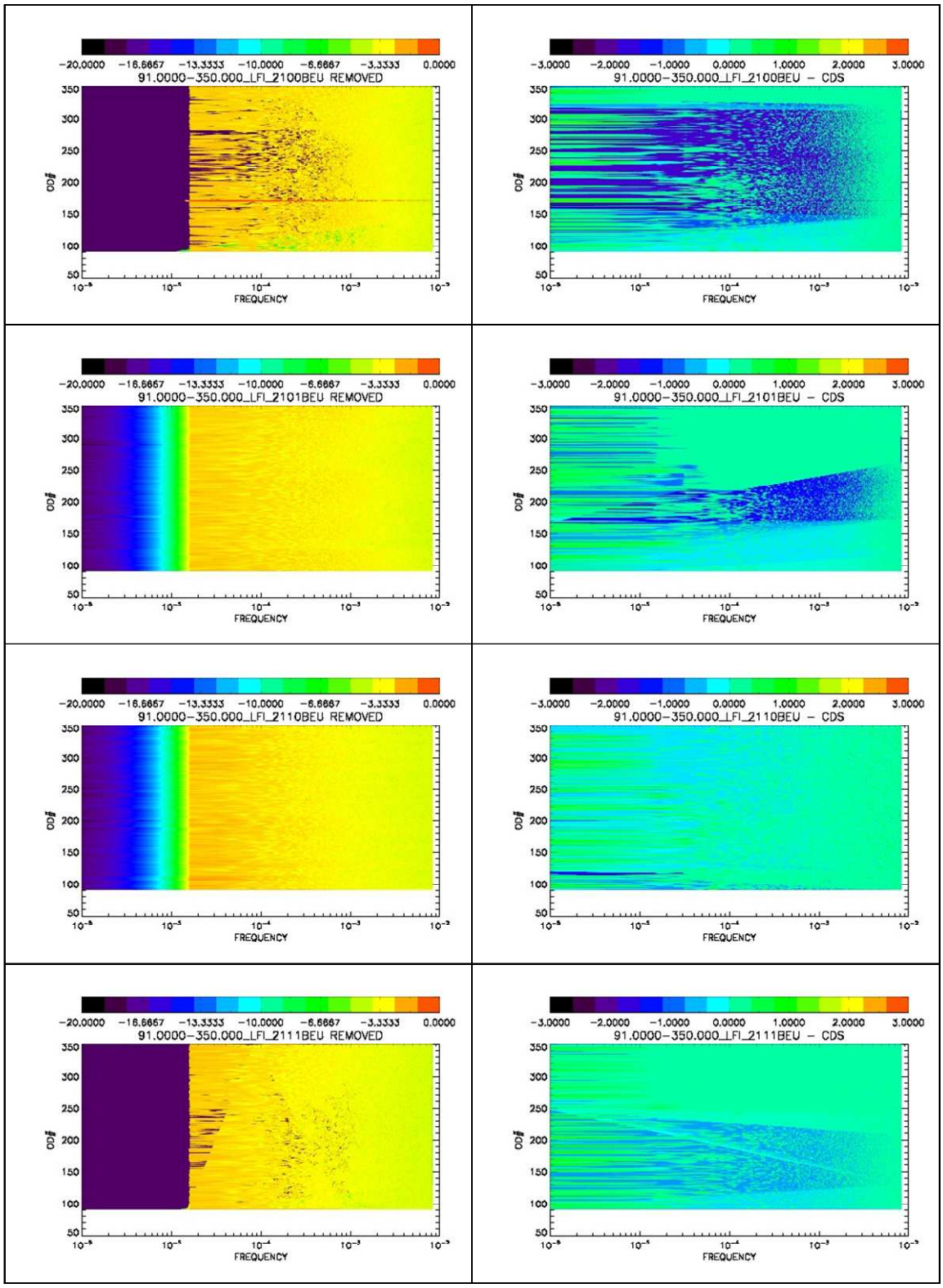

Figure 29

LFI-22

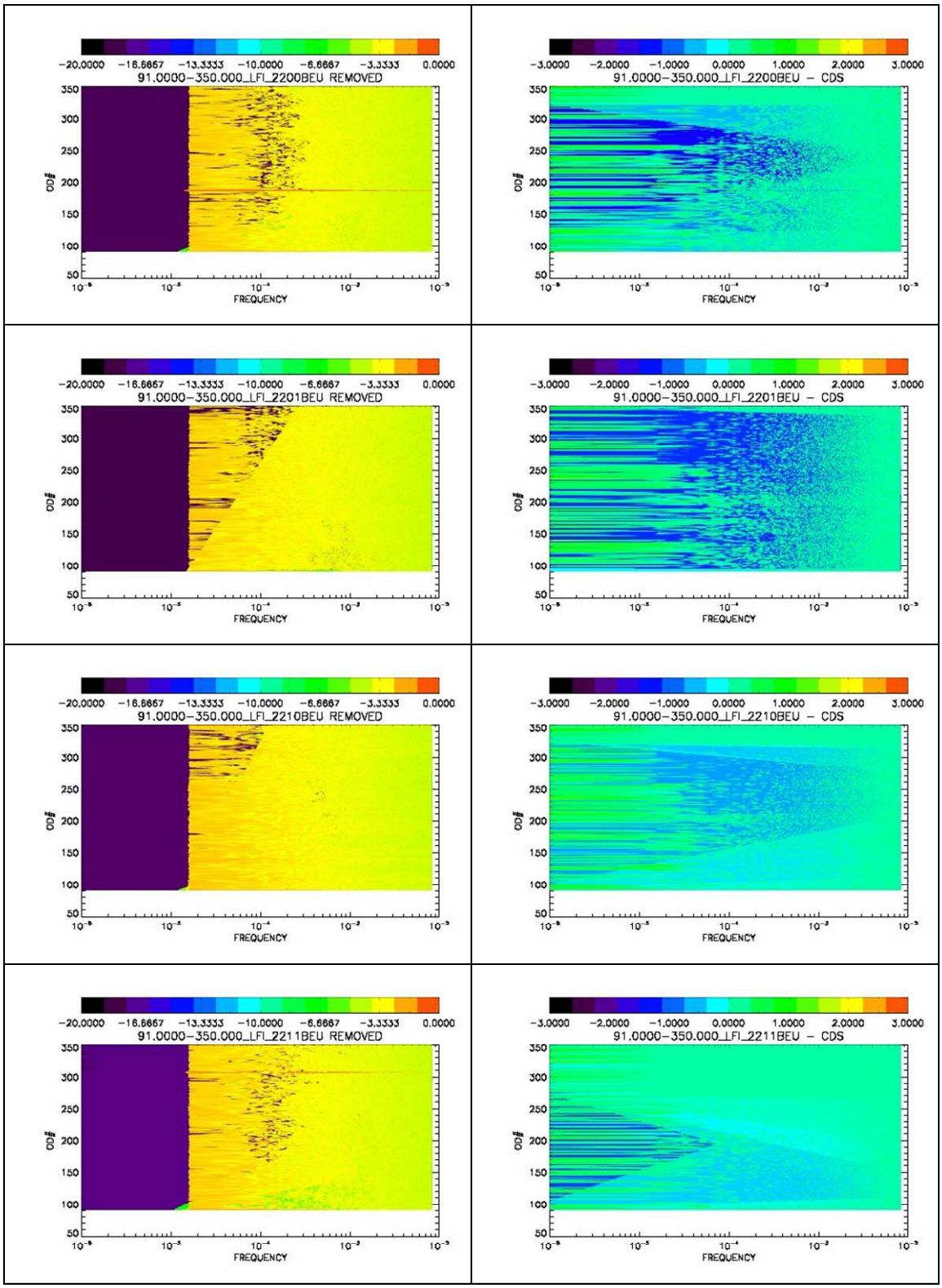

Figure 30

LFI-23

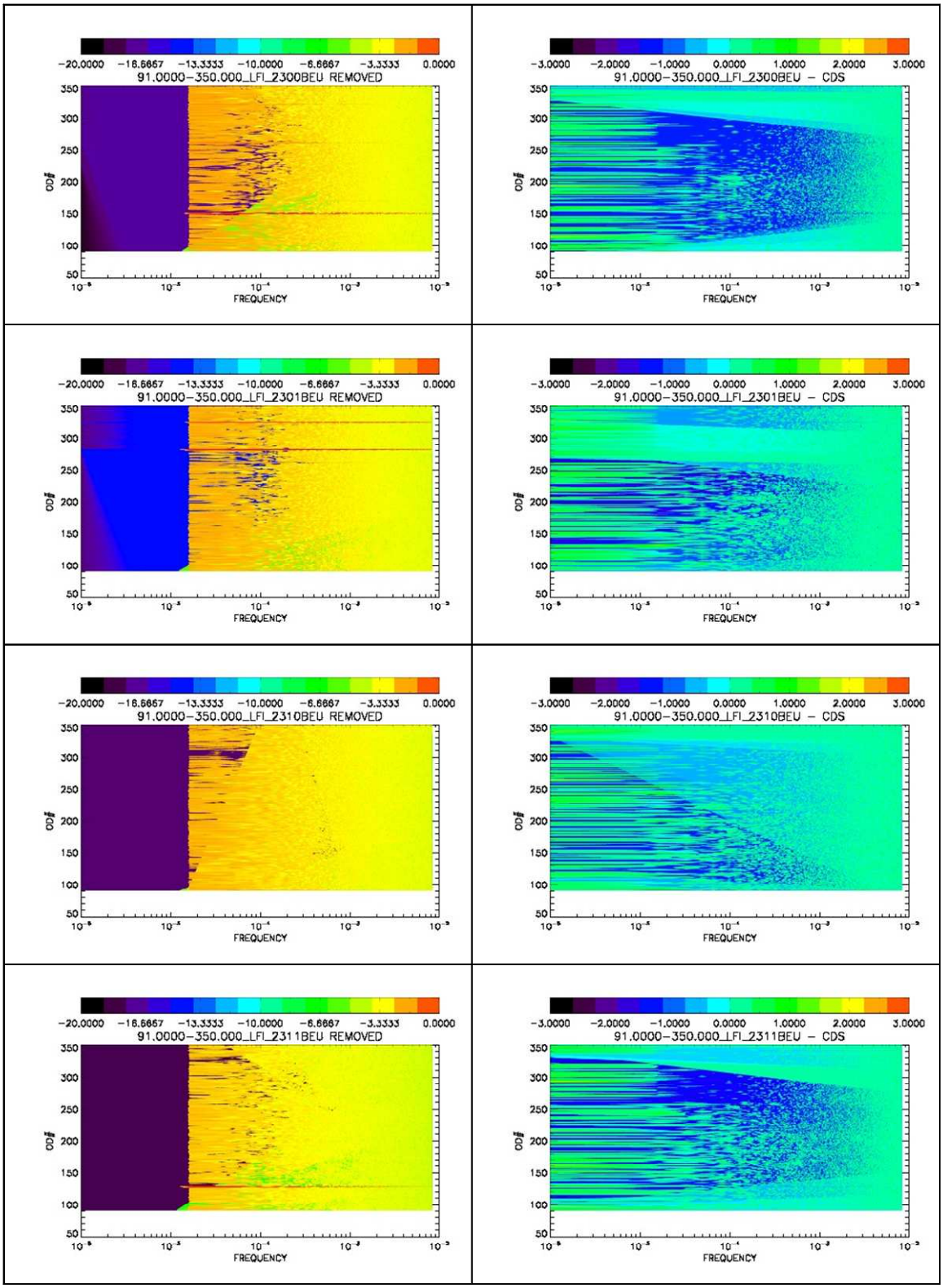

Figure 31

LFI-24

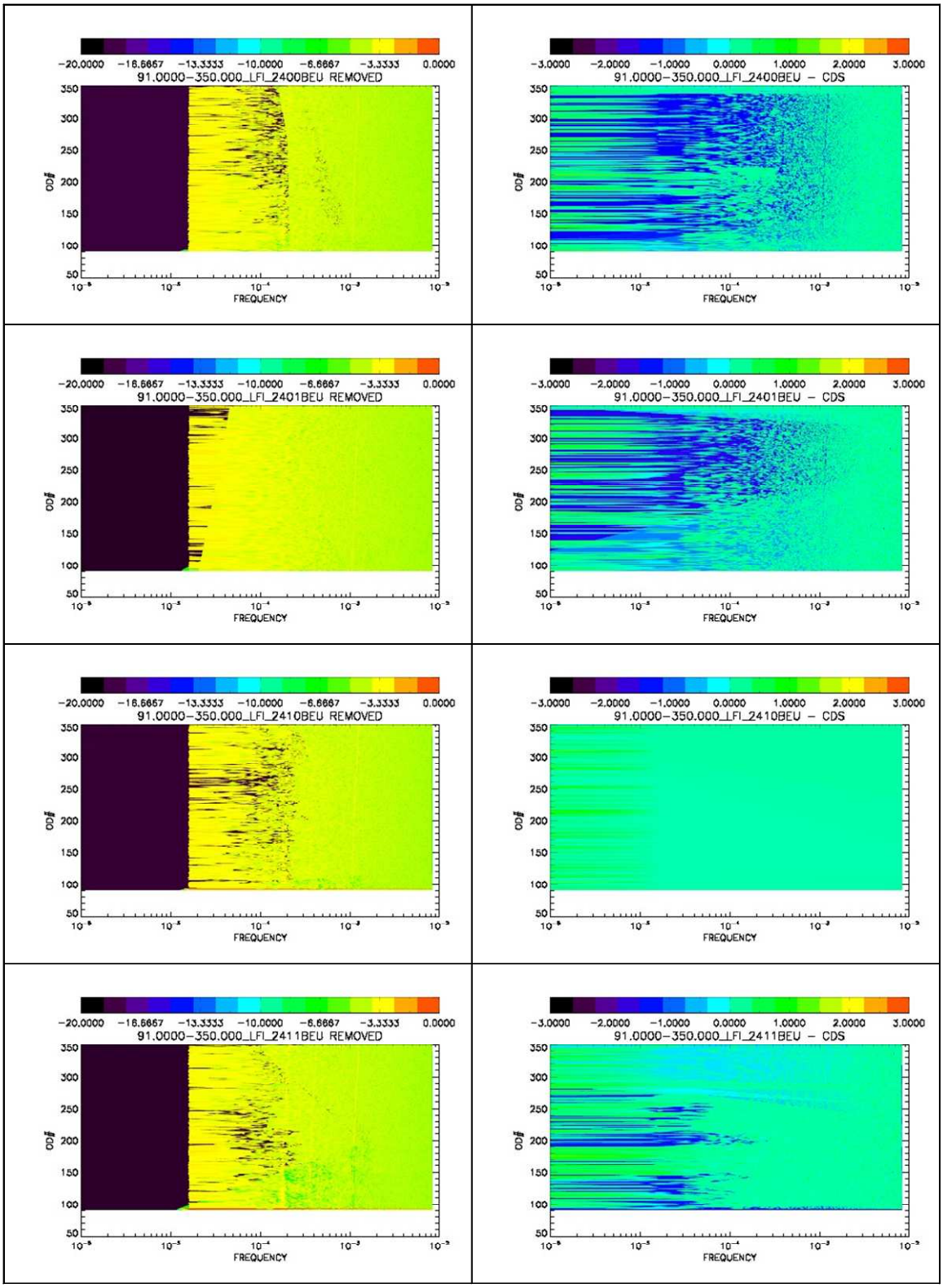

Figure 32

LFI-25

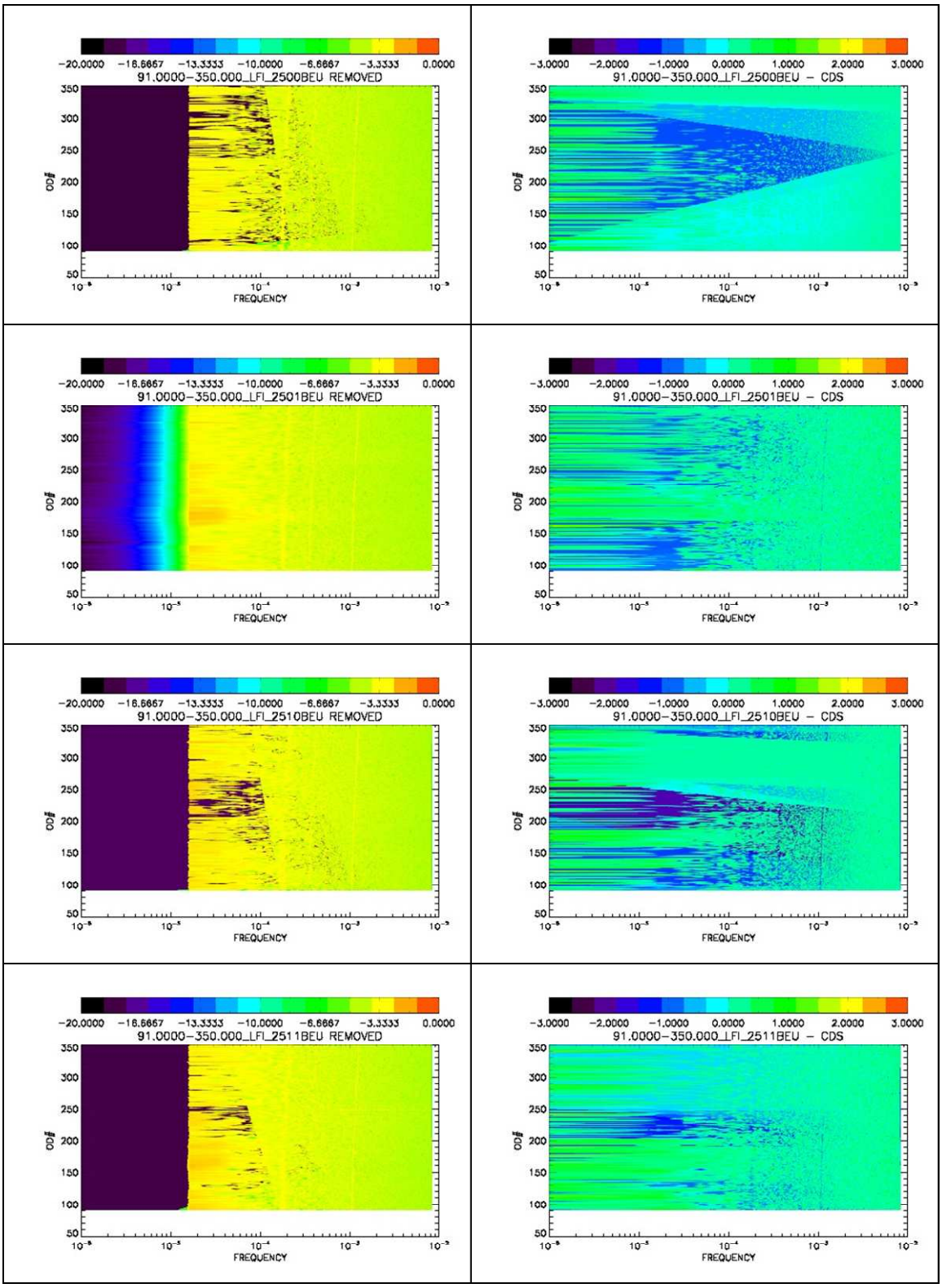

Figure 33

LFI-26

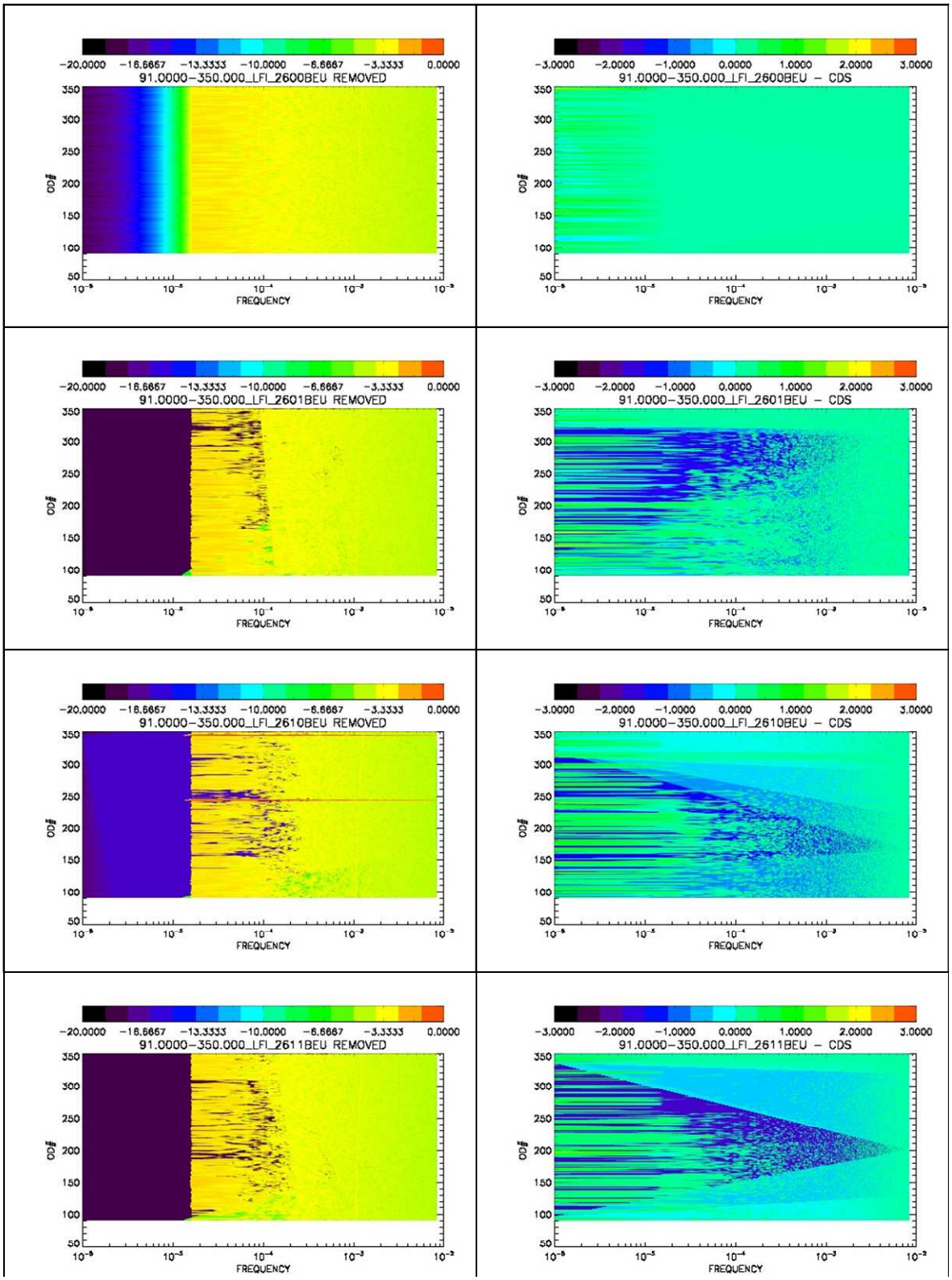

Figure 34

LFI-27

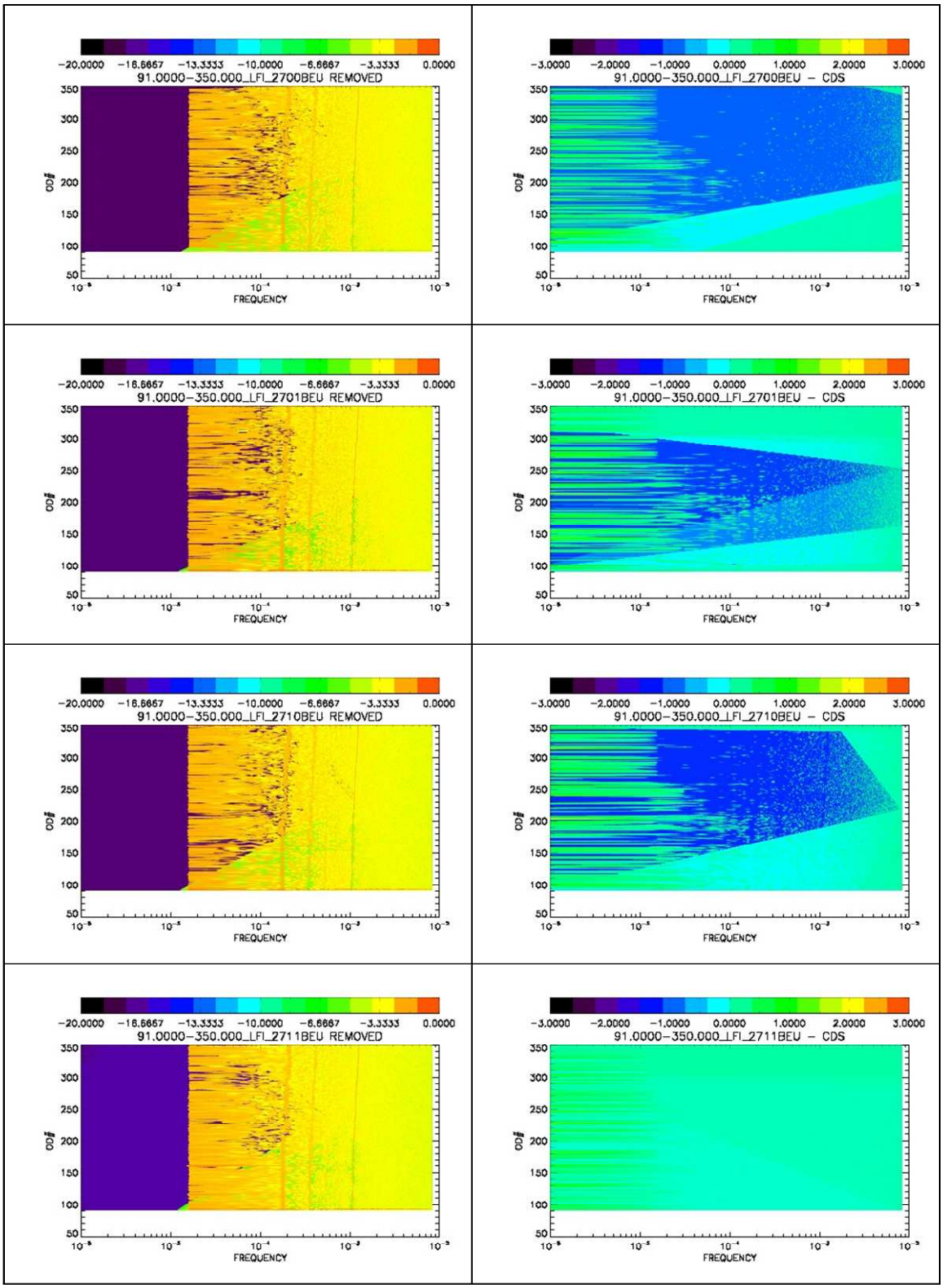

Figure 35

LFI-28

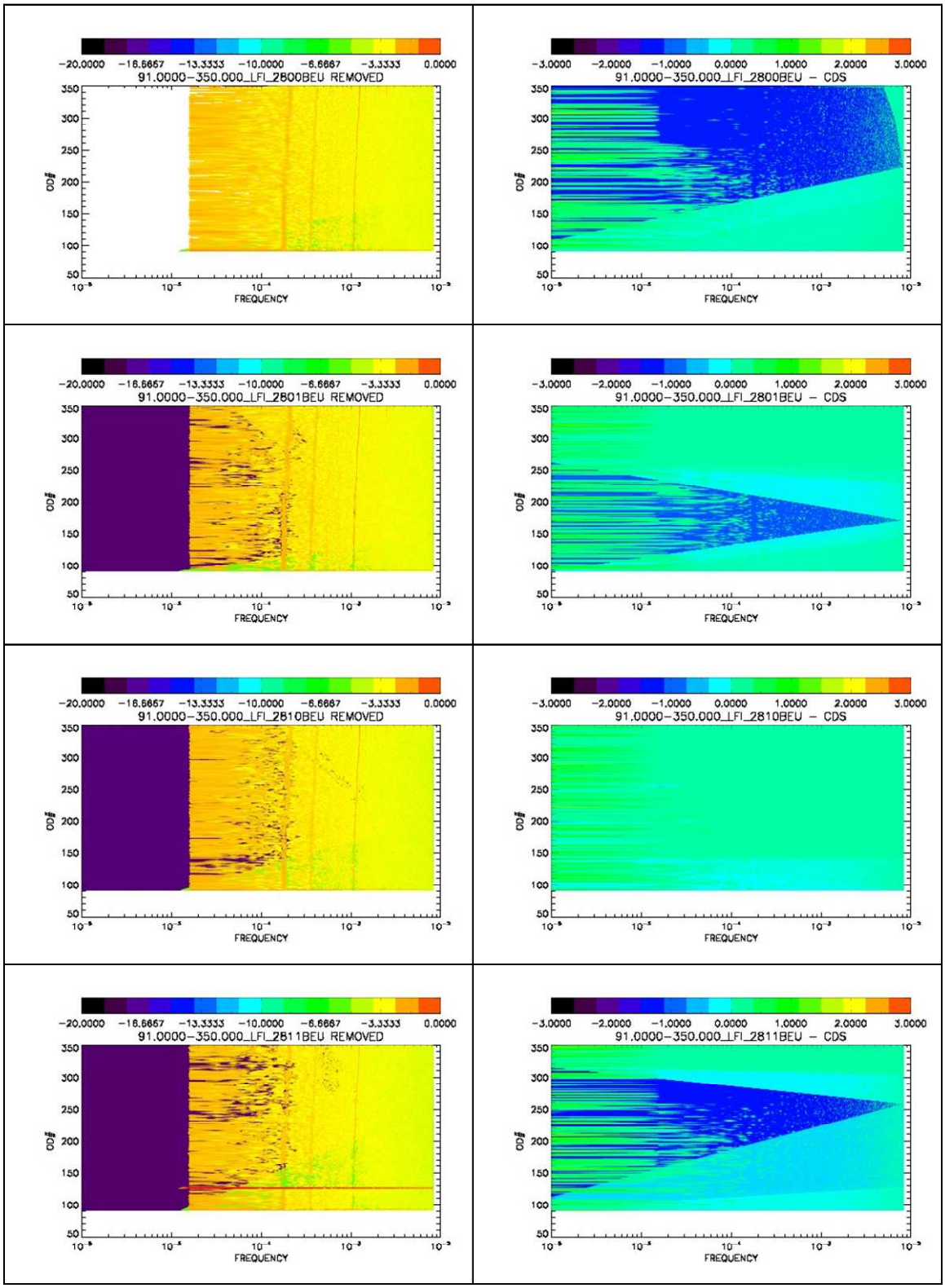

Figure 36

6.6 Spectra

Amplitude spectral density in the interval OD91-OD350. The four left plots refer to Main Arm (R0D0 top, R0D1 bottom), the four right plots to Side Arm Arm (R1D0 top, R1D1 bottom). The two left plots of each four plots panel refer to differenced data calculated using single GMF (black line are uncorrected data, yellow are corrected data), the two right panels represent differenced data calculated using multiple GMF (as before, black line are uncorrected data, yellow are corrected data).

LFI- 18

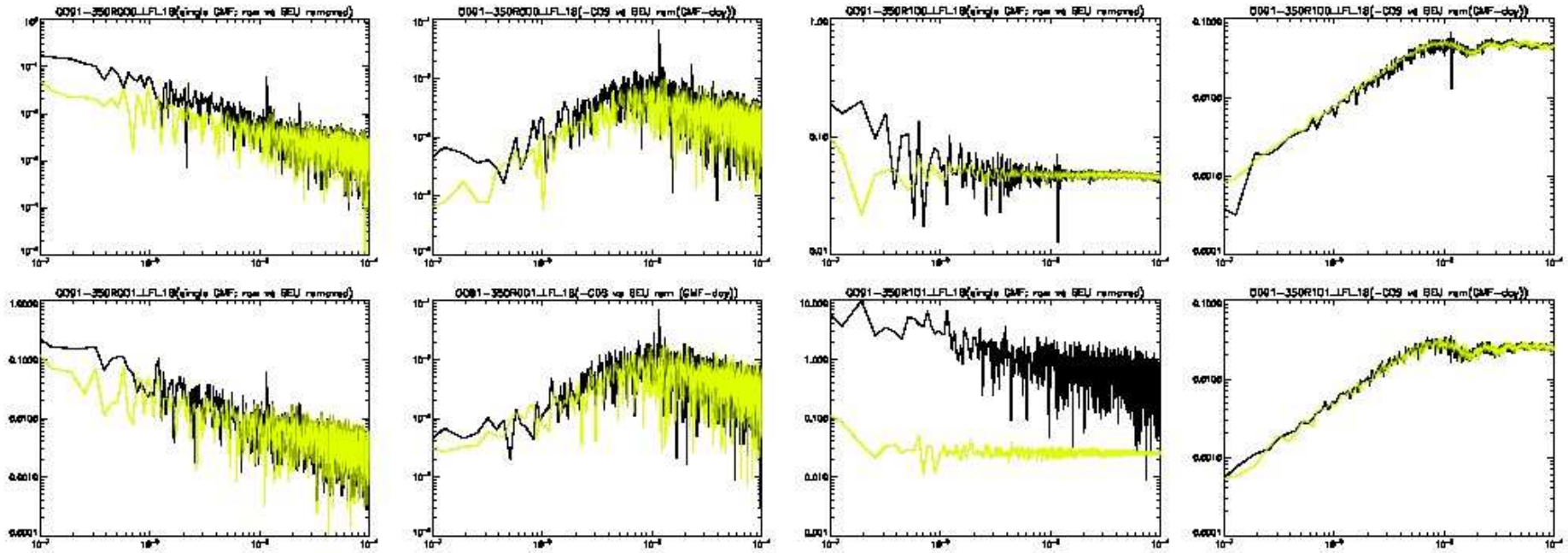

Figure 37

LFI -19

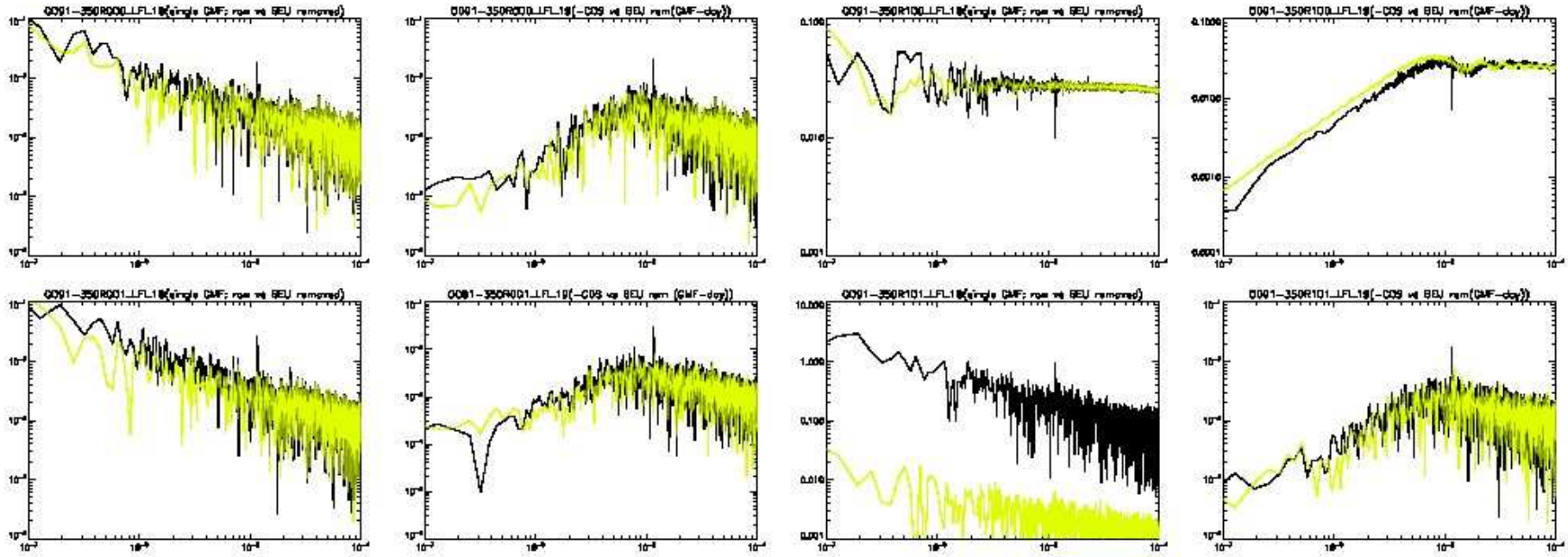

Figure 38

LFI-20

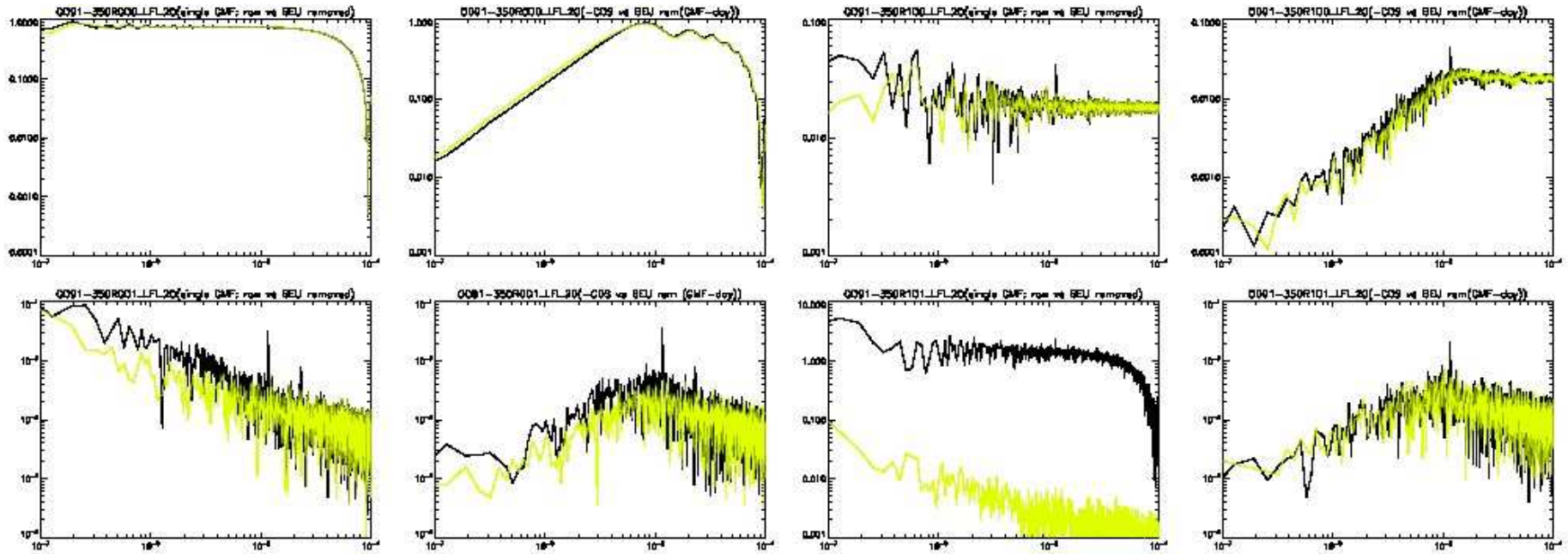

Figure 39

LFI-21

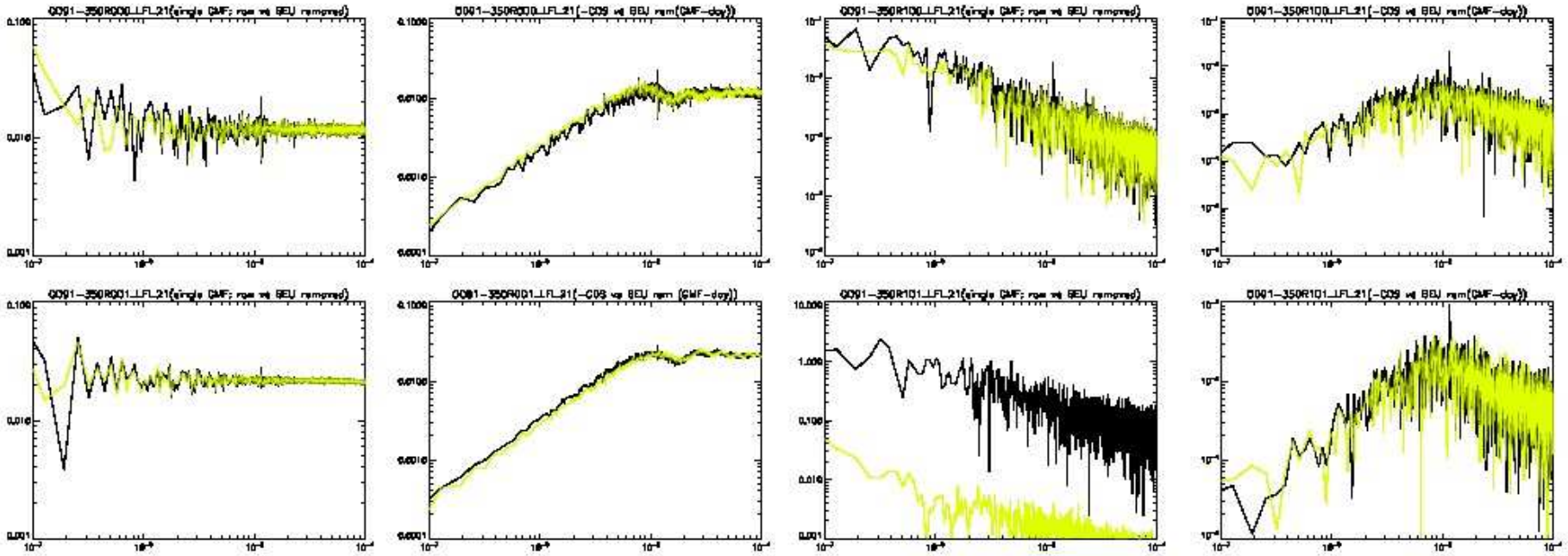

Figure 40

LFI-22

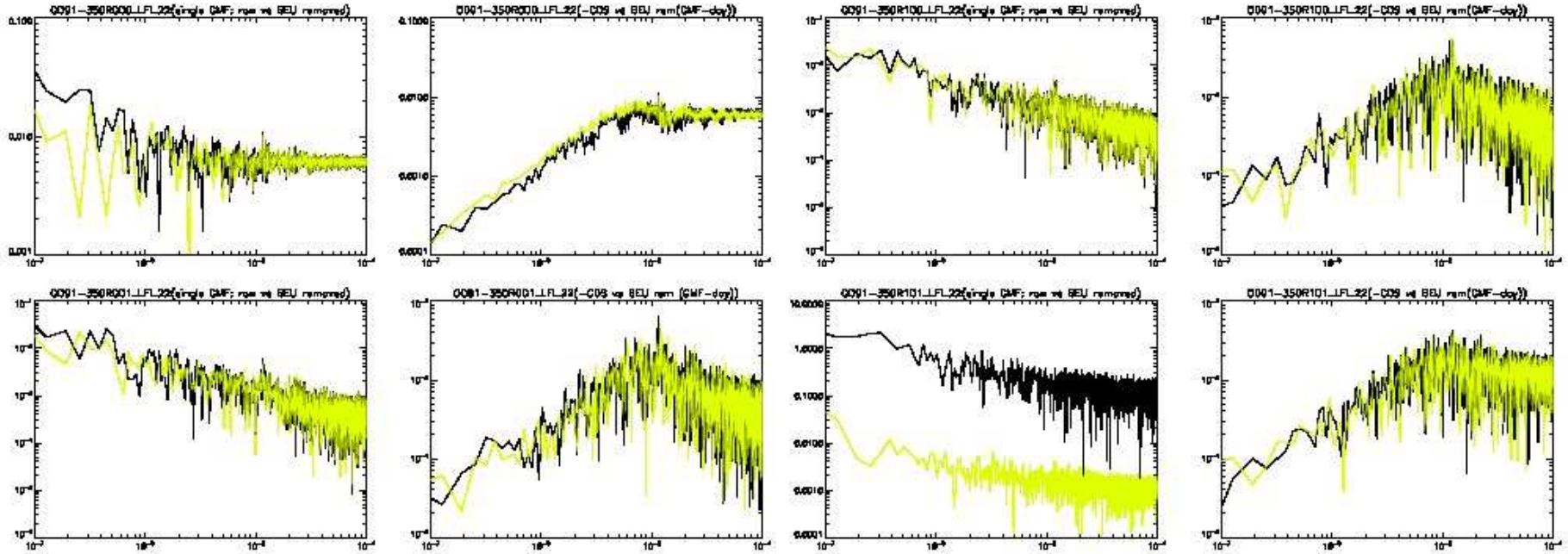

Figure 41

LFI-23

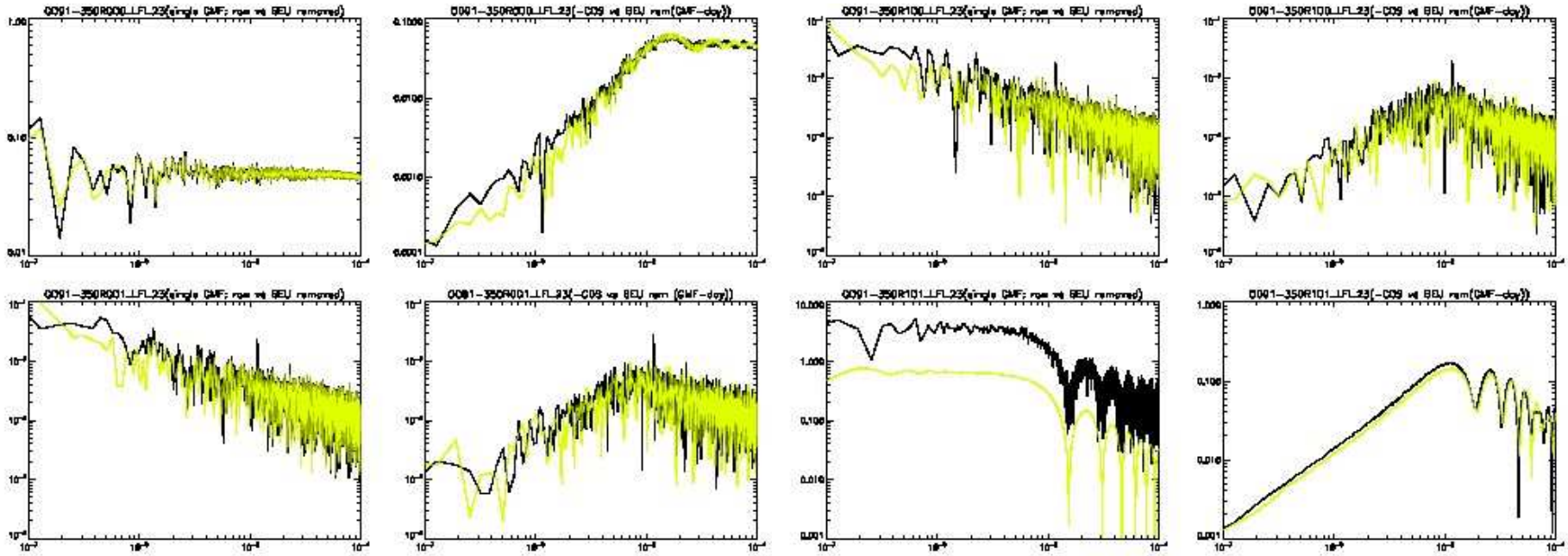

Figure 42

LFI-24

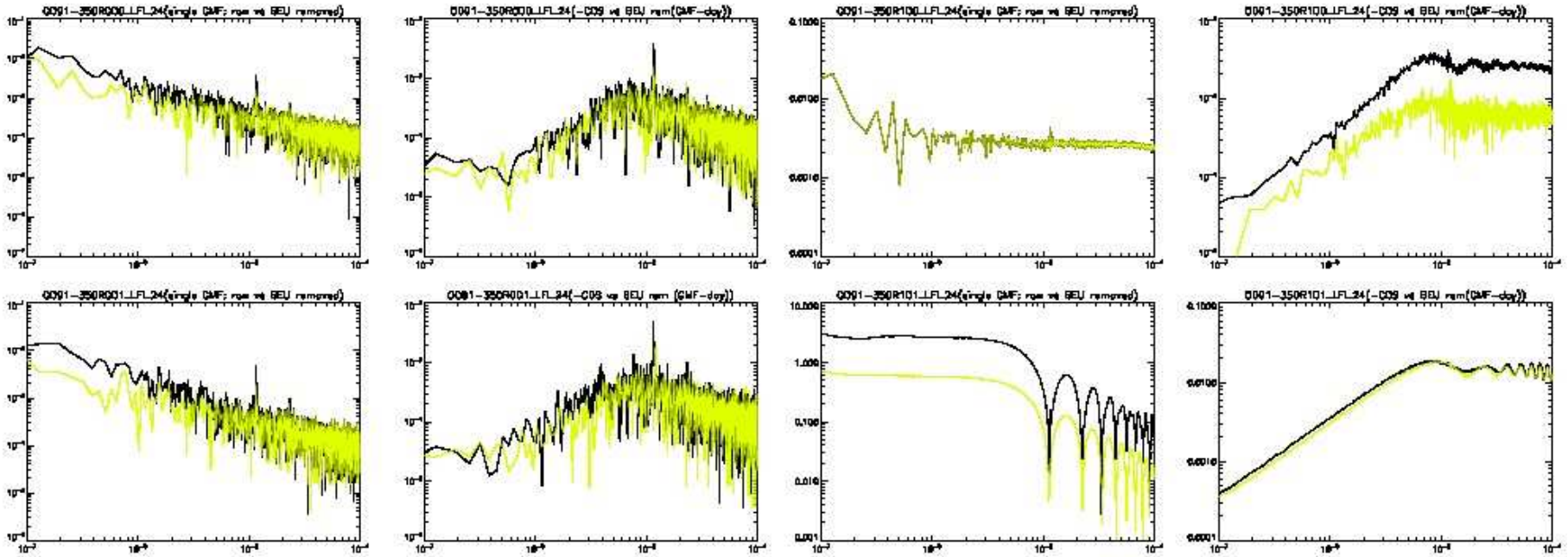

Figure 43

LFI-25

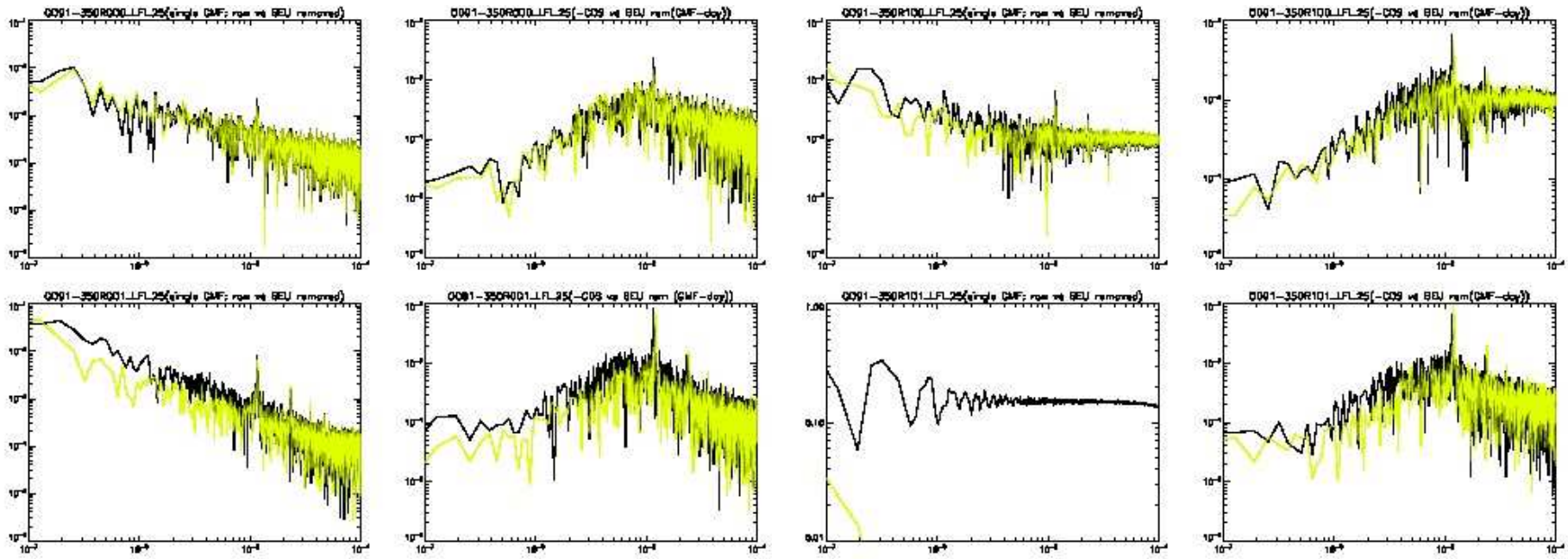

Figure 44

LFI-26

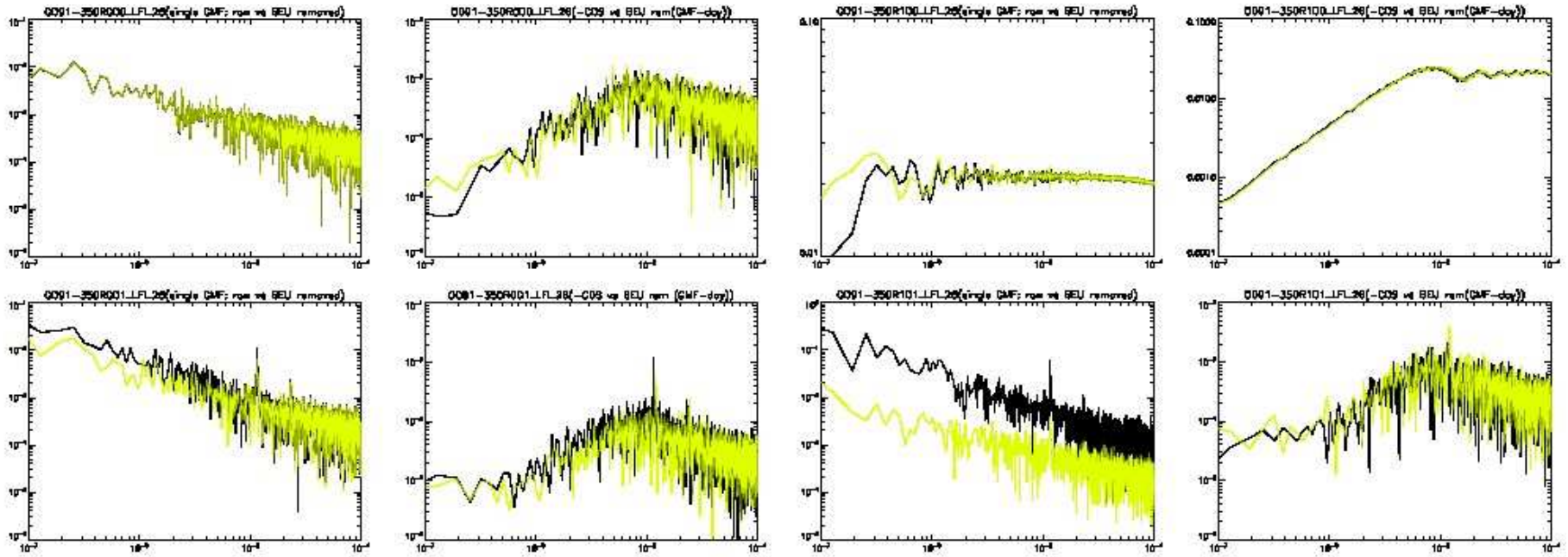

Figure 45

LFI-27

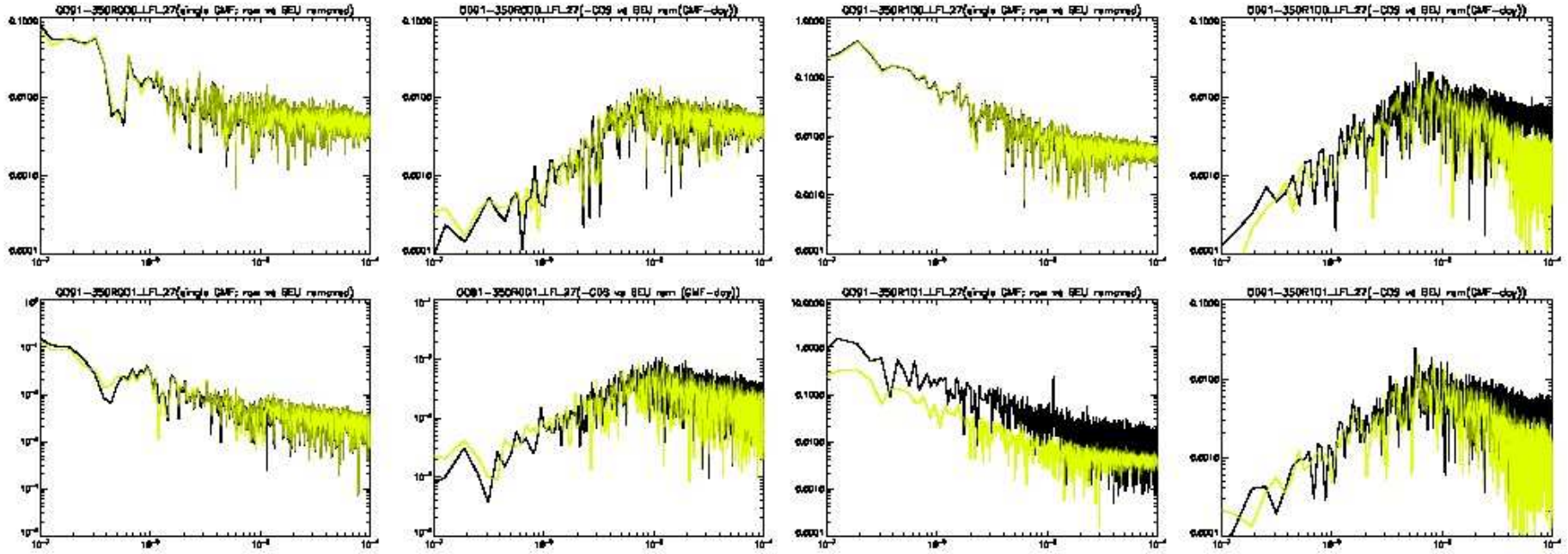

Figure 46

LFI-28

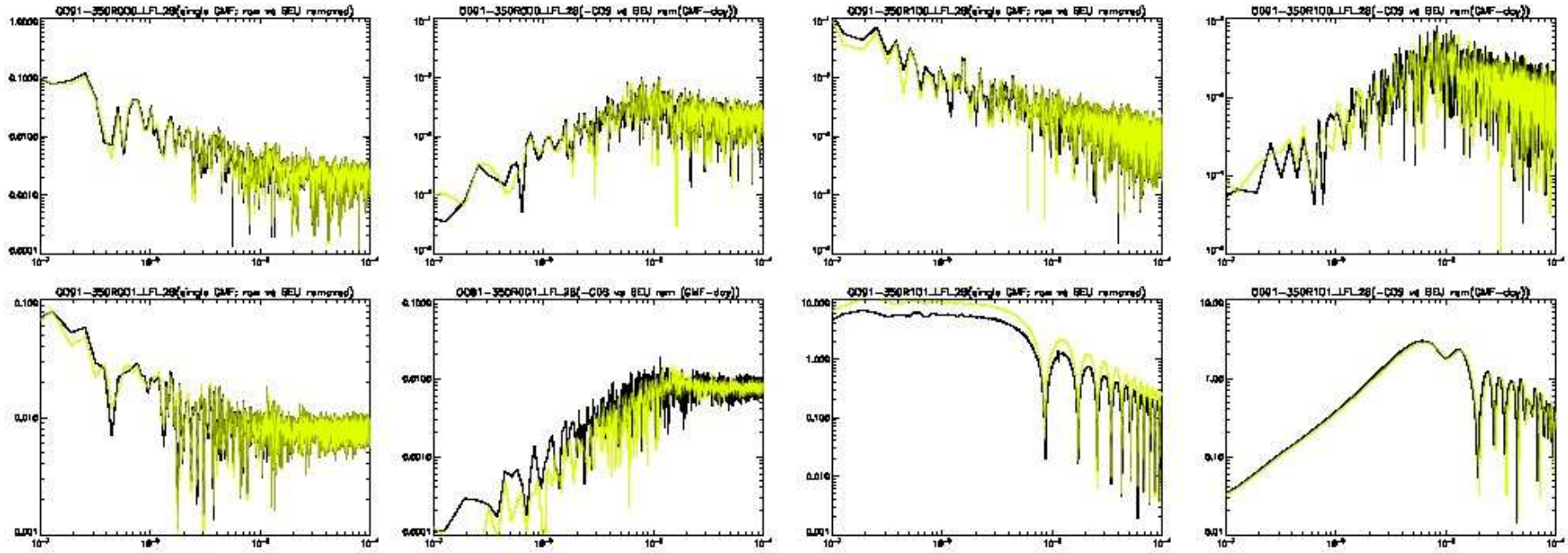

Figure 47